THE USE OF TRANSFER FUNCTION METHODS IN THE FEEDBACK CONTROL OF DISTRIBUTED PARAMETER SYSTEMS

by

Richard Morris Amato Goff

Dissertation submitted to the faculty of the

Virginia Polytechnic Institute and State University

in partial fulfillment of the requirements for the degree of

DOCTOR OF PHILOSOPHY

in

Aerospace Engineering

APPROVED:

F. H. Lutze Jr., Chairman

J. A. Burns

W. L. Hallauer Jr.

E. M. Cliff

L. Meirovitch

July, 1981

Blacksburg, Virginia

ACKNOWLEDGEMENTS

This is it!

I am satisfied.

To , my dead father, who started all this by sharing with me the joy of flying model airplanes. You have been my guide. To , my mother, whose absolute love for me was at times the only ember glowing on this project. We did it, mom.

To , my wife, whose love, enthusiasm, insanity, and joyous zest for living have been constant reminders to me of who we really are. You're great, I love you, .

To Dr. Fred Lutze, my committee chairman, whose friendship and willingness to work many hours with me through the peaks and the valleys made this a satisfying pilgrimage, and who once said, "I'll believe it, when I see it." Thank you for believing it all along. To the other members of my committee: Dr. John Burns and Dr. Gene Cliff for their lighthearted input to this heavy-headed field, Dr. Bill Hallauer for his assistance, enthusiasm and model of thoroughness in his teaching and work, and Dr. Leonard Meirovitch for his inspiring example of the quantity of quality work one man is capable of completing. Thank you all for serving on my committee.

To the following people who made a direct contribution to getting this job done: , for her truly outstanding typing; , my stepfather, who knew I could do it; , who suggested I make this a starring role; , my business manager, who

was there when I needed her; , my sister, who demonstrated to me the power of commitment;

; my siblings,

and ;

, the AOE faculty and graduate students;

; my students and my teachers. Without your support, I could not have done it.

There can be no list long enough to include the names of all the people who supported me in completing this cycle in my life. If you are reading this, know that you are one of them. Thank you.

TABLE OF CONTENTS

LIST OF TABLES

LIST OF FIGURES

NOMENCLATURE

A	a constant
a	segment designator
B	a constant
b	segment designator
D	dynamic stiffness matrix
d	differential operator
d_{ij}	dynamic stiffness influence coefficients
E	modulus of elasticity
EI	flexural rigidity
$\bar{F}$	generalized force vector
f	a force
G	transfer function scaler or matrix
g_{ij}	element of transfer function matrix
I	moment of inertia
I_r	identity matrix, (dimension r x r)
i	square root of -1, arbitrary number
j	an arbitrary number
K	feedback gain scaler or matrix
k	an integer number
L	length, element length
M	moment
m	mass, an arbitrary number, mode number
MIMO	multi-input-multi-output

n	real part of a complex number
r	an arbitrary number
s	Laplace variable
SISO	single-input-single-output
T	cable tension
t	time
$[U]$	a matrix
u	reference control input
V	shear force
$[W]$	a matrix
x	spacial coordinate, a length
y	transverse displacement
z	a length
∞	infinity
α	a complex variable
Δ	a change in, denominator
δ	displacement
$\bar{\delta}$	generalized displacement vector
∂	partial derivative operator
ζ	damping ratio
θ	slope, an angle
π	3.14159
ρ	mass per unit length
ω	frequency, imaginary part of a complex number

Subscripts

0	left end, initial value
1	left end, center
2	right end
a	segment designator
b	segment designator
CL	closed loop
D	displacement
d	denominator
i	range index
j	range index
L	at the end
n	numerator
r	range index
v	velocity
vel	velocity
x	arbitrary position

Superscripts

•	derivative wrt time
'	derivative wrt space
-	a vector
-1	matrix inverse
~	condensed matrix

I. INTRODUCTION

The design of controllers for structural systems, particularly those associated with large space structures, has received a considerable amount of attention in the past few years.[1,2,3,4,5] During this time methods for providing structural control for problems ranging from simple flexible beams[6,7] to complex satellite configurations[8,9,10,11] have been reported. These flexible structures are usually required to satisfy not only strength and deflection design criteria, but also stringent pointing and vibrational stability criteria. In addition, the structural frequencies of large structures tend to approach orbital frequencies, possibly leading to instabilities. Therefore, active positioning control and vibration suppression control of these structures appear to be required. For the design of these controllers, in almost all cases, concepts from modern control theory have been applied to a linear model of the original system which in turn was obtained from finite element analysis[12,13,14] or from a truncated modal analysis of the distributed parameter model.[15,16,17]

Inherent in these approaches are questions dealing with how many modes or elements are necessary in order to generate a good model,[17,18] how many sensors and actuators must be used and where should they be located,[19,20,21] and finally what is the effect of truncation on the control design.

An even more important question concerns the effect of the control design on the unmodeled or truncated modes (a phenomenon called

spillover). The excitation of these so-called residual modes has a potentially destabilizing effect on the actual structure. The control forces which are designed using a truncated model to control the modes of the truncated model tend to spill over into the residual modes, which are not included in the control design analysis, thus creating possible instabilities.[6] In addition, implementation of these methods requires the ability to sense the displacement or velocity at some point on the structure and process the signal into components for each mode. These signals in turn are fed back into the appropriate actuators. Hence reasonably sophisticated electronics are required to implement such controller designs. Although considerable advances in the state-of-the-art have been made these past few years and, most likely, these techniques will be used to design structural controllers of the future, one should be willing to explore alternative approaches to structural control, especially if they are significantly different, in order to extract any additional information which may be revealed about the subject.

The purpose of this work is to offer an alternative approach to the problem of designing controllers for systems governed by partial and ordinary differential equations. The technique is based on the classical concept of transfer functions which relate the output or response of a system to the input. For simple structures, the displacement (velocity, or slope) at one point can be related to the force applied at another point by an exact transfer function. The accuracy of the transfer function is limited only by the accuracy of the mathematical model used to describe the structure. This open-loop

transfer function can be used to construct the closed-loop transfer function for the case where the displacement (velocity, or slope) is fed back to the force. By examining the characteristic equation of the closed-loop transfer function the stability of the closed-loop system can be analyzed in detail. The price you pay for this exactness is the amount of algebra that is needed to obtain the final result.

In the chapters which follow, this method will be applied in some detail to a flexible cable under tension and to a flexible beam. These structural members could also be considered to be elements of a larger, more complex flexible structure. The approach taken is to develop the transfer function for a cable or beam element and to use this fundamental element to obtain the open-loop transfer functions for several sensor and actuator locations.

Utilizing the Laplace transform nature of the solution for certain structural elements, more complex structures can be considered and modeled through the use of dynamic stiffness influence coefficients. The procedure is similar to the dynamic stiffness matrix analysis used for structures,[22,23] but is carried out here in the domain of the Laplace transform. Workability of the dynamic stiffness influence coefficients in the Laplace transform plane, for the solution of flexural forced vibration problems, has been demonstrated by Beskos and Boley.[24]

Chapter Two is concerned with the vibrating cable. The Laplace transform technique will be used to obtain the open-loop transfer functions for cables with various boundary conditions. A basic cable element will then be developed and the dynamic stiffness matrix method applied to examples of varied sensor-actuator configurations.

The dynamics, stability and control for the cable will be investigated in Chapter Three. Typical sensor-actuator pairs of interest will be examined with appropriate root-loci indicating the behavior of the system with various feedback gains. Selected single-input-single-output (SISO) systems and multi-input-multi-output (MIMO) systems will be investigated.

Chapter Four is devoted to the development of various transfer functions for the cantilever beam.

Stability and control of the cantilever beam is addressed in Chapter Five.

Chapter Six discusses the development of free-free beam transfer functions, along with stability analysis and feedback control.

In Chapter Seven the dynamic stiffness matrix is developed for the beam element and a structure is created and modeled using the dynamic stiffness matrix approach.

Results, conclusions and recommendations for future research are contained in Chapter Eight. The developments presented, coupling the Laplace transform and the dynamic stiffness approach with classical feedback analysis is unique with this work. Furthermore, little or no work has previously been done using multi-input-multi-output control with transcendental transfer function matrices. The work done here opens the door to an area of research which commands considerable attention. It is intended that this investigation will offer alternative approaches to the analysis of feedback control of systems governed by ordinary and partial differential equations, and provide a stimulus for future research.

II. FLEXIBLE CABLE

The first structural member to be investigated is a vibrating cable. From the governing partial differential equation for the cable, several transfer function relationships will be developed. The concept of a generic cable element dynamic stiffness matrix will be explored. This cable element stiffness matrix will then be used to generate transfer functions for more complex actuator-sensor configurations along the cable. It will also be shown that any specific cable boundary conditions and control configuration can be obtained by simple construction from the cable element dynamic stiffness matrix.

The vibrating cable is considered to be a continuous or distributed parameter system, that is one governed by a partial differential equation. As shown in Figure 1a, $f(x,t)$, $\rho(x)$, and $T(x)$ are the distributed force, mass density, and tension in the cable, respectively, expressed as a function of position, x along the cable. For this analysis, negligible structural damping and no transverse stiffness is assumed. The inclusion of damping would not affect the procedure to be described at all. It is only omitted to simplify the results. As demonstrated in previous work,[25] damping improves the overall stability of the system without changing the relative character of the results.

The equation of motion describing the transverse motion of the cable can be obtained by examining a differential element of the cable. Figure 1b represents the free body diagram corresponding to a differential element of cable of length dx. Applying Newton's second law

in the vertical direction, assuming small deflections, only vertical motion and ignoring second-order terms in dx, we find that the governing partial differential equation of motion of the cable is given by[26]

$$\frac{\partial}{\partial x}\left[T(x)\,\frac{\partial y(x,t)}{\partial x}\right] + f(x,t) = \rho(x)\,\frac{\partial^2 y(x,t)}{\partial t^2}\,, \quad 0 \le x \le L \qquad (2\text{-}1)$$

While Eq. (2-1) is the general equation of motion of the cable, it can be simplified by certain appropriate assumptions. In addition, any solution of Eq. (2-1) will depend on the particular boundary conditions of the cable configuration under consideration. In this chapter, several configurations are considered.

Fixed-free cable with a discrete mass at end

The first configuration to be investigated is a cable of length L with constant mass per unit length, ρ, subjected to a constant tension T. This cable is fixed at one end, while the other end is free with a concentrated mass attached. A control force is acting vertically on the mass at the free end. Furthermore, there is no distributed force f(x,t) acting along the cable, (see Figure 2a). For this particular problem Eq. (2-1) reduces to

$$\rho\,\frac{\partial^2 y(x,t)}{\partial t^2} = T\,\frac{\partial^2 y(x,t)}{\partial x^2}\,, \qquad 0 \le x \le L \qquad (2\text{-}2)$$

with the associated boundary condition at the fixed end x = 0,

$$y(0,t) = 0 \qquad (2\text{-}3)$$

By writing Newton's second law for the free end, shown in Figure 2b, the boundary condition for the free end x = L becomes,

$$f_L - T \left.\frac{\partial y(x,t)}{\partial x}\right|_{x=L} = m \left.\frac{\partial^2 y(x,t)}{\partial t^2}\right|_{x=L} \tag{2-4}$$

Eq. (2-2) can now be solved for the lateral deflection $y(x,t)$. However, rather than obtain the solution, we seek the relationship between the displacement at one point (output) due to a force at another (or the same) point (input), in this case that of the mass. The Laplace transform of this output over input ratio is known as a transfer function and relates the output to the input. Hence the solution of Eq. (2-2) will be obtained by making use of the Laplace transform. This method of solution also admits any type of excitation or control force, harmonic as well as non-periodic.[26] In order to generate unique transfer functions using the Laplace transform method, it is assumed that the initial conditions of displacement and velocity are zero.

$$y(x,t) = \dot{y}(x,t) = 0 \tag{2-5}$$

The Laplace transform with respect to time of Eq. (2-2) is

$$\rho s^2 y(x,s) = T \frac{d^2 y(x,s)}{dx^2} \quad , \qquad 0 \leq x \leq L \tag{2-6}$$

where s is the Laplace transform variable. The transformed boundary conditions are

$$y(0,s) = 0 \tag{2-7a}$$

and

$$f_L - T \left.\frac{dy(x,s)}{dx}\right|_{x=L} = ms^2 y(L,s) \tag{2-7b}$$

Rearranging Eq. (2-6) yields,

$$\frac{d^2y(x,s)}{dx^2} - \frac{\rho}{T} s^2 y(x,s) = 0 \tag{2-8}$$

The solution to Eq. (2-8) is

$$y(x,s) = A \sinh \sqrt{\rho/T}\, sx + B \cosh \sqrt{\rho/T}\, sx \tag{2-9}$$

where constants A and B are determined from the boundary conditions, Eq. (2-7). The transfer function $G_{xL}(s)$ relating the general displacement response to a force on the mass at the end of the fixed-free cable is found to be

$$\frac{y(x,s)}{f_L(s)} = G_{xL}(s) = \frac{\sinh\sqrt{\rho/T}\, sx}{s(\sqrt{\rho T}\cosh\sqrt{\rho/T}\, sL + ms \sinh\sqrt{\rho/T}\, sL)} \tag{2-10}$$

where the first subscript (x) is the location of the response and the second subscript (L) is the location of the force. By taking the derivative with respect to x we have the transfer function relating the general slope response to a force on a mass at the end of the cable

$$\frac{y'(x,s)}{f_L} = \frac{\sqrt{\rho/T}\cosh\sqrt{\rho/T}\, sx}{\sqrt{\rho T}\cosh\sqrt{\rho/T}\, sL + ms \sinh\sqrt{\rho/T}\, sL} \tag{2-11}$$

Looking at the special case of the response at the free end due to a force on a mass at the free end of the cable yields the transfer functions:

for displacement,

$$\frac{y(L,s)}{f_L} = \frac{\sinh\sqrt{\rho/T}\, sL}{s(\sqrt{\rho T}\cosh\sqrt{\rho/T}\, sL + ms \sinh\sqrt{\rho/T}\, sL)} \tag{2-12}$$

and similarly for slope,

$$\frac{y'(L,s)}{f_L} = \frac{\sqrt{\rho/T}\cosh\sqrt{\rho/T}\, sL}{\sqrt{\rho T}\cosh\sqrt{\rho/T}\, sL + ms \sinh\sqrt{\rho/T}\, sL} \tag{2-13}$$

The velocity-force transfer function is obtained by taking the derivative of y(L,s) with respect to time. In the s domain this is done by multiplying by the transfer variable s.

$$\dot{y}(L,s) = s\, y(L,s) \tag{2-14}$$

or specifically

$$\frac{\dot{y}(L,s)}{f_L} = \frac{\sinh\sqrt{\rho/T}\, sL}{\sqrt{\rho T}\cosh\sqrt{\rho/T}\, sL + ms \sinh\sqrt{\rho/T}\, sL} \tag{2-15}$$

Free-free cable, discrete masses on both ends

In this case we will examine a constant mass density cable that is free at both ends, subjected to a constant tension, with concentrated masses at both boundaries. Control forces are applied vertically at both ends of the cable (see Figure 3a). The governing partial differential equation is again given by Eq. (2-2). The boundary conditions at both ends are found by applying Newton's second law to the free bodies at each end of the cable (see Figure 3b). The boundary conditions are, at x=0

$$f_1 + T \left.\frac{\partial y(x,t)}{\partial x}\right|_{x=0} = m_1 \left.\frac{\partial^2 y(x,t)}{\partial t^2}\right|_{x=0} \tag{2-16a}$$

and at x=L

$$f_2 - T \left.\frac{\partial y(x,t)}{\partial x}\right|_{x=L} = m_2 \left.\frac{\partial^2 y(x,t)}{\partial t^2}\right|_{x=L} \tag{2-16b}$$

Again transfer function relationships are desired so the Laplace transform method will be applied. Taking the Laplace transform of Eqs. (2-2) and (2-16) with respect to time, assuming initial conditions of Eq. (2-5),

we obtain a solution of the form of Eq. (2-9). Enforcing the boundary conditions yields the desired result. Letting

$$\Delta = s(m_1\sqrt{\rho T}\cosh\sqrt{\rho/T}\,sL + \rho T\sinh\sqrt{\rho/T}\,sL + m_1m_2\,s^2\sinh\sqrt{\rho/T}\,sL + m_2\,s\sqrt{\rho/T}\cosh\sqrt{\rho/T}\,sL)\,, \tag{2-17}$$

then the displacement reponse in the s domain is

$$y(x,s) = \{[-\sqrt{\rho T}\sinh\sqrt{\rho/T}\,sL - m_2 s\cosh\sqrt{\rho/T}\,sL]\sinh\sqrt{\rho/T}\,sx + \frac{[\sqrt{\rho T}\cosh\sqrt{\rho/T}\,sL + m_2 s\sinh\sqrt{\rho/T}\,sL]\cosh\sqrt{\rho/T}\,sx\}}{\Delta}[f_1] + \frac{\{m_1 s\sinh\sqrt{\rho/T}\,sx + \sqrt{\rho T}\cosh\sqrt{\rho/T}\,sx\}}{\Delta}[f_2] \tag{2-18}$$

Eq. (2-18) now gives an algebraic expression relating the displacement of any point on the cable to the vertical control forces at either end. Notice that this free-free cable is a very simple case of an unrestrained continuous and discrete parameter system. Several cases of interest can be reduced from Eq. (2-18). One such case is that of the free-free cable without the discrete masses on the ends. This free-free cable can be thought of as a basic element which can be used to construct more complex structural configurations. This construction method, known as the dynamic stiffness matrix method, will be carried out here in the Laplace domain.

Cable configurations having various boundary conditions and control force configurations can be constructed from the dynamic stiffness matrix of the free-free cable element. The analysis of these more complex configurations tends to be cumbersome when directly applying the Laplace transform method used above. The dynamic stiffness method

uses exact continuous elements rather than approximate or discrete elements as in the case of the finite element method. Therefore, it gives the exact solution of the dynamic problem, within the limits of the original mathematical model. This method also does not require knowledge of the natural frequencies and mode shapes for the computation of the response as in the case of the finite element method in conjunction with modal analysis.[24]

Dynamic stiffness matrix for the cable element

The dynamic stiffness influence coefficients d_{ij} which make up the dynamic stiffness matrix in the Laplace transform plane are expressions that are a function of s and describe the generalized boundary forces of a structural element in terms of the generalized boundary displacements. In this case the dynamic stiffness matrix for a cable element can be developed starting with Eq. (2-18). Assuming the discrete masses equal to zero and evaluating the displacement of the cable only at the ends yields a matrix equation of the form

$$\bar{y}(x) = G(s)\ \bar{f}(s) \tag{2-19}$$

where

$$\bar{y}^{T}(s) = (y(0,s),y(L,s))$$

and

$$\bar{f}^{T}(s) = (f_1,f_2)$$

and G(s) is the open-loop transfer function matrix of the free-free cable. Solving Eq. (2-19) for the force in terms of the displacement yields

$$\bar{f}(s) = G^{-1}(s)\,\bar{y}(s) \tag{2-20}$$

or

$$\bar{f}(s) = D(s)\,\bar{y}(s) \tag{2-21}$$

where D(s) the dynamic stiffness matrix for the free-free cable element is found to be

$$D(s) = \frac{1}{\sinh\sqrt{\rho/T}\,sL}\begin{bmatrix} s\sqrt{\rho T}\cosh\sqrt{\rho/T}\,sL & -s\sqrt{\rho T} \\ -s\sqrt{\rho T} & s\sqrt{\rho T}\cosh\sqrt{\rho/T}\,sL \end{bmatrix} \tag{2-22}$$

Having obtained the dynamic stiffness matrix in the Laplace domain, a powerful tool is now available for constructing other cable configurations.

To demonstrate the construction of other cable configurations by the dynamic stiffness method, the following examples will be developed:

Example 1 is a fixed-free cable with a force at the free end;

Example 2 is a fixed-free cable with a force at the end and at an arbitrary interior point;

Example 3 is a fixed-free cable with three forces including one at the free end;

Example 4 is a free-free cable with three forces, including one at each end.

Example 1. Fixed-free cable, force at free end

The development starts with the dynamic stiffness matrix given by Eq. (2-22). Because the cable is fixed at x=0, we assume $f_1(s)$ in Eq. (2-21) sufficient to hold $y_1(s) = 0$, and can therefore delete the first row and column of the stiffness matrix of Eq. (2-22), yielding

$$f_2(s) = \frac{s\sqrt{\rho T}\cosh\sqrt{\rho/T}\,sL}{\sinh\sqrt{\rho/T}\,sL}\,y_2(s) \tag{2-23}$$

Solving Eq. (2-23) for $y_2(s)$ yields

$$y_2(s) = \frac{\sinh\sqrt{\rho/T}\,sL}{s\sqrt{\rho T}\cosh\sqrt{\rho/T}\,sL}\,f_2(s) \tag{2-24}$$

We can see by comparing Eq. (2-24) with Eq. (2-10) that they are identical, if the discrete mass in Eq. (2-10) is set equal to zero, thus validating the dynamic stiffness method for this case.

Example 2. Fixed-free cable with force at end and an arbitrary point

The basic dynamic stiffness matrix for the cable element, Eq. (2-22) can be expressed symbolically in Eq. (2-21) as

$$\begin{Bmatrix} f_1(s) \\ f_2(s) \end{Bmatrix} = \begin{bmatrix} d_{11} & d_{12} \\ d_{21} & d_{22} \end{bmatrix} \begin{Bmatrix} y_1(s) \\ y_2(s) \end{Bmatrix} \tag{2-25}$$

By joining two cable elements (see Figure 4), it can be shown that we can match displacement boundary conditions to obtain

$$\begin{Bmatrix} f_0 \\ f_1 \\ f_2 \end{Bmatrix} = \begin{bmatrix} d_{11a} & d_{12a} & 0 \\ d_{21a} & d_{22a} + d_{11b} & d_{12b} \\ 0 & d_{21b} & d_{22b} \end{bmatrix} \begin{Bmatrix} y_0 \\ y_1 \\ y_2 \end{Bmatrix} \tag{2-26}$$

where the extra subscript indicates to which cable segments, a or b the coefficient refers. The cable segment, a is fixed at x=0 and therefore can assume f_0 sufficient to hold $y_0 = 0$. This allows us to delete the first row and column of the dynamic stiffness matrix of Eq. (2-26), yielding

$$\begin{Bmatrix} f_1 \\ f_2 \end{Bmatrix} = \begin{bmatrix} d_{22a} + d_{11b} & d_{12b} \\ d_{21b} & d_{22b} \end{bmatrix} \begin{Bmatrix} y_1 \\ y_2 \end{Bmatrix} . \tag{2-27}$$

Solving Eq. (2-27) for $\bar{y}$ in terms of $\bar{f}$ yields the transfer function matrix equation

$$\begin{Bmatrix} y_1(s) \\ y_2(s) \end{Bmatrix} = \frac{1}{s\sqrt{\rho T}\,\cosh\sqrt{\rho/T}\,sL} \begin{bmatrix} \sinh\sqrt{\rho/T}\,sx \cdot \cosh\sqrt{\rho/T}\,s(L-x) & \sinh\sqrt{\rho/T}\,sx \\ \sinh\sqrt{\rho/T}\,sx & \sinh\sqrt{\rho/T}\,sL \end{bmatrix} \begin{Bmatrix} f_1 \\ f_2 \end{Bmatrix} \tag{2-28}$$

This is an exact relationship of the displacement at an arbitrary point, (1) and the end, (2) with forces at the point and the end of the fixed-free cable. Note that it is important when constructing the elements of the dynamic stiffness matrix that the length L of the element of the stiffness matrix Eq. (2-22) be replaced with the length of the cable segment for which the matrix is being applied, e.g. here d_{22a} contains the length x and d_{22b} contains the length (L-x) in place of the L in d_{22} of Eq. (2-22).

It is now evident that we can, in theory, piece together many cable segments with many control forces using the dynamic stiffness method. The basic cable element relationship Eq. (2-22) can be repeatedly applied for any number of forces acting on the cable by considering the cable between any two forces or displacements as a basic cable element and superimposing them for each element of the cable. To reduce the complexity of the terms in Eq. (2-22) we will, for future convenience, select the length of the cable as unity and set $\rho = T = 1$.

Eq. (2-21) with Eq. (2-22) can now be written as

$$\begin{Bmatrix} f_1(s) \\ f_2(s) \end{Bmatrix} = \frac{s}{\sinh s\ell} \begin{bmatrix} \cosh s\ell & -1 \\ -1 & \cosh s\ell \end{bmatrix} \begin{Bmatrix} y_1(s) \\ y_2(s) \end{Bmatrix} \tag{2-29}$$

Example 3. The fixed-free cable, three forces including one at the free end.

The cable shown in Figure 5 can be described by

$$\bar{f}(s) = D(s)\, \bar{y}(s) \tag{2-21}$$

where

$$\bar{f}^T(s) = (f_0, f_1, f_2, f_3)$$

and

$$\bar{y}^T(s) = (y_0, y_1, y_2, y_3)$$

and the dynamic stiffness matrix, D(s) obtained from repeated superposition of Eq. (2-29) is given by

$$D(s) = s \begin{bmatrix} \frac{\cosh xs}{\sinh xs} & \frac{-1}{\sinh xs} & 0 & 0 \\ \frac{-1}{\sinh xs} & \frac{\cosh xs}{\sinh xs} + \frac{\cosh(z-x)s}{\sinh(z-x)s} & \frac{-1}{\sinh(z-x)s} & 0 \\ 0 & \frac{-1}{\sinh(z-x)s} & \frac{\cosh(z-x)s}{\sinh(z-x)s} + \frac{\cosh(\ell-z)s}{\sinh(\ell-z)s} & \frac{-1}{\sinh(\ell-z)s} \\ 0 & 0 & \frac{-1}{\sinh(\ell-z)s} & \frac{\cosh(\ell-z)s}{\sinh(\ell-z)s} \end{bmatrix} \tag{2-30}$$

where x and z are the locations of f_1 and f_2 measured from f_0. Again if we assume that f_0 is sufficient to hold $y_0 = 0$, the first row and column of the matrix in Eq. (2-30) can be neglected and the remaining matrix

inverted to obtain the transfer function matrix. The result has the form

$$\bar{y}(s) = G(s)\ \bar{f}(s) \tag{2-19}$$

where

$$\bar{y}^T(s) = (y_1, y_2, y_3)$$

and

$$\bar{f}^T(s) = (f_1, f_2, f_3)$$

and the transfer function matrix becomes[27]

$$G(s) = \frac{1}{s\ \cosh s} \begin{bmatrix} \sinh xs \cdot \cosh(1-x)s & \sinh xs \cdot \cosh(1-z)s & \sinh xs \\ \sinh xs \cdot \cosh(1-z)s & \cosh(1-z)s \cdot \sinh zs & \sinh zs \\ \sinh xs & \sinh zs & \sinh s \end{bmatrix} \tag{2-31}$$

Example 4. The free-free cable, three forces, including one at each end.

This is an interesting case which has all the ingredients of a satellite problem (i.e. rigid body motion as well as structural vibration). Here the cable is under constant tension and free to translate (see Figure 6). The transfer function matrix for this case can be obtained by using the procedures outlined above. The result is given by

$$\bar{y}(s) = G(s)\ \bar{f}(s) \tag{2-19}$$

where

$$\bar{y}^T = (y_0, y_1, y_2)$$

and

$$\bar{f}^T = (f_0, f_1, f_2)$$

and

$$G(s) = \frac{1}{s \sinh s} \begin{bmatrix} \cosh s & \cosh(1-x)s & 1 \\ \cosh(1-x)s & \cosh xs \cosh(1-x)s & \cosh xs \\ 1 & \cosh xs & \cosh s \end{bmatrix} \qquad (2\text{-}32)$$

Note that by letting $f_1 = 0$ and ignoring y_1, we can delete the second row and column of the above matrix. This yields Eq. (2-18) (with appropriate change of nomenclature) with $m_1 = m_2 = 0$, for the special cases of $x = 0$ and $x = L$.

In this chapter we have seen the development of force-deflection and force-velocity relationships for several cases of flexible cable configurations. We have also illustrated the dynamic stiffness matrix approach for generating various cable element-control force configurations and have obtained the transfer functions for several examples. Having done this let us now turn our attention to the system dynamics and stability of the vibrating cable, and the characteristics of vibration suppression control via closed-loop feedback using root locus analysis.

III. FLEXIBLE CABLE--STABILITY AND CONTROL

When one looks at the question of the stability and control design for a dynamical system many avenues of approach can be taken. The method chosen for this examination is the classical root-locus analysis technique.

In Chapter Two we developed transfer function matrices relating the displacements and forces at a finite number of points along the cable. These are exact transfer functions for the system governed by Eq. (2-1). The system natural frequencies can be obtained by setting the denominator of each transfer function equal to zero and solving for s, where $s = n + i\omega$. It is easily verified that the solution of $\cosh s = 0$ from Eq. (2-24) will yield imaginary values of s corresponding to the frequencies associated with a fixed-free cable. In addition $\sinh s = 0$ (the free-free cable characteristic equation) yields the frequencies associated with a free-free cable including $\omega = 0$ corresponding to the rigid body motion (in this case pure translation).

The transfer functions associated with cable velocity at specified points can be easily obtained from those developed in Chapter Two for the displacement, by simply multiplying through by s, the derivative operator in the Laplace plane. By taking the derivative of G(s) with respect to x, the position of some generic point on the cable, transfer functions relating the cable slope and the force can be determined.

Feedback control

Consider a system with inputs f_i, i = 1,2,...,m and outputs y_j, j = 1,2,...,r. Associated with this system is an r x m transfer function matrix G(s). One could sense all the outputs and in turn feed those back with some gain to all the inputs, requiring a m x r feedback matrix K. A block diagram of the system is shown in Figure 7. The closed-loop transfer function matrix can be shown to be (for $\bar{u}$ the same dimension as $\bar{f}$)

$$G(s)_{CL} = [I_r + G(s)K]^{-1} G(s) \tag{3-1}$$

where I_r is an r x r identity matrix. The closed-loop system dynamics can be determined from the closed-loop characteristic equation

$$|I_r + G(s)K| = 0 \tag{3-2}$$

For the case of a single force and a single displacement, i.e., a single-input-single-output-system (SISO), all the classic tools for control design can be utilized.[28] Again it should be emphasized that all results obtained have no assumptions other than those inherent in Eq. (2-2).

The SISO open-loop transfer function for a fixed-free cable which relates the displacements at some arbitrary point, x, to a force at the end of the cable can be obtained from the matrix in Eq. (2-31) by selecting the G(1,3) element:

$$\frac{y(x,s)}{f(1,s)} = \frac{\sinh xs}{s \cosh s} = G(s) \tag{3-3}$$

If $s = n + i\omega$ is substituted into the transfer function, Eq. (3-3), the

open-loop poles and zeros can be determined to be:

$$\begin{aligned} &\text{zeros} \quad n = 0 \quad , \quad \omega = \frac{k_n \pi}{2x} \quad , \quad k_n \text{ even} \\ &\text{poles} \quad n = 0 \quad , \quad \omega = 0 \quad , \quad \omega = \frac{k_d \pi}{2} \quad , \quad k_d \text{ odd} \end{aligned} \tag{3-4}$$

The open-loop pole and zero locations for various sensor positions, x are shown in Figure 8.

The closed-loop transfer function can be obtained from Eq. (3-1) with Eq. (3-3) and is given by

$$G(s)_{CL} = \frac{\text{sinhxs}}{\text{s coshs + K sinhxs}} \tag{3-5}$$

with the associated closed loop characteristic equation, Eq. (3-2) of

$$\text{s coshs + K sinhxs} = 0 \tag{3-6}$$

where K is the feedback gain which we can select.

In order to determine the dynamic characteristics of the closed-loop system we can solve the characteristic equation for various values of K ranging from zero to infinity or we can make use of the rules for constructing a root locus.

For the case of displacement feedback from the end of the cable to a force at the end of the cable, x = 1, the root locus can be predicted from the pole-zero plot of Figure 8. Since poles migrate to zeros for increasing values of K it is suspected that increasing the gain simply changes the frequency of the system but provides no damping. With an infinite gain the frequencies of the closed-loop system approach those of a fixed-fixed cable as would be expected. Furthermore, we would expect that higher gains are necessary to drive the closed-loop poles a

given distance away from the open-loop poles at the higher frequencies. For this particular problem an analytic expression relating the change in frequency to the gain can be developed and is given by

$$(\omega_0 + \Delta\omega) \text{ Tan } \Delta\omega = K \tag{3-7}$$

where ω_0 is the open-loop pole from which the locus starts. Table 1 shows some solutions of Eq. (3-7) for selected frequencies. As can be seen from Table 1, it does in fact require more gain to drive a closed-loop pole a given distance away from an open-loop pole at the higher frequencies.

The solution of the closed-loop characteristic equation, Eq. (3-6) for various values of gain from zero to infinity verifies that displacement feedback for this case changes frequency and provides no damping.

If velocity feedback at the cable end is used instead of displacement feedback, the open-loop transfer function has the form

$$G(s) = \frac{\text{sinhxs}}{\text{coshs}} \tag{3-8}$$

where x = 1, with the associated closed loop characteristic equation

$$\text{coshs} + K \text{ sinhxs} = 0 \tag{3-9}$$

The pole-zero plot of the open-loop transfer function is similar to that in Figure 8 with the exception of the pole-zero cancellation at the origin which is now just a zero. If we let $s = n + i\omega$ we can obtain analytic solutions for the feedback of velocity. The results are given by

$$\text{Tanh } n = -K \quad ; \quad \omega = \frac{m\pi}{2} \quad (m \text{ odd})$$
$$\text{Tanh } n = -\frac{1}{K} \quad ; \quad \omega = \frac{m\pi}{2} \quad (m \text{ even}) \tag{3-10}$$

The root locus plot is shown in Figure 9.

It is seen from the root locus that all the modes are controlled by feeding back the velocity at the end of the cable to a force at the end. Furthermore no special filter is needed to process the sensor signal. For this particular case all modes are affected the same for a given gain. For gains less than one, the frequencies of vibration are the same as the open-loop frequencies but the motion is damped out. For gains greater than one the frequencies jump to those of a fixed-fixed cable and the motion is also damped. At a gain of one, $n = -\infty$ and it can be shown that the system comes to rest in a finite time.[29]

Let us now observe what happens to the zeros of the system when we move the sensor from the end where it is co-located with the force, to some arbitrary point, x. From Figure 8 it can be seen that the zeros of the system move upward on the imaginary axis as the value of x is decreased. Decreasing x corresponds to physically moving the sensor farther away from the force. Furthermore, the zeros farthest away from the origin of the s plane move a greater distance than those closer to the origin for a given sensor position. Hence one can see that the pole-zero-pole pattern which occurs with the sensor at the end, $x = 1$, will be disrupted as x decreases from the value of 1. The alternating pattern will be changed initially at large values of ω. It can easily be shown from Eq. (3-4) that such a change in pattern will

occur for the zero associated with k_n when

$$x = \frac{k_n}{1 + k_n} \tag{3-11}$$

As an example for $k_n = 2$, $x = 0.667$, while for $k_n = 24$, $x = 0.96$. It is significant that these represent node positions which, for these cases, are for the second and thirteenth mode shapes respectively.

It can also be noted that the node of some mode will be crossed when moving a sensor any distance away from the end. When the sensor is located just beyond the node of a particular mode, the displacement and velocity of this location are opposite those of the end where the force is located. Therefore, feeding back information sensed at this location to the force at the end is detrimental to control of this mode.

Root-loci for both displacement and velocity feedback from a sensor located away from the end can be generated from the solution of Eqs. (3-6) and (3-9), respectively.

The generation of root-loci analytically is, in general, not practical. Consequently, a computer routine will be employed. Most computer routines that generate root-loci need to be supplied with polynomial functions or factors.[30] In this work the solution of a transcendental equation is required. One method of solution, for the generation of the root loci, is the use of a computer routine which includes an IMSL routine called ZSCNT[31] which solves for the roots of a set of non-linear simultaneous equations, the complex characteristic equation, Eq. (3-2) being one of these sets when separated into real and imaginary equations. The procedure is to apply repeatedly the ZSCNT routine starting with the open-loop pole position with zero gain

as the first guess. Then, incrementing the gain, solve for the first closed-loop pole position. This pole is then used as the guess for solving for the pole at the next gain value and so on. This method is found to be highly reliable for calculating root-loci, although occasionally sensitive to abrupt changes in locus direction.

Using this computer routine, the cases where a sensor is located at either $x = 0.667$ or $x = 0.50$ are examined and the root-loci constructed for both the displacement and velocity feedback situations. The results are presented in Figures 10 and 11. As seen from Figure 8, both of these cases have a repeated pattern open-loop pole-zero distribution along the imaginary axis. The case where $x = 0.667$ represents a displacement or a velocity feedback from the node of the second, fifth, etc., modes, and shows up as a pole-zero cancellation for those modes. At $x = 0.50$ on the other hand, there is no node at that point for any mode (similar to the point at the end of the cable), but two poles associated with the first two modes are no longer separated by a zero.

By examining Figures 10 and 11 we can make the following observations: 1) As far as the root locus is concerned, if an open-loop pole-zero cancellation occurs, two open-loop poles appear adjacent to each other on the imaginary axis, 2) If two open-loop poles appear adjacent to each other because of the sensor location, an instability will occur for either displacement or velocity feedback. With these observations in mind we can return to Eq. (3-11). Here, for example, we see that a sensor at $x = 0.96$ will cause a pole-zero cancellation for $k_n = 24$ or for the thirteenth mode. Up to that point on the imaginary axis there is an alternating pole-zero pattern on the imaginary axis. We expect

that velocity feedback from that sensor location to the force at the end of the cable would provide damping up through the thirteenth mode but would cause instabilities for selected higher modes.

The cases for velocity and displacement feedback for a sensor located at x = 0.9 are shown in Figure 12 . Here we see that displacement feedback does indeed simply change the frequencies of the modes except where the two poles appear adjacent where gains above a certain value cause an instability. For velocity feedback from the same point (x = 0.9) it is seen that the lower modes are damped while the modes immediately above the two poles which appear adjacent are unstable for all gains.

The cases where open-loop pole-zero cancellations take place on the imaginary axis, such as when x = 0.4, 0.667, 0.80 (see Figure 8), correspond to the placement of the sensor at the node of the mode shape associated with the pole cancelled. Consequently this mode is uncontrolled and continues to oscillate unattenuated. As might be expected, a sensor at the node of a mode cannot transmit any information about that mode.

It has been shown that velocity feedback to a co-located actuator is always stabilizing.[7,32] This case can be examined here by obtaining the transfer function relating the velocity output at some arbitrary point x to the input at the same point. From Eq. (2-31) this transfer function is equivalent to $s \cdot G(1,1)$ or

$$G(s) = \frac{\sinh xs \cdot \cosh(1-x)s}{\cosh s} = \left.\frac{\dot{y}(s)}{f(s)}\right|_x \qquad (3\text{-}12)$$

The open-loop pole-zero plots for Eq. (3-12) for various values of x are shown in Figure 13. Here we see the alternate pole-zero pattern is retained for all values of x. Furthermore, where pole-zero cancellations occur (at nodes) there is a second zero to retain the apparent alternating pattern, hence damping is assured for all co-located actuator and sensor locations. The modes which have nodes where the sensor and actuator are located are uncontrolled as indicated previously.

Closing the loop by applying Eq. (3-1) to Eq. (3-12) the characteristic equation, Eq. (3-2), can be solved on the computer as previously indicated.

The root-loci for the case where $x = 0.667$ and $x = 0.9$ are presented in Figure 14. Here the expected results have been verified. As can be seen, the effectiveness of the controller on a given mode depends upon how far the sensor is from a node of that mode as might be expected.

Multivariable feedback

In the previous section we saw how one actuator could control all the modes of motion. It might be expected however that a better job could be done with more than one sensor and actuator. Here we will examine two cases for the fixed-free cable. Velocity and displacement at one point fed back into one actuator at the same point and velocity at two points fed back into an actuator at each point. We will then examine two cases for the free-free cable. Velocity and displacement fed back to an actuator at one end and velocity and displacement fed back to actuators at both ends.

Case 1. Velocity and displacement fed back to one force at the end of the fixed-free cable.

The transfer function for this case is given by

$$\begin{Bmatrix} y_1(s) \\ \dot{y}_1(s) \end{Bmatrix} = \begin{bmatrix} \frac{\sinh s}{s \cosh s} \\ \frac{\sinh s}{\cosh s} \end{bmatrix} f_1 = \begin{bmatrix} g_{11} \\ g_{21} \end{bmatrix} f_1 \tag{3-13}$$

If the feedback control takes the form,

$$f_1 = -[K_{11} \quad K_{12}] \begin{bmatrix} y_1 \\ \dot{y}_1 \end{bmatrix} , \tag{3-14}$$

the term in brackets from Eq. (3-1) has the form

$$I_r + G(s)K = \begin{bmatrix} 1 + g_{11} K_{11} & g_{11} K_{12} \\ g_{21} K_{11} & 1 + g_{21} K_{12} \end{bmatrix} \tag{3-15}$$

and the characteristic equation, Eq. (3-2) becomes

$$1 + g_{21} K_{12} + g_{11} K_{11} = 0 \tag{3-16}$$

or

$$s \cosh s + (K_{11} + s K_{12}) \sinh s = 0 \tag{3-17}$$

Eq. (3-17) is the multivariable feedback closed-loop characteristic equation for which a two gain root locus can be constructed.

Before we proceed, however, a definition of the zeros of a MIMO system is needed. The term "zeros of G(s)" has sometimes been used for the individual entries of G(s).[33] Although a broader definition has been given for polynomial functions,[33] the definition proposed here is

a simple and useful one. A system zero will be defined as "any root of any term or group of terms which is a coefficient of a specific feedback gain or group of cross gains in the closed-loop characteristic equation." The purpose of this definition is to illuminate where the closed-loop poles will tend to go when the feedback gains are very high. This definition will be used when referring to the system zeros of the MIMO systems to follow.

From Eq. (3-17), it can be seen that the open-loop pole locations (i.e., $K_{11} = K_{12} = 0$) are the same as for the case of only displacement feedback, as would be expected since the open-loop pole locations are dependent on boundary conditions. The system zeros, by the definition given previously, are also found to be the same as the individual velocity and displacement open-loop transfer function zeros, an expected result since the zeros depend on sensor location.

A two gain root locus will now be generated from the solution of Eq. (3-17). Obviously with a two gain root locus there are many choices of how to increment the feedback gains. Two approaches are investigated here. The first is while maintaining constant velocity gain, the displacement gain is increased. The second is while maintaining constant displacement gain, the velocity gain is increased. For the first approach, three values of constant velocity gain will be used. They are $K_v = 0.7617$ which yields $n = -1$ for ω equal to the frequencies of the open-loop poles, $K_v = 0.964$ which yields $n = -2$ for ω equal to the frequencies of the open-loop poles, and $K_v = 1.04$ which yields $n = -2$ for ω equal to the frequencies of the system zeros. For each of these constant velocity gains the displacement gain is incremented from

K_D = 0 to 25. The second approach is with constant displacement gains, K_D = 0.2, 0.5 and 3.5, and incrementing the velocity gain from K_V = 0 to 25. Both of these approaches generate a family of root-loci, shown in Figure 15. As can be seen from Figure 15, if both velocity and displacement feedback are used the damping is limited. Increasing the displacement gain drives the system back toward the imaginary axis (i.e., no damping, just oscillation at a higher frequency). Increasing the velocity gain with a small amount of displacement feedback generates some damping, but the amount of available damping decreases with increasing displacement gain. Even the slightest amount of displacement feedback causes the amount of damping to be limited. With no displacement feedback we saw in Figure 9 that there was no limit to the amount of damping. This situation corresponds to a pole located equidistant from two zeros. With some displacement feedback the closed-loop poles are moved closer to the zero above it and we now see from Figure 15 that the closer the closed-loop pole is to the zero initially the smaller the amount of damping that can be generated from velocity feedback. This result indicates that there is no advantage in using both velocity and displacement feedback for the fixed-free cable unless a change of frequency is desired.

Case 2 - Velocity feedback from an arbitrary point and the end to actuators at the arbitrary point and the end.

The transfer function matrix for this case can be obtained from Eq. (2-31) as

$$\begin{Bmatrix} \dot{y}_1(s) \\ \dot{y}_2(s) \end{Bmatrix} = \frac{1}{\cosh s} \begin{bmatrix} \sinh xs \cdot \cosh(1-x)s & \sinh xs \\ \sinh xs & \sinh s \end{bmatrix} \begin{Bmatrix} f_1 \\ f_2 \end{Bmatrix} \tag{3-18}$$

If the feedback control is given by

$$\begin{Bmatrix} f_1 \\ f_2 \end{Bmatrix} = -\begin{bmatrix} K_{11} & K_{12} \\ K_{21} & K_{22} \end{bmatrix} \begin{Bmatrix} \dot{y}_1 \\ \dot{y}_2 \end{Bmatrix} \tag{3-19}$$

the term in brackets from Eq. (3-1) has the form

$$I_r + G(s)K = \begin{bmatrix} 1 + g_{11}K_{11} + g_{12}K_{21} & g_{11}K_{12} + g_{12}K_{22} \\ g_{21}K_{11} + g_{22}K_{21} & 1 + g_{21}K_{12} + g_{22}K_{22} \end{bmatrix} \tag{3-20}$$

We could now follow the procedure used in case one, that is, simply extending the SISO controller to a MIMO control system directly. For most systems, the extension of SISO design methods to MIMO systems is not advisable,[34] the difficulty being the need, in general, to design all the entries in the gain matrix, K, simultaneously. A properly designed K matrix assures that the interactive effects of the MIMO system will contribute to stability rather than instability. It was found for SISO feedback for the cable that feeding back velocity and displacement to other than co-located actuators can lead to system instabilities. For this reason (although at this stage possibly an invalid reason), we suspect that for the MIMO system this interactive effect would continue to be a destabilizing influence. The problem which could arise by the elimination of this cross-gain feedback interaction is that the system could become unstable when high values of gain are applied in both feedback loops. A high value of gain in either loop alone usually can be tolerated.[34] Since there are

limitless combinations of the values for the elements of a fully populated K matrix, initially the system stability will be analyzed without cross-gains. Some selected cross-gain cases will then be discussed.

The characteristic equation associated with Eq. (3-20) is given by

$$1 + g_{11}K_{11} + g_{22}K_{22} + g_{12}K_{21} + g_{21}K_{12} + (g_{12}g_{21} - g_{11}g_{22})K_{12}K_{21} + (g_{11}g_{22} - g_{21}g_{12})K_{11}K_{22} = 0 \qquad (3\text{-}21)$$

Eliminating cross-gains, $K_{12} = K_{21} = 0$, Eq. (3-21) becomes

$$1 + g_{11}K_{11} + g_{22}K_{22} + (g_{11}g_{22} - g_{21}g_{12})K_{11}K_{22} = 0 \ . \qquad (3\text{-}22)$$

With appropriate substitutions, the above equation is the closed-loop characteristic equation for the system described by the open-loop transfer function matrix in Eq. (3-18). Eq. (3-22) can be used to generate a two gain root-locus.

It is clear from Eq. (3-22) that even though we are feeding back the velocities only to the co-located forces, there still is some interaction between the two points. It cannot be determined without analyzing Eq. (3-22) if this interaction is favorable or not. An important point to be noted, however, is that the interaction of co-located sensor-actuator pairs is more complex than just a simple superposition of individual contributions.

Proceeding with the analysis, substituting in appropriate values from Eq. (3-18) into Eq. (3-22) yields the closed-loop characteristic equation

$$\cosh s + (\sinh xs \cdot \cosh(1-x)s)K_{11} + \sinh s\, K_{22} + [(\sinh xs \cdot \cosh(1-x)s)\sinh s - \sinh^2 xs]K_{11}K_{22} = 0 \qquad (3\text{-}23)$$

In this case the open-loop poles are still the same as the previous case. The system zeros in this case correspond to the zeros of a SISO system with a sensor at the end, and the zeros of a SISO system with a sensor at some specific location x. There are also additional zeros from the interactive term (the last term). For solution of Eq. (3-23) three approaches are taken for each of two cases. The first case is velocity feedback from sensors at x = 0.67 and the end to co-located forces. The second case is velocity feedback from sensors at x = 0.5 and the end to co-located forces. The second case was selected since for each location individually SISO velocity feedback provided a means for driving the real parts of the closed-loop poles to negative ∞ for the case of K = 1 and K = 2 for x = 1 and 0.5, respectively.

For each case, first the end gain will be fixed and the gain of the interior point feedback will be increased. Next the interior point feedback will be fixed and the end gain will be increased. Finally both feedback gains will be varied simultaneously. Figure 16 shows the results for co-located sensor actuator pairs at x = 0.67 and the end. For co-located sensor-actuator pairs at x = 0.5 and the end, the general MIMO characteristic equation, Eq. (3-23) reduces to the form

$$\cosh s + \sinh s \left(\frac{K_{11}}{2} + K_{22}\right) + \left(\frac{1}{2}\sinh^2 s - \sinh^2 \frac{s}{2}\right)K_{11}K_{22} = 0 \qquad (3\text{-}24)$$

Figure 17 shows the results for co-located sensor-actuator pairs at x = 0.5 and the end.

As can be seen from the results in Figures 16 and 17, for this case, the addition of another velocity sensor-actuator pair to the system is seen to cause degradation in the performance, (i.e., a reduction of damping rather than an increase in damping) for the fixed-free cable, even for the case (x = 0.5, 1) where individually outstanding damping was obtained. This result seems counter to what would be expected. A possible explanation is that, even though the signal from one sensor is only fed back to its co-located actuator, there is the interaction term seen in both Eqs. (3-23) and (3-24). Also, each force appears as a forced oscillation at the other sensor location. In addition, it can be seen from Figure 14 (individual co-located sensors and actuators) that increasing feedback gain beyond a certain value reduces the amount of damping, the only exceptions being a co-located sensor-actuator at x = 1 or at x = 0.5, so it is seen that more than the slightest amount of feedback from a sensor-actuator pair at a location other than at the end of the fixed-free cable causes degradation of the performance of the boundary control alone. In no case, however, even with both gains very high, does the system become unstable. The elimination of the off-diagonal cross-gain terms has not adversely affected the stability of the system.

System performance might, however, be improved by the inclusion of the cross-gain terms. To examine the effect of cross gains, the same two cases (co-located sensor-actuators at x = 0.67 and 1 and at x = 0.5 and 1) will be investigated using the general characteristic equation, Eq. (3-21). For each case, two procedures will be employed. First, maintaining constant cross-gain values of $K_{12} = K_{21} = 0.5$,

K_{11} and K_{22} are increased from values of 0 to 25. Second, all gains are increased simultaneously. The root-loci for these cases are shown in Figures 18 and 19. As can be seen in both cases for a constant cross-gain of $K_{12} = K_{21} = 0.5$, the system is unstable for low values of direct gain. The closed-loop pole moves from the right-half-plane to the left-half-plane when the direct gain values reach $K_{11} = K_{22} = 0.5$. In Figure 18, at higher gains the inclusion of this specific value of cross-gain, $K_{12} = K_{21} = 0.5$, is shown to improve damping, but in Figure 19 it reduces damping as compared with the same cases without cross-gains. It also can be seen, in Figures 18 and 19, that having cross-gains of the same magnitude as the direct gains neutralizes the damping effect of velocity feedback altogether except for the first mode. From these results it can be seen that the question of how to handle cross-gain feedback is, indeed, not a simple one and requires further investigation. One can conclude, however, that arbitrary inclusion of cross gains is risky, but for these cases, elimination of cross gains does not effect stability and appears to be a viable approach to analysis.

Up to this point our analysis has been directed toward fixed-free cable configurations. We will now investigate the behavior of the free-free cable under tension.

Free-free cable stability and control

Two cases will be examined. The first case is a free-free cable with velocity and displacement fed back to a co-located force at one end. The second case is a free-free cable with velocity and displacement fed

back to co-located forces at both ends.

First we will examine a free-free cable with both velocity and displacement feedback to a co-located force at one end (Figure 6 with a force acting at one end only). The transfer function for this case is given by

$$\begin{Bmatrix} y_1(s) \\ \dot{y}_1(s) \end{Bmatrix} = \begin{bmatrix} \frac{\cosh s}{s \sinh s} \\ \frac{\cosh s}{\sinh s} \end{bmatrix} f_1 \tag{3-25}$$

If the feedback control takes the form,

$$f_1 = -[K_{11}, K_{12}] \begin{Bmatrix} y_1 \\ \dot{y}_1 \end{Bmatrix}, \tag{3-26}$$

the term in brackets from Eq. (3-1) has the form

$$I_r + G(s)K = \begin{bmatrix} 1 + g_{11}K_{11} & g_{11}K_{12} \\ g_{21}K_{11} & 1 + g_{21}K_{12} \end{bmatrix} \tag{3-15}$$

and the characteristic equation, Eq. (3-2) becomes

$$1 + g_{21}K_{12} + g_{11}K_{11} = 0$$

or

$$s \sinh s + (K_{11} + s K_{12}) \cosh s = 0 \tag{3-27}$$

If we let $s = n + i\omega$ we can obtain analytic solutions for the open-loop poles and system zeros.

Poles $n = 0$; $\omega = 0$, $\omega = \frac{k_d \pi}{2}$, k_d even

Zeros for displacement

$$n = 0 \quad ; \quad \omega = \frac{k_n \pi}{2} \quad , \quad k_n \text{ odd}$$

No solution $\omega = 0$ (3-28)

Zeros for velocity

$$n = 0 \quad ; \quad \omega = 0 \quad , \quad \omega = \frac{k_n \pi}{2} \quad , \quad k_n \text{ odd}$$

so for the free-free cable we have for the open loop, a pole at $n = 0$, $\omega = 0$, corresponding to the rigid body translation. Pure displacement feedback and pure velocity feedback is shown in Figure 20. As can be seen in Figure 20, displacement feedback causes the vibrational frequencies to increase without damping, and the rigid body pole at zero frequency with feedback becomes a rigid body oscillation pole. Velocity feedback for the free-free cable, force at one end is similar (with different frequencies), to the fixed-free cable velocity feedback result (Figure 9), in that poles can be driven to $n = -\infty$ for all modes, the exception being the zero frequency rigid body mode, where we see a pole-zero cancellation, which only means that this mode is uncontrolled with velocity feedback alone.

Three two gain root loci plots are shown in Figures 21 and 22. In Figure 21 there are two gain sequencing schemes shown. The first is using a constant velocity feedback gain, the displacement feedback gain is increased. The second scheme is using a constant displacement feedback gain, the velocity gain is increased. It can be seen that, feeding back velocity with some specific constant gain while increasing the value of the displacement feedback gain to the force at one end of the free-free cable causes the closed-loop poles to migrate from an initial velocity damped position back toward the imaginary axis (two

initial values of velocity feedback gain are illustrated). This reduction of damping behavior is true of all the vibrational modes. The pattern is similar to the pattern for the fixed-free cable. The effect on the rigid body mode is to limit the velocity feedback damping, but not to drive the pole back to the imaginary axis.

The scheme using constant displacement feedback gain of $K_D = 0.5$ and increasing the velocity feedback gain exhibits the same behavior as the corresponding fixed-free cable case. At low values of velocity feedback gain, damping is increased with increasing gain and at higher values, damping is decreased with increasing gain. The value of velocity feedback gain where this switching occurs is the same for all modes, $K_V = 1.0$. The higher the modal frequency, the smaller the adverse effect of any particular value of displacement feedback gain on the movement of the closed-loop pole into the left half plane. These results indicate that, for the vibrational modes, there is no advantage in using both displacement and velocity feedback for the free-free cable unless a change of frequency is desired. Control of the rigid body mode, however, necessitates the use of displacement feedback, as velocity feedback alone cannot control the rigid body position of the cable.

In Figure 22, the root loci are generated by increasing both velocity feedback and displacement feedback gains simultaneously. We observe that, for the vibrational modes, increasing feedback gain for low values of gain increases the damping. Increasing feedback gain for values of gain greater than $K = 1.0$ causes a decrease in damping from the maximum damped condition. This behavior is also exhibited by the open-loop rigid body zero frequency mode when the loop is closed.

With high gain the free-free cable takes on the vibrational characteristics of the uncontrolled fixed-free cable.

We will now examine a free-free cable with both velocity and displacement feedback to co-located forces at both ends, Figure 6, with forces acting only at the ends. The open-loop free-free cable transfer function for displacement feedback to three forces is given by Eq. (2-32). Eliminating the second row and second column we obtain the transfer function for displacement feedback of forces only at the free ends of the cable;

$$G_D(s) = \frac{1}{s \sinhs} \begin{bmatrix} \coshs & 1 \\ 1 & \coshs \end{bmatrix} \tag{3-29}$$

By taking the time derivative of Eq. (3-29), which is simply a multiplication by s, we obtain the velocity feedback transfer function

$$G_v = \frac{1}{\sinhs} \begin{bmatrix} \coshs & 1 \\ 1 & \coshs \end{bmatrix} \tag{3-30}$$

Now recognizing that

$$\bar{y}(s) = G_D(s)\, \bar{f}(s) \tag{3-31}$$

and

$$\dot{\bar{y}}(s) = G_v(s)\, \bar{f}(s) \tag{3-32}$$

where

$$\bar{y}^T = (y_1, y_2)$$

$$\dot{\bar{y}}^T = (\dot{y}_1, \dot{y}_2)$$

and

$$\bar{f}^T = (f_1, f_2)$$

we can write

$$\begin{Bmatrix} \bar{y} \\ \hdashline \bar{\dot{y}} \end{Bmatrix} = \begin{bmatrix} G_D(s) \\ \hdashline G_V(s) \end{bmatrix} \bar{f} \tag{3-33}$$

If the feedback takes the form

$$\bar{f} = - \left[\begin{array}{cc:cc} K_{11} & K_{12} & K_{13} & K_{14} \\ K_{21} & K_{22} & K_{23} & K_{24} \end{array}\right] \begin{Bmatrix} \bar{y} \\ \hdashline \bar{\dot{y}} \end{Bmatrix} \tag{3-34}$$

then the term in brackets from Eq. (3-1) has the form

$$I_r + \begin{bmatrix} G_D(s) \\ \hdashline G_V(s) \end{bmatrix} K \tag{3-35}$$

and the complete characteristic equation is obtained by applying Eq. (3-2).

Recognizing that feeding back displacements and velocities to other than co-located actuators can lead to instabilities, we will again set cross-coupled gain values to zero (i.e., $K_{12} = K_{14} = K_{21} = K_{23} = 0$). In addition, notice that $g_{11} = g_{22}$, $g_{21} = g_{12}$, $g_{31} = g_{42}$ and $g_{32} = g_{41}$ from Eqs. (3-29) and (3-30), so further simplification can be made. Finally, as a result of symmetry of the free-free cable, the choice of equal displacement feedback gains $K_{11} = K_{22}$ and equal velocity feedback gains $K_{13} = K_{24}$ is made.

Under these conditions, the characteristic equation associated with Eq. (3-35) becomes:

$$1 + (g_{31}^2 - g_{41}^2) K_{13}^2 + 2 g_{31} K_{13} + (g_{11}^2 - g_{21}^2) K_{11}^2 + 2 g_{11} K_{11} + 2(g_{11} g_{31} - g_{21} g_{41}) K_{11} K_{13} = 0 \tag{3-36}$$

Substituting in appropriate values from Eq. (3-29) and Eq. (3-30) yields the closed-loop characteristic equation

$$s^2 \sinhs + s^2 \sinhs \cdot K_{13}^2 + 2\, s^2 \coshs \cdot K_{13} + \sinhs \cdot K_{11}^2 + 2s \coshs \cdot K_{11} + 2\, s \sinhs \cdot K_{11} K_{13} = 0 \qquad (3\text{-}37)$$

By substituting in $s = n + i\omega$ and expanding Eq. (3-37) into real and imaginary equations, the open-loop poles and system zeros can be obtained analytically. The open-loop poles are the same as the previous case with a force only at one end, (i.e., poles at $n = 0$; $\omega = 0$, $\omega = k_d\pi$, $k_d = 1,2,3,\cdots$. The system zeros can be obtained by using the definition given in Chapter Three in conjunction with Eq. (3-37) expanded into real and imaginary equations. This results in system zeros at $n = 0$, $\omega = 0$, $\omega = k_n\pi$, $k_n = 1,2,3,\cdots$. By observing the pole-zero locations given above, it would appear that they are a series of pole-zero cancellations. However, coincidence of system poles and system zeros does not insure cancellation when dealing with MIMO systems.[33] It is helpful to keep this in mind when looking at the root-loci for this case.

Figure 23 demonstrates that displacement feedback to the co-located forces at the ends of the free-free cable causes the vibrational frequencies to increase without damping. The pole at zero frequency corresponding to the rigid body motion, with feedback, becomes another oscillatory mode as a result of restraining the free ends of the cable. At high gains the cable behaves as if it is fixed-fixed. For velocity feedback alone (Figure 23), increasing the values of gain, drive the closed-loop poles to $n = -\infty$ at a value of gain of 1.0. Increasing the

gain further drives the closed-loop poles back toward the imaginary axis, most at the same frequency.

Three two gain root loci plots are shown in Figures 24 and 25. Figure 24 illustrates two gain sequencing schemes. The first scheme is, using a constant velocity feedback gain, displacement feedback gain is increased. The second scheme is, using a constant displacement feedback gain, the velocity feedback gain is increased.

We can observe that feeding back velocity with some specific constant gain, while increasing the value of the displacement feedback gain to the forces at the ends of the free-free cable, causes the closed-loop poles to migrate from an initial velocity damped position back toward the imaginary axis (two initial values of velocity feedback gain are illustrated). This reduction of damping is similar for all modes except for the zero frequency mode where the closed-loop pole moves straight in along the negative real axis.

The scheme using constant displacement feedback gain of $K_D = 0.5$ and increasing the velocity feedback gain is similar to previous results for the force at only one end. At low values of velocity feedback gain, damping is increased with increasing gain, and at higher than $K_V = 1.0$ damping is decreased with increasing gain. The higher the modal frequency, the smaller the effect of any particular value of displacement feedback on the movement of the closed-loop pole into the left half plane. Similar conclusions can be made for this case as for the case of a force only at one end.

Figure 25 is a plot of the root loci generated by increasing both the velocity feedback and displacement feedback gains simultaneously.

We observe that for all modes, increasing feedback gain for low values of gain increases the damping. Increasing feedback gain for high values of gain (greater than K = 1.0) causes a decrease in damping from the maximum damped condition. Notice again, that the elimination of cross-gain feedback, while possibly not being the best feedback scheme, does create a stable closed-loop system even at high values of velocity and displacement gain at both ends of the cable.

In this chapter we have examined the open-loop and closed-loop characteristics of various cable configurations. These results yield much information useful for the design of flexible structures. To expand this body of knowledge we will in subsequent chapters examine the characteristics of the flexible beam.

IV. CANTILEVER BEAM

In this chapter, the open-loop transfer functions for a cantilever beam will be developed for, displacement feedback and velocity feedback to a force actuator, and slope and angular rate feedback to a moment actuator.

Transverse vibration of the beam is described by a fourth order partial differential equation. The solution of this equation requires four boundary conditions, two at each end of the beam.[35] From the basic governing partial differential equation for the beam, we will develop through the use of the Laplace transform, open-loop transfer functions corresponding to various free-end boundary conditions. These open-loop transfer functions will then be used in Chapter Five to form the closed-loop transfer functions needed for stability and control analysis.

A beam element in bending vibration is shown in Figure 26, where transverse displacement is given by $y(x,t)$; mass distribution by, $m(x)$; flexural rigidity by, $EI(x)$ and force per unit length by $f(x,t)$.

The classical Bernoulli-Euler beam theory assumes the rotation of the beam element to be insignificant when compared to the vertical translation, and the shearing deformation to be small in relation to the bending deformation.[26,35] Timoshenko beam theory does not make these assumptions. Neglecting these effects only contributes about 2% error in the frequency, if the length of the beam is about 10 times its height.[36] Therefore, the mathematically simpler Bernoulli-Euler

theory which yields essentially the same results, in terms of characteristic behavior, will be used in this development. Again, negligible structural damping is assumed. The governing partial differential equation of motion for the beam is, therefore, given by[26]

$$-\frac{\partial^2}{\partial x^2}\left[EI(x)\,\frac{\partial^2 y(x,t)}{\partial x^2}\right] + f(x,t) = m(x)\,\frac{\partial^2 y(x,t)}{\partial t^2}\quad,$$

$$0 \leq x \leq L \quad . \tag{4-1}$$

While Eq. (4-1) is the general equation of motion for the beam in bending vibration, it can be simplified by certain assumptions. In addition, the solution to Eq. (4-1) will depend on the particular boundary conditions of the beam configuration under consideration. Several configurations will be considered.

Cantilever beam, force at free end

Assuming a uniform cantilever beam with no distributed load (Figure 27a), Eq. (4-1) reduces to

$$EI\,\frac{\partial^4 y(x,t)}{\partial x^4} + m\,\frac{\partial^2 y(x,t)}{\partial t^2} = 0 \quad , \quad 0 \leq x \leq L \tag{4-2}$$

The deflection and the slope of the cantilever beam must be zero at the fixed end, $x = 0$; therefore, at $x = 0$ the boundary conditions are

$$\left.\begin{aligned} &y(0,t) = 0 \\ \text{and}\quad &y'(0,t) = 0 \end{aligned}\right\} \tag{4-3}$$

At the free end, only a force is acting (Figure 27a,b). Therefore, at $x = L$ the boundary conditions are

$$EI \left.\frac{\partial^3 y(x,t)}{\partial x^3}\right|_{x=L} = - f_L$$

and (4-4)

$$EI \left.\frac{\partial^2 y(x,t)}{\partial x^2}\right|_{x=L} = 0$$

Again as was stated in Chapter Two, a transfer function relating the input to the output is desired.

Assuming initial conditions of displacement and velocity are zero, Eq. (2-5), the Laplace transform of Eq. (4-2) with respect to the time variable, t, is given by

$$EI \frac{d^4 y(x,s)}{dx^4} + m s^2 y(x,s) = 0 \quad , \quad 0 \leq x \leq L \tag{4-5}$$

The transformed boundary conditions are, at x = 0

$$\left.\begin{aligned} & y(0,s) = 0 \\ \text{and} \quad & \\ & y'(0,s) = 0 \end{aligned}\right\} \tag{4-6}$$

and at x = L

$$EI \left.\frac{d^3 y(x,s)}{dx^3}\right|_{x=L} = - f_L$$

and (4-7)

$$EI \left.\frac{d^2 y(x,s)}{dx^2}\right|_{x=L} = 0$$

The solution to Eq. (4-5) in the Laplace transform plane is given by

$$y(x,s) = A_1(\cosh\alpha x\cdot\cos\alpha x + \sinh\alpha x\cdot\cos\alpha x) + A_2(\cosh\alpha x\cdot\cos\alpha x - \sinh\alpha x\cdot\cos\alpha x) + A_3(\cosh\alpha x\cdot\sin\alpha x + \sinh\alpha x\cdot\sin\alpha x) + A_4(\cosh\alpha x\cdot\sin\alpha x - \sinh\alpha x\cdot\sin\alpha x) \quad (4\text{-}8)$$

where

$$\alpha = \sqrt[4]{\frac{m\,s^2}{4EI}} \quad (4\text{-}9)$$

The constants A_1, A_2, A_3 and A_4 in Eq. (4-8) are determined by applying the boundary conditions Eqs. (4-6) and (4-7) to Eq. (4-8). The result in the s domain is a transfer function $G_{xL}(s)$, relating the displacement at an arbitrary point, $y(x,s)$ to a control force at the end of the beam, f_L and is found to be

$$\frac{y(x,s)}{f_L} = G_{xL}(s) = \left[\frac{L^3}{2(\alpha L)^3 EI}\right]\left[\frac{1}{\cosh^2\alpha L + \cos^2\alpha L}\right][(-\cosh\alpha L\cdot\cos\alpha L)(\cosh\alpha x\cdot\sin\alpha x - \sinh\alpha x\cdot\cos\alpha x) + (\cosh\alpha L\cdot\sin\alpha L + \sinh\alpha L\cdot\cos\alpha L)(\sinh\alpha x\cdot\sin\alpha x)] \quad (4\text{-}10)$$

By taking the derivative of Eq. (4-10) with respect to x, the transfer function relating the slope at any point on the beam to a control force at the end can be obtained. Also by taking the derivative of Eq. (4-10) with respect to time we can obtain the transfer function relating the velocity at any point to a control force at the end. Taking a time derivative in the s plane is simply

$$\frac{\dot{y}(x,s)}{f_L} = s\,\frac{y(x,s)}{f_L} \quad . \quad (4\text{-}11)$$

Applying Eq. (4-11) to Eq. (4-10) and by rearranging Eq. (4-9) such that

$$s = 2(\alpha L)^2 \sqrt{\frac{EI}{mL^4}} \quad , \tag{4-12}$$

We can eliminate the explicit s term from Eq. (4-11) to obtain the general velocity-force open-loop transfer function as

$$\frac{\dot{y}(x,s)}{f_L} = \left[\frac{L}{(\alpha L)\sqrt{EIm}}\right]\left[\frac{1}{\cosh^2\alpha L + \cos^2\alpha L}\right][(-\cosh\alpha L \cdot \cos\alpha L)$$
$$(\cosh\alpha x \cdot \sin\alpha x - \sinh\alpha x \cdot \cos\alpha x) + (\cosh\alpha L \cdot \sin\alpha L$$
$$+ \sinh\alpha L \cdot \cos\alpha L)(\sinh\alpha x \cdot \sin\alpha x)] \; . \tag{4-13}$$

A special case of the relationship of the displacement at the free end and the control force at the free end can now be examined. From Eq. (4-10) by letting x = L we obtain the expression

$$\frac{y(L,s)}{f_L} = \left[\frac{L^3}{2(\alpha L)^3 EI}\right]\left[\frac{\cosh\alpha L \cdot \sinh\alpha L - \cos\alpha L \cdot \sin\alpha L}{\cosh^2\alpha L + \cos^2\alpha L}\right] \tag{4-14}$$

Likewise the special case of relating the velocity at the free end to a control force at the free end can be obtained by applying Eqs. (4-11) and (4-12) to Eq. (4-14) and utilizing the result. This yields the velocity at x = L, force at x = L open-loop transfer function,

$$\frac{\dot{y}(L,s)}{f_L} = \frac{L}{(\alpha L)\sqrt{EIm}}\left[\frac{\cosh\alpha L \cdot \sinh\alpha L - \cos\alpha L \cdot \sin\alpha L}{\cosh^2\alpha L + \cos^2\alpha L}\right] \tag{4-15}$$

Cantilever beam, moment at free end

The transfer functions for feeding back the slope and angular rate to a moment at the end of a cantilever beam can be developed in a similar manner. For these cases, the transformed governing differential equation, Eq. (4-5), is subject to transformed boundary conditions of:

at $x = 0$,

$$y(0,s) = 0$$

and

$$y'(0,s) = 0 \tag{4-16}$$

and at $x = L$,

$$EI \left.\frac{d^3y(x,s)}{dx^3}\right|_{x=L} = 0$$

and

$$EI \left.\frac{d^2y(x,s)}{dx^2}\right|_{x=L} = -M_L \tag{4-17}$$

Applying Eqs. (4-16) and (4-17) to Eq. (4-8), the open-loop transfer function relating the slope at any point, $\theta(x,s)$ to the moment at the end of the beam, M_L, is given by

$$\frac{\theta(x,s)}{M_L} = G_{xL}(s) = \frac{L}{(\alpha L)EI}\left[\frac{1}{\cosh^2\alpha L + \cos^2\alpha L}\right]$$
$$[-(\cos\alpha L\cdot\cosh\alpha L)(\cos\alpha x\cdot\sinh\alpha x + \sin\alpha x\cdot\cosh\alpha x)$$
$$+ (\cos\alpha L\cdot\sinh\alpha L - \sin\alpha L\cdot\cosh\alpha L)(\sin\alpha x\cdot\sinh\alpha x)] . \tag{4-18}$$

Applying Eqs. (4-11) and (4-12) to Eq. (4-18), yields the open-loop transfer function relating the angular rate at any point to the control moment at the end of the beam,

$$\frac{\dot\theta(x,s)}{M_L} = G_{xL}(s) = \frac{2(\alpha L)}{L\sqrt{EIm}}\left[\frac{1}{\cosh^2\alpha L + \cos^2\alpha L}\right]$$
$$[-(\cos\alpha L\cdot\cosh\alpha L)(\cos\alpha x\cdot\sinh\alpha x + \sin\alpha x\cdot\cosh\alpha x)$$
$$+ (\cos\alpha L\cdot\sinh\alpha L - \sin\alpha L\cdot\cosh\alpha L)(\sin\alpha x\cdot\sinh\alpha x)] . \tag{4-19}$$

By letting $x = L$ in Eqs. (4-18) and (4-19) slope at free end to moment at free end and angular rate at free end to moment at free end relations

can be easily obtained.

General force-displacement, force-velocity, moment-slope and moment-angular rate open-loop transfer functions and specific free-end transfer functions for the cantilever (fixed-free) beam have now been obtained.

Let us now turn our attention to the question of stability and feedback control of the cantilever beam.

V. CANTILEVER BEAM--STABILITY AND CONTROL

In this chapter we will examine the closed-loop characteristics of the cantilever beam in the same manner as the analysis of the cable in Chapter Three. In general we will determine the open-loop pole-zero locations and attempt to construct a root locus. In addition we will form the closed-loop characteristic equation from Eq. (3-2) and solve it directly.

Displacement and velocity fed back from the end of the beam to a force at the end, and velocity and displacement fed back from other points on the beam to a force at the end will be examined. In addition to the above analysis which will be done for a generic beam, (i.e. $E = I = m = 1$) parameters for a specific beam will be developed and some comments about damping ratio will be made.

Displacement at end fed back to co-located force actuator

Examining the roots of the numerator and the roots of the denominator of the open-loop transfer function Eq. (4-14), a pole-zero plot can be generated. For proper interpretation, one needs to recognize that the poles and zeros, s are actually a multiple of the square of αL. Therefore a solution that yields equal real and imaginary parts of αL, actually results in values of s which lie on the imaginary axis of the s plane. Since no structural damping is assumed, the open-loop poles and zeros for the cantilever beam modeled here are always on the imaginary axis. Figure 28 shows the open-loop pole-zero locations for the sensor and actuator co-located at the free end of the beam.

It can be seen that the pole-zero pattern is alternating as would be expected, but that the poles and zeros are not equally spaced as they were with the cable.

By closing the feedback loop, as shown in Figure 7, we can write the closed-loop transfer function and obtain the closed-loop characteristic equation, from which the root locus may be generated, by incrementing the value of feedback gain in a manner similar to that described in Chapter Three.

The characteristic equation for this case can be obtained by applying Eq. (3-1) to the open-loop transfer function, Eq. (4-14). From Eq. (3-2) the closed-loop characteristic equation for displacement feedback at the end of the beam to a co-located force is given by

$$\left[\frac{L^3}{(\alpha L)^3\, 2EI}\right] (\cos^2\alpha L + \cosh^2\alpha L)$$

$$+ K\,(\cosh\alpha L \cdot \sinh\alpha L - \cos\alpha L \cdot \sin\alpha L) = 0 \quad . \qquad (5\text{-}1)$$

The root loci are generated by obtaining the roots of Eq. (5-1) while increasing the values of gain, K.

Velocity at end fed back to co-located force actuator

Applying Eq. (3-1) to Eq. (4-15), and writing Eq. (3-2) for this case, the closed-loop characteristic equation for velocity feedback at the end to a force at the end is given by

$$\left[\frac{L}{\alpha L\sqrt{EIm}}\right] (\cos^2\alpha L + \cosh^2\alpha L)$$

$$+ K\,[\cosh\alpha L \cdot \sinh\alpha L - \cos\alpha L \cdot \sin\alpha L] = 0 \quad . \qquad (5\text{-}2)$$

The roots of Eq. (5-2) for increasing values of K generates the root

loci for velocity feedback. The root loci curves for velocity feedback and displacement feedback are displayed in Figure 28. Here we see that, for displacement feedback, increasing gain causes the frequencies to increase to values corresponding to those of a fixed-pinned beam.[37] Displacement feedback does not affect the damping. As a result, the system is neutrally stable with or without feedback. Notice that for a specific value of gain, for instance K = 25, the poles for the higher modes do not move as far as the poles for the lower modes. This supports the fact that more energy is required to excite the higher modes.

We also see in Figure 28 that velocity feedback will stabilize the beam oscillations, although not in the same dramatic manner as occurred with the cable. The damping of the system increases with increasing velocity feedback gain up to a point where, as the gain is further increased, the system starts to return to being neutrally stable. The constrained frequencies,[38] those for which $K = \infty$, are again for a beam that is fixed-pinned.[37] The optimum gain for maximum damping for each mode appears to be approximately 1.8 times the optimum value of gain for the next lower mode. Therefore, more gain is needed at higher modes to achieve maximum damping for the higher modes. This result is significant from the standpoint of controller design. Since for a single sensor-actuator only one gain is available, different gains cannot be used for each mode. Picking the gain that results in maximum damping for the first mode, K = 1.6, we can see from Figure 28 that the location of the roots for the higher modes are such that the damping for these modes is less than the maximum possible for these modes. On the other hand, picking a value of gain which maximizes the damping

of a higher mode, for example K = 5.2 for mode three, the position of the roots for higher and lower modes is less than that for maximum damping. Hence for design purposes some tradeoff must be considered.

Figure 28 displays general root loci that apply to a generic uniform cantilever beam. The complex values of s from

$$s = 2(\alpha L)^2 \cdot \sqrt{\frac{EI}{mL^4}} \tag{4-12}$$

are plotted with

$$\sqrt{\frac{EI}{mL^4}} = 1 \tag{5-3}$$

In addition for displacement feedback the computed gain values assume

$$\frac{L^3}{2EI} = 1 \tag{5-4}$$

and for velocity feedback the computed gain values assume

$$\frac{L}{\sqrt{EIm}} = 1 \quad . \tag{5-5}$$

To obtain the actual values of s for a specific beam, the computed values of s must be multiplied by the factor $\sqrt{\frac{EI}{mL^4}}$ for the specific beam. To obtain the actual values of displacement feedback gain for a specific beam

$$K_{actual} = K_{computed} \left(\frac{2EI}{L^3}\right) \tag{5-6}$$

and for velocity feedback

$$K_{actual} = K_{computed} \left(\frac{\sqrt{EIm}}{L}\right) \quad , \tag{5-7}$$

As a demonstration, one can obtain values of s and values of gain for a specific beam. Parameters of a particular graphite-epoxy tubular beam[39] and the computation of the factors shown in Eqs. (5-3), (5-4) and (5-5), for this beam, are given in Appendix A.

Using these factors, Figure 29 shows the most stable closed-loop pole positions for the first few modes of the cantilever beam, feeding back the velocity at the end to the force at the end. The damping ratio, ζ, can be calculated from the expression

$$\zeta = - \sin \theta \tag{5-8a}$$

where θ is given by

$$\theta = \sin^{-1} \frac{n}{\omega} \tag{5-8b}$$

Damping ratio is independent of beam parameters, since the values of n and ω are multiplied by the same quantities for a specific beam.

For a generic cantilever beam, the most stable closed-loop pole position for any mode (beyond mode one) is described by the following expressions:

The imaginary value is given by,

$$\omega = (32\ m^2 - 40\ m + 13)\ \frac{\pi^2}{32} \tag{5-9a}$$

and the real value is bounded by

$$-(8m + 3)\ \frac{\pi^2}{32} < n < -(8m - 5)\ \frac{\pi^2}{32} \tag{5-9b}$$

where m is the mode number.

From Eq. (5-9) and Figure 29 it can be seen that although the damping ratio, ζ, decreases for increasing mode number, global stability of all modes is assured.

To see the effect of moving the sensor away from the free end of the beam (see Figure 30), we can examine first, the open-loop pole-zero locations for various sensor positions, x, and second, selected cases of closed-loop displacement and velocity feedback.

The open-loop pole-zero locations for various sensor positions, x, force at the end, x = L, are obtained from the general displacement-force open-loop transfer function given by Eq. (4-10). From Figure 31 it can be seen that the poles and zeros have an alternating pattern with the sensor co-located with the force at the free end. As the sensor location is moved down the beam away from the force location, the zero locations begin to move up the imaginary axis, as was true in the similar case for the cable. When the sensor location is moved past the location of a node of a particular mode, the pole-zero pattern is no longer alternating, and we see two poles appearing in sequence without a zero between them. As was observed with the cable, it is expected for the beam, that for these sensor locations instability will occur when the feedback gain is high enough.

To investigate this further, displacement and velocity feedback for sensors located at x = 0.5 and x = 0.8 will be examined.

Displacement feedback, separated sensor-actuator

For the case of displacement feedback from a sensor located at any point on the beam to a control force at the end of the beam, applying Eq. (3-1) to Eq. (4-10), the characteristic equation, Eq. (3-2), of the closed-loop transfer function is found to be,

$$\left[\frac{L^3}{2(\alpha L)^3 EI}\right](\cos^2\alpha L + \cosh^2\alpha L)$$

$$+ K\,[(-\cosh\alpha L\cdot\cos\alpha L)(\cosh\alpha x\cdot\sin\alpha x - \sinh\alpha x\cdot\cos\alpha x)$$

$$+ (\cosh\alpha L\cdot\sin\alpha L + \sinh\alpha L\cdot\cos\alpha L)(\sinh\alpha x\cdot\sin\alpha x)] = 0 \qquad (5\text{-}10)$$

To generate the root loci, for displacement feedback from a sensor located at any specific point to a force at the end, the roots of Eq. (5-10) are obtained as K is increased. Figure 32 shows the root loci of the first few vibrational modes due to feeding back displacement sensed at x = 0.5 and x = 0.8 individually to a control force located at the free end. It can be seen in Figure 32 that, as expected, at high values of feedback gain, poles not separated by zeros can be driven unstable. It can also be observed from Figure 32, that for non-co-located sensor-actuator pairs, displacement feedback does not affect stability if the displacement feedback gains are small. The closer the sensor is to the actuator, the larger the value of displacement feedback gain that can be used before creating instability problems.

Velocity feedback, separated sensor-actuator

For the case of velocity feedback from a sensor located at any point on the beam to a control force located at the end of the beam, applying Eq. (3-1) to Eq. (4-13), the characteristic equation, Eq. (3-2), of the closed-loop transfer function is found to be

$$\left[\frac{L}{(\alpha L)\sqrt{EIm}}\right](\cos^2\alpha L + \cosh^2\alpha L)$$

$$+ K\,[(-\cosh\alpha L\cdot\cos\alpha L)(\cosh\alpha x\cdot\sin\alpha x - \sinh\alpha x\cdot\cos\alpha x)$$

$$+ (\cosh\alpha L\cdot\sin\alpha L + \sinh\alpha L\cdot\cos\alpha L)(\sinh\alpha x\cdot\sin\alpha x)] = 0 \qquad (5\text{-}11)$$

Again the root loci are generated from the solution of Eq. (5-11) as the value of K is increased. Figure 33 displays the root loci of the first few vibrational modes due to feeding back velocity sensed at $x = 0.5$ and $x = 0.8$ individually to a control force located at the free end of the beam.

In Figure 33, it can be observed by looking at the first four modes, that feedback from a velocity sensor located away from the actuator causes instabilities for some modes. Positions of the sensor that generate a stable response for a particular mode, correspond to positions on the beam that are in phase with position of the control force, as the beam oscillates. A sensor located at a node of a particular mode cannot sense the motion of that mode. Locations of the sensor that generate an unstable response for a particular mode are those that are out of phase with the motion of the actuator location.

It can also be noted that the stability of a particular mode is independent of the value of feedback gain. Unlike the case of displacement feedback, unstable closed-loop poles are unstable even for small values of gain. Although for extremely high values of gain some unstable poles can be driven neutrally stable. It can be seen from Figure 33 that feedback from a velocity sensor located at $x = 0.5$, generates stability of mode one, instability of mode two and has little effect on mode three, $x = 0.5$ being very close to a node of mode three for the cantilever beam. From this we can conclude, for single-input-single-output systems, that having a separated velocity sensor and a force actuator is at best a risky proposition, although some destabilizing energy in the higher modes may not be a problem with a

small amount of structural damping.[25] At worst, it could lead to unstable excitation of the lower modes, aggravating the structural vibration problem rather than alleviating it.

In this chapter, we have examined the open-loop pole-zero patterns, as well as the closed-loop characteristics of velocity and displacement feedback to a force actuator for co-located and separated sensor-actuator pairs for the cantilever beam.

In the following chapter, selected transfer functions will be developed and closed-loop characteristics of the free-free beam will be discussed.

VI. FREE-FREE BEAM

The free-free beam in contrast to the cantilever beam has two rigid body degrees of freedom, translation and rotation, which makes it a good model of a missile in free flight[40] or of an orbiting satellite. In this chapter, several open-loop transfer functions for the free-free beam with various control boundary conditions will be developed. Stability analysis and feedback control will then be discussed.

A uniform beam that is free of supports at both ends and has a control force and a moment at each end is shown in Figure 34a. Again the partial differential equation governing the motion of the beam is given by[26] Eq. (4-1). As a result of the simplifying assumptions made in Chapter Four, Eq. (4-1) reduces to Eq. (4-2). The boundary conditions can be determined by referring to Figure 34a and using the sign convention[41] shown in Figure 34b.

The boundary conditions at x = 0 are

$$V(x,t)\Big|_{x=0} = EI \left.\frac{\partial^3 y(x,t)}{\partial x^3}\right|_{x=0} = f_1$$

and (6-1)

$$M(x,t)\Big|_{x=0} = EI \left.\frac{\partial^2 y(x,t)}{\partial x^2}\right|_{x=0} = M_1$$

and at x = L

$$V(x,t)\Big|_{x=L} = EI \left.\frac{\partial^3 y(x,t)}{\partial x^3}\right|_{x=L} = -f_2$$

and (6-2)

$$M(x,t)\Big|_{x=L} = EI \left.\frac{\partial^2 y(x,t)}{\partial x^2}\right|_{x=L} = -M_2 .$$

Transforming Eqs. (4-2), (6-1) and (6-2) into the s domain by Laplace transform, the relationship of the displacement at any point on the free-free beam as a function of the forces and moments at its boundaries can be found to be

$$
\begin{aligned}
y(x,s) = \Bigg\{ & \frac{f_1}{2\alpha^3 EI}\left[\frac{\sinh\alpha L\cdot\cosh\alpha L - \sin\alpha L\cdot\cos\alpha L}{\sinh^2\alpha L - \sin^2\alpha L}\right] \\
& + \frac{f_2}{2\alpha^3 EI}\left[\frac{\cos\alpha L\cdot\sinh\alpha L - \sin\alpha L\cdot\cosh\alpha L}{\sinh^2\alpha L - \sin^2\alpha L}\right] \\
& + \frac{M_1}{2\alpha^2 EI}\left[\frac{\cos^2\alpha L\cdot\sinh^2\alpha L + \sin^2\alpha L\cdot\cosh^2\alpha L}{\sinh^2\alpha L - \sin^2\alpha L}\right] \\
& + \frac{M_2}{\alpha^2 EI}\left[\frac{\sin\alpha L\cdot\sinh\alpha L}{\sinh^2\alpha L - \sin^2\alpha L}\right]\Bigg\}\cos\alpha x\cdot\cosh\alpha x \\
& + \Bigg\{\frac{-f_1}{4\alpha^3 EI}\left[\frac{\sin^2\alpha L\cdot\cosh^2\alpha L + \cos^2\alpha L\cdot\sinh^2\alpha L}{\sinh^2\alpha L - \sin^2\alpha L}\right] \\
& + \frac{f_2}{2\alpha^3 EI}\left[\frac{\sin\alpha L\cdot\sinh\alpha L}{\sinh^2\alpha L - \sin^2\alpha L}\right] \\
& - \frac{M_1}{2\alpha^2 EI}\left[\frac{\sin\alpha L\cdot\cos\alpha L + \sinh\alpha L\cdot\cosh\alpha L}{\sinh^2\alpha L - \sin^2\alpha L}\right] \\
& - \frac{M_2}{2\alpha^2 EI}\left[\frac{\sin\alpha L\cdot\cosh\alpha L + \cos\alpha L\cdot\sinh\alpha L}{\sinh^2\alpha L - \sin^2\alpha L}\right]\Bigg\} \\
& (\sin\alpha x\cdot\cosh\alpha x + \cos\alpha x\cdot\sinh\alpha x) \\
& + \frac{M_1}{2\alpha^2 EI}\left[\frac{\sinh^2\alpha L - \sin^2\alpha L}{\sinh^2\alpha L - \sin^2\alpha L}\right]\sin\alpha x\cdot\sinh\alpha x \\
& + \frac{f_1}{4\alpha^3 EI}\left[\frac{\sinh^2\alpha L - \sin^2\alpha L}{\sinh^2\alpha L - \sin^2\alpha L}\right](\sin\alpha x\cdot\cosh\alpha x - \cos\alpha x\cdot\sinh\alpha x)
\end{aligned}
\tag{6-3}
$$

It is known from previous results for the free-free beam,[25,42] that feeding back the velocity or displacement to a non co-located force

actuator, or feedback using a co-located sensor of a different degree of freedom than the actuator (e.g., angular rate fed back to a force actuator) leads to instabilities. The relationships of interest, therefore, are those sensor-actuator pairs that are co-located and of the same degree of freedom type. The open-loop transfer function relating the displacement at x = 0 to the force at x = 0 is one of these pairs, and from Eq. (6-3) is given by

$$\frac{y(0,s)}{f_1} = \frac{1}{2\alpha^3 EI}\left[\frac{\sinh\alpha L\cdot\cosh\alpha L - \sin\alpha L\cdot\cos\alpha L}{\sinh^2\alpha L - \sin^2\alpha L}\right] \tag{6-4}$$

Similarly, the displacement-force open-loop transfer function at x = L, can be obtained.

Other relationships of interest are; the slope $\theta(0,s)$ to moment, M_1, the velocity, $\dot{y}(0,s)$ to force, f_1, and the angular rate $\dot{\theta}(0,s)$ to moment, M_1, open-loop transfer functions.

Taking the derivative of Eq. (6-3) with respect to x, the general slope equation can be obtained. From this equation, the relationship of the slope at x = 0 to the moment at x = 0 is given by

$$\frac{\theta(0,s)}{M_1} = \frac{1}{\alpha EI}\left[\frac{\sin\alpha L\cdot\cos\alpha L + \sinh\alpha L\cdot\cosh\alpha L}{\sinh^2\alpha L - \sin^2\alpha L}\right] \tag{6-5}$$

Similarly, the slope at x = L to the moment at x = L relationship can also be obtained. The time derivative of Eq. (6-3) yields the relationship of the velocity to the force and moments at either end of the free-free beam, and desired transfer functions can be obtained.

Free-free beam, closed-loop characteristics

Displacement at one end of the beam feeding back to a co-located force will be examined, as well as slope at one end of the beam feeding back to a co-located moment.

Feeding back displacement at one end of the free-free beam to a co-located force drives the frequencies toward those of a free-pinned beam. Likewise, feeding back slope at one end to a co-located moment, drives the frequencies toward those of a free-guided beam. In both of these cases, as expected, no damping is introduced. In a similar manner, velocity can be fed back to a co-located force or angular rate to a co-located moment. Results similar to these can be found elsewhere.[42]

In this chapter selected transfer functions for a free-free beam were developed and a brief discussion of closed-loop characteristics was presented.

VII. BEAM--DYNAMIC STIFFNESS APPROACH

In previous chapters dealing with the beam, single span beams, with single-input-single-output feedback, were investigated. Recognizing that most practical structures consist of more than a single span beam, it is desirable to expand to more complex structures, the technique of controlling the exact partial differential equation system. It is also desirable to be able to handle multi-input-multi-output control systems. That is, more than one actuator-sensor pair on the beam-like structures. A convenient method for handling both of these requirements is the dynamic stiffness matrix method mentioned in Chapter Two. In that chapter it was used for several cases involving the flexible cable. The feasibility of this method for synthesizing structures from beam elements has been demonstrated in the past.[22] Specifically the use of the dynamic stiffness influence coefficients in the Laplace transform plane has been investigated with regard to a single external exciting force.[24] The use of this method in conjunction with feedback of control forces, in particular multi-input-multi-output control, has not been previously demonstrated.

In this chapter the dynamic stiffness matrix for a beam element in flexure will be developed. This element matrix will then be used to construct an example case for which the stability and control will be investigated. The boundary forces and displacements for a uniform beam segment[22] shown in Figure 35 are used in a standard development of the dynamic stiffness matrix, although in this case using the Laplace

transform. The general solution for the transverse vibration of a beam in the Laplace transform plane was shown in Chapter four to be

$$\begin{aligned} y(x,s) = {} & A_1 (\cosh\alpha x \cdot \cos\alpha x + \sinh\alpha x \cdot \cos\alpha x) \\ & + A_2 (\cosh\alpha x \cdot \cos\alpha x - \sinh\alpha x \cdot \cos\alpha x) \\ & + A_3 (\cosh\alpha x \cdot \sin\alpha x + \sinh\alpha x \cdot \sin\alpha x) \\ & + A_4 (\cosh\alpha x \cdot \sin\alpha x - \sinh\alpha x \cdot \sin\alpha x) \end{aligned} \tag{4-8}$$

Taking the derivative with respect to x, expressions for $y'(x,s)$, $y''(x,s)$ and $y'''(x,s)$ can be obtained. Expressing the displacement, $y(x,s)$ and the slope $y'(x,s)$ evaluated at the two ends (or nodal points) of the beam segment, in terms of the constants, $\bar{A}$ yields

$$\bar{\delta}(s) = [W]\,\bar{A} \tag{7-1}$$

where $\bar{\delta}^T(s) = (y(0,s), -y'(0,s), y(L,s), -y'(L,s)) = (\delta_1(s), \theta_1(s), \delta_2(s), \theta_2(s))$ and $\bar{A}^T = (A_1, A_2, A_3, A_4)$. The nodal forces and moments using the sign convention established earlier in Figure 34b are given by,

$$\begin{aligned} f_1(s) &= EIy'''(0,s) \\ f_2(s) &= -EIy'''(L,s) \\ M_1(s) &= EIy''(0,s) \\ M_2(s) &= -EIy''(L,s) \end{aligned} \tag{7-2}$$

Writing the nodal forces in terms of the same constants, $\bar{A}$ yields

$$\bar{F}(s) = [U]\,\bar{A} \tag{7-3}$$

where

$$\bar{F}^T(s) = (f_1(s), M_1(s), f_2(s), M_2(s))$$

By solving Eq. (7-1) for the unknown constants

$$\bar{A} = [W]^{-1}\,\bar{\delta}(s) \quad , \tag{7-4}$$

the nodal forces can be found as a function of the nodal displacements by

$$\bar{F}(s) = [U]\cdot[W]^{-1}\,\bar{\delta}(s) \tag{7-5}$$

where

$$D(s) = [U]\cdot[W]^{-1} \quad , \tag{7-6}$$

D(s) is the dynamic stiffness matrix in the Laplace transform plane. The elements of the dynamic stiffness matrix, D(s) for the beam element are given in Appendix B. The use of the beam element dynamic stiffness matrix D(s), relating the nodal forces to the nodal displacements

$$\bar{F}(s) = D(s)\,\bar{\delta}(s) \quad , \tag{7-7}$$

will facilitate the analysis of more complex structures and sensor-actuator configurations. Structures consisting of beams of various lengths, stiffnesses, and moments of inertia, and having various control configurations can be formulated by the dynamic stiffness matrix method.

To illustrate the method, an example will be utilized. A cantilever beam will be constructed from two beam elements (see Figure 36) with two co-located sensor-actuator pairs on the beam. One pair will be at the free end and one pair at the intersection of the two beam elements. The result for this example is given by

$$\bar{F}(s) = D(s)\,\bar{\delta}(s) \tag{7-7}$$

where

$$\bar{F}^{T} = (f_0, M_0, f_1, M_1, f_2, M_2)$$

and

$$\bar{\delta}^T = (\delta_0, \theta_0, \delta_1, \theta_1, \delta_2, \theta_2)$$

and the dynamic stiffness matrix, D(s) is given symbolically by

$$D(s) = \left[\begin{array}{cc:cc:cc} d_{11} & d_{12} & d_{13} & d_{14} & 0 & 0 \\ d_{21} & d_{22} & d_{23} & d_{24} & 0 & 0 \\ \hdashline d_{31} & d_{32} & d_{33}+d_{11} & d_{34}+d_{12} & d_{13} & d_{14} \\ d_{41} & d_{42} & d_{43}+d_{21} & d_{44}+d_{22} & d_{23} & d_{24} \\ \hdashline 0 & 0 & d_{31} & d_{32} & d_{33} & d_{34} \\ 0 & 0 & d_{41} & d_{42} & d_{43} & d_{44} \end{array}\right] \qquad (7\text{-}8)$$

where the upper left-hand 4 x 4 pertains to the first beam segment and the lower right-hand 4 x 4 to the second beam segment. If we assume f_0 and M_0 sufficient to hold $\delta_0 = 0$ and $\theta_0 = 0$ (the cantilever condition), the first two rows and columns of the matrix in Eq. (7-8) can be neglected. Since only force actuators will be used there will be no external moment at the end and the internal moments at the intersection match leaving a force vector of

$$\bar{F}^T = (f_1, 0, f_2, 0) \quad . \qquad (7\text{-}9)$$

The remaining 4 x 4 dynamic stiffness matrix can, because of Eq. (7-9), be reduced to a 2 x 2 matrix by solving explicitly for the slopes in Eq. (7-7) in terms of the deflections. The resulting relationship is given by

$$\begin{Bmatrix} f_1 \\ \\ f_2 \end{Bmatrix} = \tilde{D}(s) \begin{Bmatrix} \delta_1 \\ \\ \delta_2 \end{Bmatrix} \qquad (7\text{-}10)$$

where $\tilde{D}(s)$ is the condensed stiffness matrix.

The remaining 2 x 2 can then be inverted to obtain the transfer function matrix. The result has the form

$$\bar{\delta}(s) = G(s)\,\bar{F}(s) \tag{7-11}$$

for the open-loop force-displacement relationship or

$$\dot{\bar{\delta}}(s) = s\,G(s)\,\bar{F}(s) \tag{7-12}$$

for the velocity-force relationship.

If the feedback control for velocity feedback takes the form,

$$\begin{Bmatrix} f_1 \\ f_2 \end{Bmatrix} = - \begin{bmatrix} K_{11} & K_{12} \\ K_{21} & K_{22} \end{bmatrix} \begin{Bmatrix} \dot{\delta}_1 \\ \dot{\delta}_2 \end{Bmatrix} , \tag{7-13}$$

the closed-loop transfer function is obtained by Eq. (3-1) and the closed-loop system dynamics can be determined from the closed-loop characteristic equation

$$|I_r + G(s)\,K| = 0 \tag{3-2}$$

As results in Chapter Three indicated, the inclusion of cross-gains K_{12} and K_{21} could have a destabilizing effect so they will be eliminated.

The expansion of Eq. (3-2) yields the multivariable feedback closed-loop characteristic equation for which a two gain root locus can be constructed as was done in Chapter Three.

For this example each beam segment will be chosen to be the same length and velocity feedback will be utilized. Therefore, velocity will be fed back to co-located actuators at x = 0.5 and x = 1.0 for the cantilever beam. Figure 37 illustrates that with $K_{11} = 0$, (i.e. only velocity feedback to a co-located actuator at the end), the root locus

is identical to that of Figure 28. Thus, verifying that the cantilever beam constructed by using the dynamic stiffness matrix approach is equivalent to the cantilever beam developed directly in Chapter Four. Also in Figure 37, it can be seen that feeding back velocity to a co-located actuator at x = 0.5 alone ($K_{22} = 0$) generates increased damping in modes two and four. This increase in damping is the result of x = 0.5 being the location of a peak in the mode shape of mode two and mode four. A larger velocity signal is available for feedback at these modal peaks. Mode three, on the other hand, has a node near x = 0.5. Therefore, as can be seen in Figure 37, there is no damping of mode three.

As was stated previously, MIMO control has the potential for better control of more modes than SISO control.

Figure 38 demonstrates that for the first four modes of the cantilever beam, overall damping is improved with two co-located sensor-actuator pairs. This result is what one would expect, although it is counter to the result for the similar cable case obtained in Chapter Three. Having two sensor-actuator pairs, allows us to set two feedback gains. Two cases of velocity feedback are shown in Figure 38. In the first case, $K_{11} = K_{22}$, and in the second case, $K_{11} = 2K_{22}$. In both cases, if very high feedback gain is used, modes one and two can be driven to zero frequency. For case two ($K_{11} = 2K_{22}$) more damping is available than in the case of $K_{11} = K_{22}$. This indicates that the feedback gain for sensor-actuator pairs at an interior point should, in general, be higher than the gain for the feedback of the end point, for the best damping in all modes. Obviously with two

sensor-actuator pairs, (at x = 0.5 and x = 1.0) only the first two modes can be controlled in the best manner. Although some improvement in damping is seen in those modes which have peaks at the location of the interior sensor-actuator pair, e.g. mode four for this case. Therefore, a controller design can be initiated based on the system characteristics illustrated in Figures 37 and 38.

In this chapter we have seen that the dynamic stiffness matrix method, in the Laplace transform plane, can be utilized to synthesize more complex structural and control configurations. We have also examined an example of MIMO control for a cantilever beam constructed using the dynamic stiffness approach.

VIII. RESULTS AND CONCLUSIONS

In this work, a formulation using exact transfer function methods has been applied to the control of systems governed by partial differential equations. Exact transfer functions were developed and single-input-single-output feedback was applied to various cable and beam configurations. Using the exact relationships, dynamic stiffness matrices were developed for cable and beam elements. These elements were then used to construct more complex configurations. Multi-input-multi-output feedback control was then investigated. There are several significant results:

1) Exact solutions are obtained even though a finite number of sensors and actuators are used.

2) All vibrational modes can be controlled by using a single co-located sensor-actuator at the boundary of a fixed-free cable or beam.

3) Pure signals from the sensors can be used without any additional signal processing.

4) The multi-input-multi-output investigation demonstrates that, even without cross-gains, there is still interaction between sensor-actuator pairs. It appears that this interactive effect needs to be included in any multi-input-multi-output control design.

5) By starting with fundamental elements of beams and cables, reasonably sophisticated systems can be modeled. It should be pointed out, however, that as the system becomes more general or complex, the work involved in extracting results increases significantly.

6) It would seem that the use of a multi-input-multi-output control system would yield the most benefits, since, as observed in the examples shown, a single actuator does not in general damp all the modes in possibly the best manner, the exception being the cable which has symmetric locations of poles and zeros, where MIMO control of the cable is found to be less effective than SISO. More sophisticated multivariable theory than is presently available is needed to deal with the transcendental equations encountered here.

7) Finally with the development of more advanced algebraic manipulator routines, computers will be able to do most of the algebra required for applying to more complex structures, the approach presented here. This may generate interest in developing this approach as an alternative to some of the current techniques. The usefulness of any technique can only be determined when,eventually,it is used in the control of actual hardware. The final word on which approach will prove most useful has yet to be written.

To expand the work done here, some suggested topics to be investigated are:

1) A comparison of the exact transfer function models with truncated modal models from the standpoint of control system performance, and to determine the effects of truncation on model integrity.

2) The development of multivariable theory and techniques to handle transfer function matrices of transcendental nature.

3) Expand the dynamic stiffness matrix approach in the Laplace transform plane to include Timoshenko beam, membrane and plate elements.[43]

4) Determine an acceptable limit on the spacing of sensors and actuators when co-location is not possible.

5) The development of methods to carry out more of the necessary operations numerically instead of algebraically.

REFERENCES

1. Meirovitch, L. (ed.), Proceedings of the First VPI&SU/AIAA Symposium on Dynamics and Control of Large Flexible Space Craft, Blacksburg, VA, June, 1977.

2. Meirovitch, L. (ed.), Proceedings of the Second VPI&SU/AIAA Symposium on Dynamics and Control of Large Flexible Space Craft, Blacksburg, VA, June, 1979.

3. Meirovitch, L. (ed.), Proceedings of the Third VPI&SU/AIAA Symposium on Dynamics and Control of Large Flexible Space Craft, Blacksburg, VA, June, 1981.

4. Meirovitch, L. and Oz, H. "An Assessment of Methods for the Control of Large Space Structures," Proceedings of the 1979 Joint Automatic Controls Conference, Denver, Colorado, June, 1979, pp. 34-41.

5. Balas, M. M. "Some Trends in Large Space Structure Control Theory; Fondest Hopes; Wildest Dreams," Proceedings of the 1979 Joint Automatic Controls Conference, Denver, Colorado, June, 1979, pp. 42-55.

6. Balas, M. J. "Feedback Control of Flexible Systems," IEEE Transactions on Automatic Control, Vol. AC 23, No. 4, August 1978, pp. 673-679.

7. Aubrun, J. N. "Theory of the Control of Structures by Low-Authority Controllers," Journal of Guidance and Control, Vol. 3, No. 5, Sept-Oct, 1980, pp. 444-451.

8. Meirovitch, L. and Baruh, H. "Optimal Control of Damped Flexible Gyroscopic Systems," Journal of Guidance and Control. Vol. 4, No. 2, March-April, 1981, pp. 157-163.

9. Strunce, R. R. and Henderson, T. C. "Application of Modern Controller Design to a Large Space Structure," Second VPI&SU Symposium, Blacksburg, VA, June 1979, pp. 661-676.

10. Meirovitch, L. and Oz, H. "Model-Space Control of Large Flexible Spacecraft Possessing Ignorable Coordinates," Journal of Guidance and Control, Vol. 3, No. 6, Nov-Dec., 1980, pp. 569-577.

11. Kane, T. R. and Levinson, D. A. "Formulation of Motion for Complex Spacecraft," Journal of Guidance and Control, Vol. 3, No. 2, March-April, 1980, pp. 99-112.

12. Hallauer, W. L., Jr. and Barthelemy, J. F. M. "Sensitivity of Modal-Space Control to Non-Ideal Conditions," Journal of Guidance and Control, Vol. 4, No. 4, Sept.-Oct., 1981 (To Appear).

13. Balas, M. J. and Canavin, J. R. "An Active Modal Control System Philosophy for a Class of Large Space Structures," First VPI&SU Symposium, Blacksburg, VA, June 1977, pp. 271-285.

14. Gallagher, R. H. Finite Element Analysis. Prentice Hall, Inc. Englewood Cliffs, NJ, 1975.

15. Benhabib, R. J., Iwens, R. P., Jackson, R. L. "Active Vibration Control of a Flat Plate Using Model Reference Adaptive Techniques," Second VPI&SU Symposium, Blacksburg, VA, June 1979, pp. 317-329.

16. Mason, J. M. "Some Aspects of the Control of Discrete and Continuous Systems," M.S. Thesis, Dept. of Aerospace and Ocean Engrg, VPI&SU, Oct., 1979.

17. Hughes, P. C. and Skelton, R. E. "Modal Truncation for Flexible Spacecraft," Journal of Guidance and Control, Vol. 4, No. 3, May-June 1981, pp. 291-297.

18. Balas, M. J. "Enchanced Modal Control of Flexible Structures via Inovations Feed Through," Second VPI&SU Symposium, Blacksburg, VA, June 1979, pp. 677-700.

19. Juang, J. N. and Rodriguez, G. "Formulations and Applications of Large Structure Actuator and Sensor Placements," Second VPI&SU Symposium, Blacksburg, VA, June 1979, pp. 247-259.

20. Baruh, H. and Meirovitch, L. "On the Placement of Actuators in the Control of Distributed-Parameter Systems," Part 2, Collection of Technical Papers AIAA Dynamics Specialist Conference, April 1981, Atlanta, Georgia, pp. 611-620.

21. Hughes, P. C. and Skelton, R. E. "Controllability and Observability for Flexible Spacecraft," Journal of Guidance and Control, Vol. 3, No. 5, Sept-Oct, 1980, pp. 452-459.

22. Clough, R. W. and Penzien, J. Dynamics of Structures, McGraw-Hill, New York, 1975, pp. 345-350.

23. Narayan, G. V. and Beskos, D. E. "Use of Dynamic Influence Coefficients in Forced Vibration Problems with the Aid of Fast Fourier Transform," Computers and Structures, Vol. 9, 1978, pp. 145-150.

24. Beskos, D. E. and Boley, B. A. "Use of Dynamic Influence Coefficients in Forced Vibration with the Aid of Laplace Transform," Computers and Structures, Vol. 5, 1975, pp. 263-269.

25. Gevarter, W. B. "Basic Relations for Control of Flexible Vehicles," AIAA Journal, Vol. 8, No. 4, Apr. 1970, pp. 666-672.

26. Meirovitch, L. Elements of Vibration Analysis, McGraw-Hill, Inc., New York, 1975, pp. 79-80, 195, 207-208.

27. Lutze, F. H. and Goff, R. M. A. "Application of Classical Techniques to Control of Continuous Systems," Third VPI&SU Symposium, Blacksburg, VA, June 1981.

28. D'Azzo, J. J. and Houpis, C. H. Linear Control System Analysis and Design, McGraw-Hill, Inc., New York, 1975.

29. Parks, P. C. "On How to Shake a Piece of String to a Standstill," Recent Mathematical Developments in Control, Academic Press, 1973, pp. 267-287.

30. Melsa, J. L. and Jones, S. K., Computer Programs for Computational Assistance in the Study of Linear Control Theory, Second Edition, McGraw-Hill, New York, 1973, pp. 114-120.

31. International Mathematical and Statistical Libraries, IMSL, Edition 8, IMSL, Inc., Houston, Texas, July 1980.

32. Balas, M. J. "Direct Velocity Feedback Control of Large Space Structures," Journal of Guidance and Control, Vol. 2, No. 3, May-June, 1979, pp. 252-253.

33. Rosenbrock, H. H. "The Zeros of a System," International Journal of Control, Vol. 18, No. 2, 1973, pp. 297-299.

34. MacFarlane, A. G. J. "A Survey of Recent Results in Linear Multivariable Feedback Theory," Automatica, 1972, Vol. 8, pp. 455-492.

35. Meirovitch, L. Analytical Methods in Vibrations, The Macmillan Co., New York, 1967, pp. 133,135.

36. Timoshenko, S. Vibration Problems in Engineering, D. Van Nostrand Co., Inc., New York, 1937, p. 342.

37. Blevins, R. D. Formulas for Natural Frequency and Mode Shape, Van Nostrand Reinhold Co., New York, 1979, p. 108.

38. Wang, B. P. and Pilkey, W. D. "Optimal Damper Location in the Vibration Control of Large Space Structures," Third VPI&SU Symposium, Blacksburg, VA, June 1981.

39. Aubrun, J. N. "Theory of the Control of Structures by Low-Authority Controllers," AIAA Journal of Guidance and Control, Vol. 3, No. 5, Sept-Oct 1980, pp. 444-451.

40. Meirovitch, L. Computational Methods in Structural Dynamics, Sijthoff and Noordhoff, 1980, p. 265.

41. Thomson, W. T. Theory of Vibrations with Applications, Prentice-Hall, Englewood Cliffs, NJ, 1981, pp. 218.

42. Wie, B. and Bryson, A. E., Jr. "Modeling and Control of Flexible Space Structures," Third VPI&SU Symposium, Blacksburg, VA, June 1981.

43. Poelaert, D., "A Distributed Element Technique for Dynamic Analysis of Flexible Space Structure," Second VPI&SU Symposium, Blacksburg, VA, June 1979, pp. 495-510.

APPENDIX A

NOMINAL VALUES OF EXAMPLE GRAPHITE-EPOXY BEAM

Length = 100 meters

Outside radius = 10.55 cm

Wall thickness = 2.275 mm

Tensile and compressive modulus, $E = 3.45 \times 10^{11}$ n/m^2

Mass density = 1607 $\frac{kg}{m^3}$

Area moment of inertia, $I = 8.1 \times 10^{-6}$ m^4

The mass per unit length, $m(x) = 2.397$ $\frac{kg}{m}$

Useful factors--using the above values

$$\sqrt{\frac{EI}{mL^4}} = 0.108$$

$$\frac{\sqrt{EIm}}{L} = 25.88$$

$$\frac{2EI}{L^3} = 5.589$$

APPENDIX B

BEAM ELEMENT DYNAMIC STIFFNESS MATRIX IN THE LAPLACE TRANSFORM PLANE

$$\begin{Bmatrix} f_1 \\ M_1 \\ f_2 \\ M_2 \end{Bmatrix} = \frac{EI}{\Delta} \begin{bmatrix} 4\alpha^3(S\cdot C + Sh\cdot Ch) & -2\alpha^2(C^2Sh^2 + Ch^2S^2) & -4\alpha^3(Sh\cdot C + S\cdot Ch) & -4\alpha^2(Sh\cdot S) \\ — & 2\alpha(Sh\cdot Ch - S\cdot C) & 4\alpha^2(Sh\cdot S) & 2\alpha(S\cdot Ch - C\cdot Sh) \\ \text{SYMMETRIC} & — & 4\alpha^3(S\cdot C + Sh\cdot Ch) & 2\alpha^2(C^2Sh^2 + Ch^2S^2) \\ — & — & — & 2\alpha(Sh\cdot Ch - S\cdot C) \end{bmatrix} \begin{Bmatrix} \delta_1 \\ \theta_1 \\ \delta_2 \\ \theta_2 \end{Bmatrix}$$

where:

$Sh = \sinh\alpha L$

$Ch = \cosh\alpha L$

$S = \sin\alpha L$

$C = \cos\alpha L$

$\Delta = Sh^2 - S^2$

and

$$\alpha = \sqrt[4]{\frac{ms^2}{4EI}}$$

Table 1 Gain Required for Frequency Changes

ω_o	1.570	4.712	7.854	10.996
$\Delta\omega$				
0	0	0	0	0
.2	0.359	0.996	1.633	2.269
.4	0.833	2.161	3.490	4.818
.6	1.485	3.634	5.764	7.933
.8	2.441	5.676	8.910	12.145
1.0	4.003	8.897	13.789	18.682
1.2	7.127	15.203	23.288	31.369
1.4	17.224	35.439	53.653	71.868

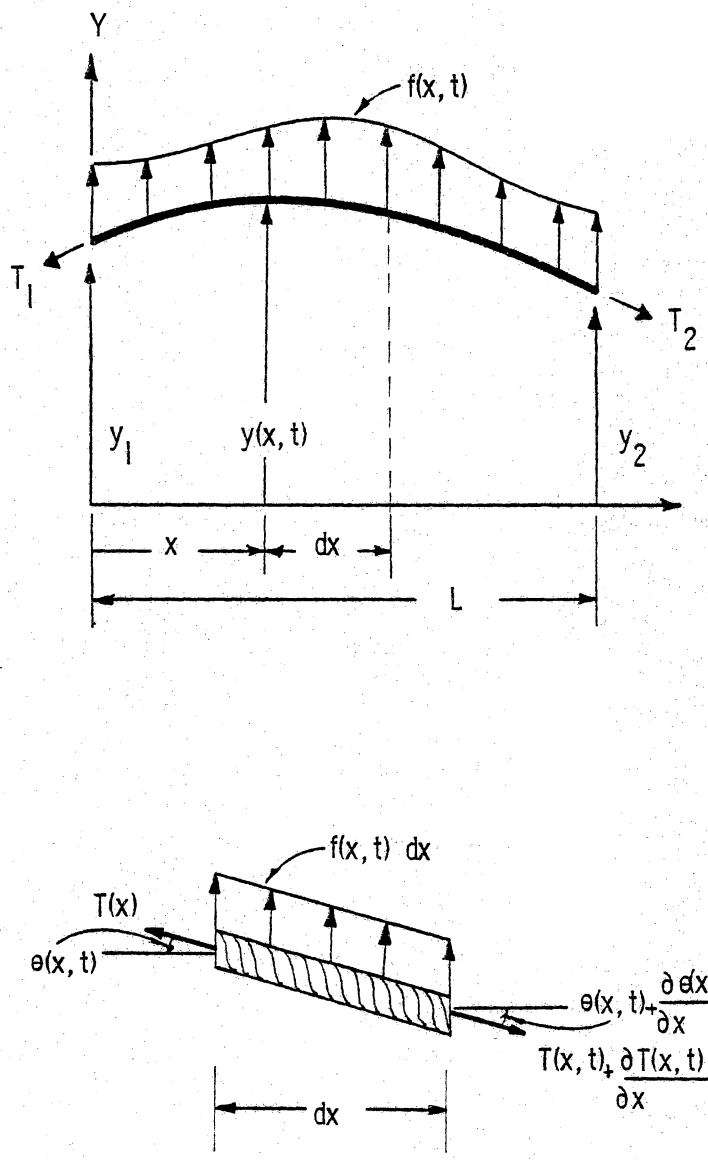

Figure 1. Cable Element

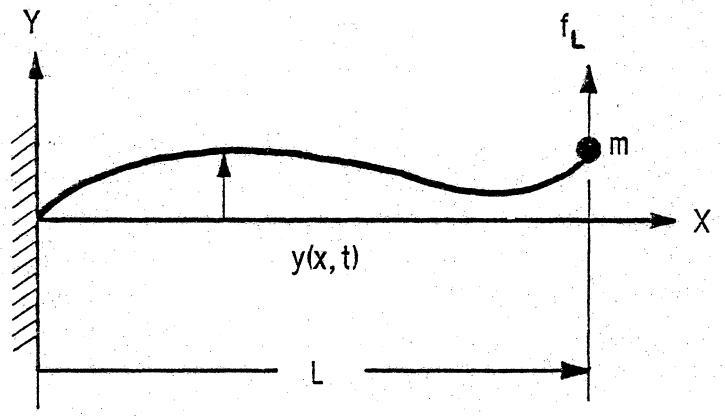

(a)

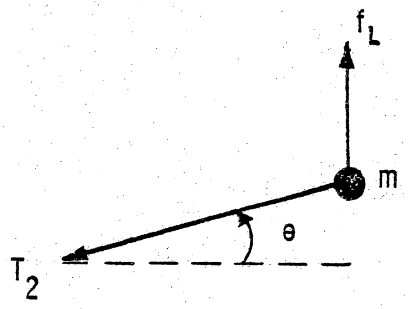

(b) free body diagram

Figure 2. Fixed-free cable--discrete mass at end

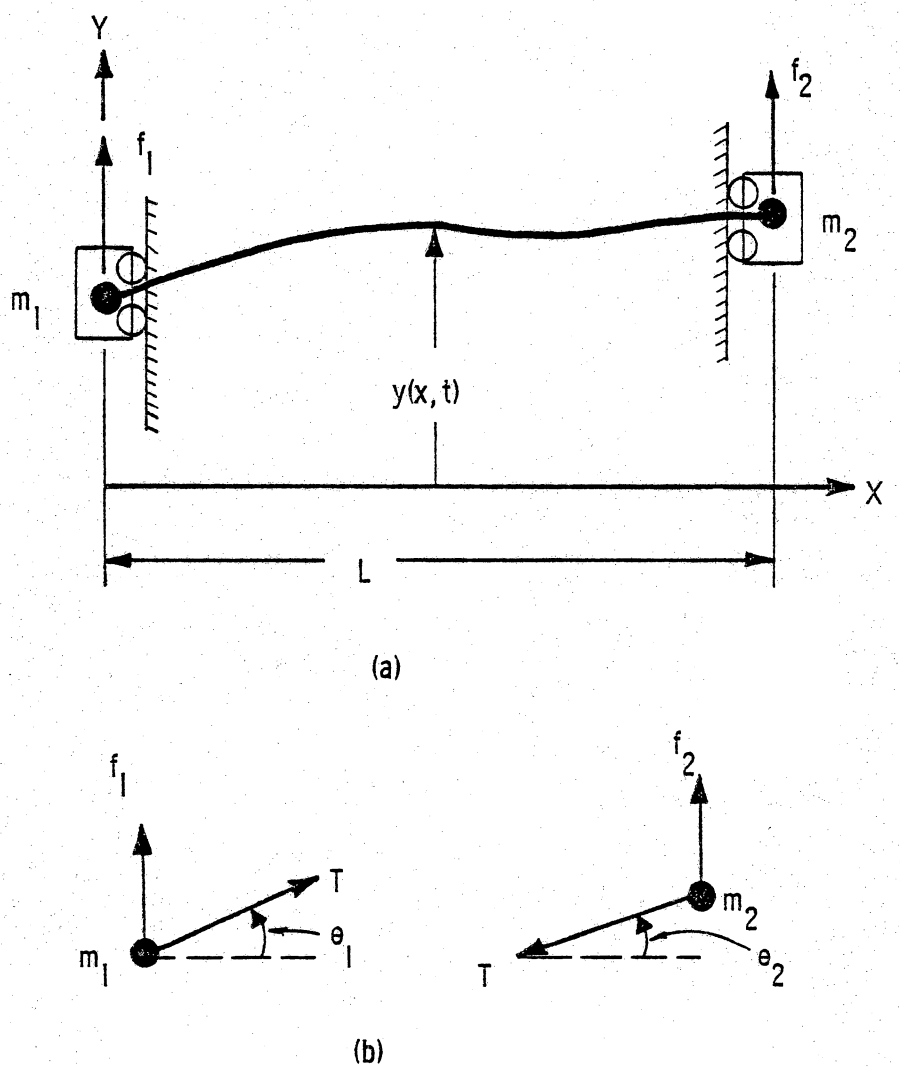

Figure 3. Free-Free Cable--Discrete Mass at Both Ends

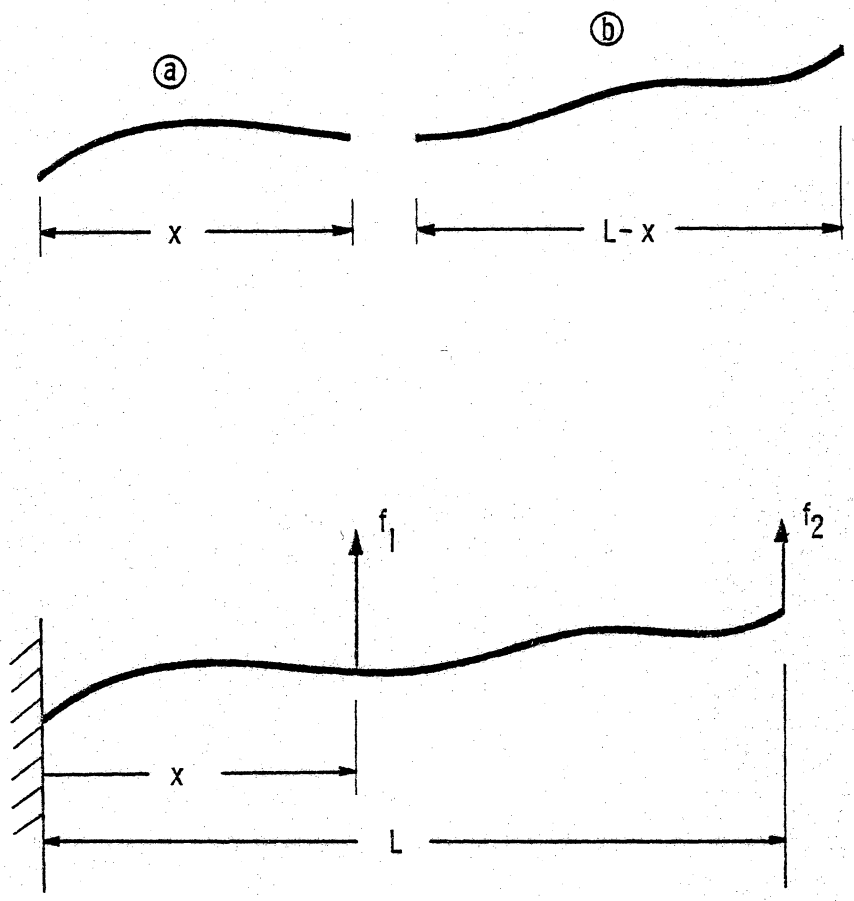

Figure 4. Fixed-Free Cable--Interior and end forces

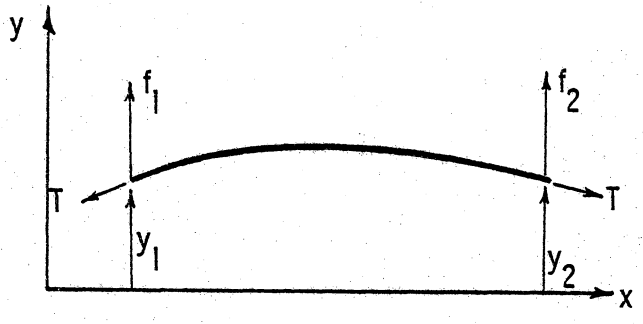

(A Single Cable Element)

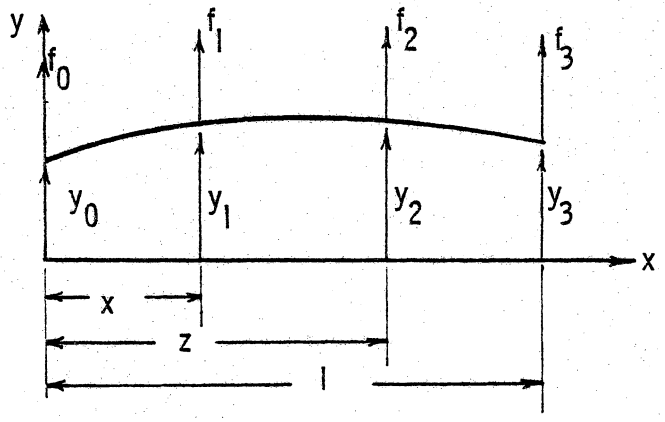

Figure 5. Cable with Several Elements

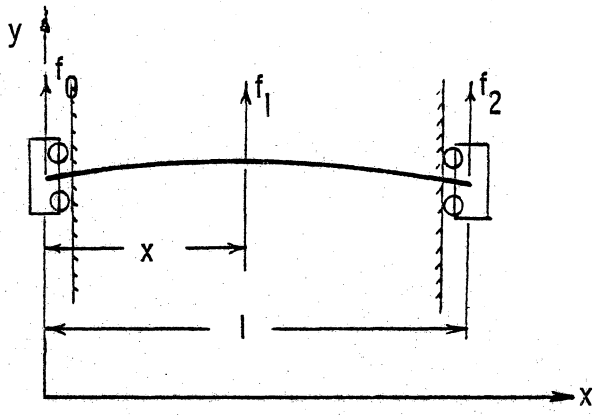

Figure 6. Free-Free Cable

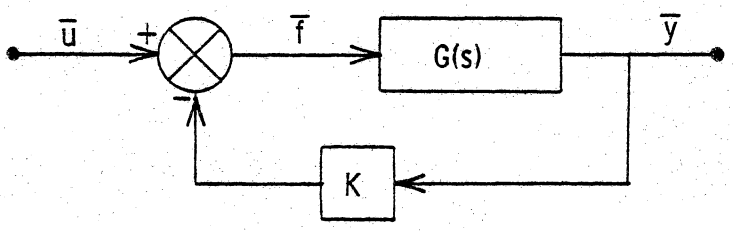

Figure 7. Feedback System

$$\frac{y(x,s)}{f(l,s)} = \frac{\sinh xs}{s \cosh s} = G(s)$$

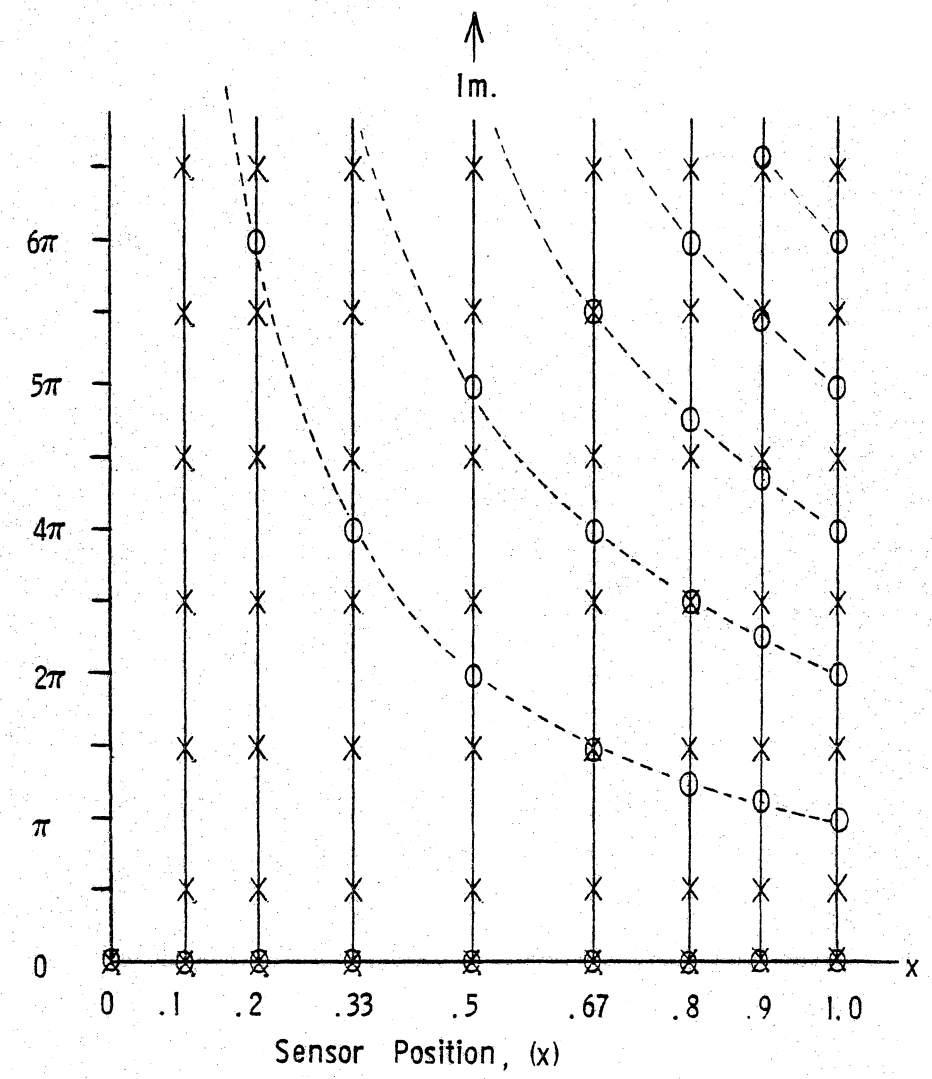

Figure 8. Open-Loop Pole-Zero Locations for Various Sensor Positions (Fixed-Free Cable)

Characteristic Equation

$$\cosh s + K \sinh s = 0$$

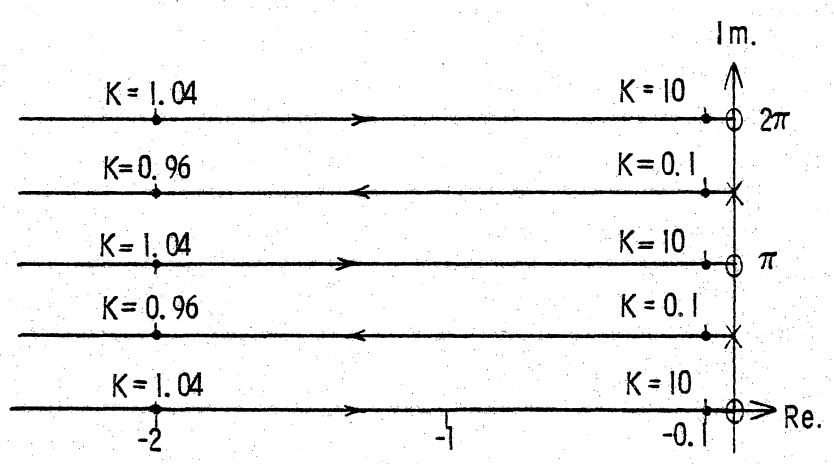

Figure 9. End-End Velocity Feedback Root locus
(Fixed-Free Cable)

$$s \cosh s + K \sinh xs = 0$$

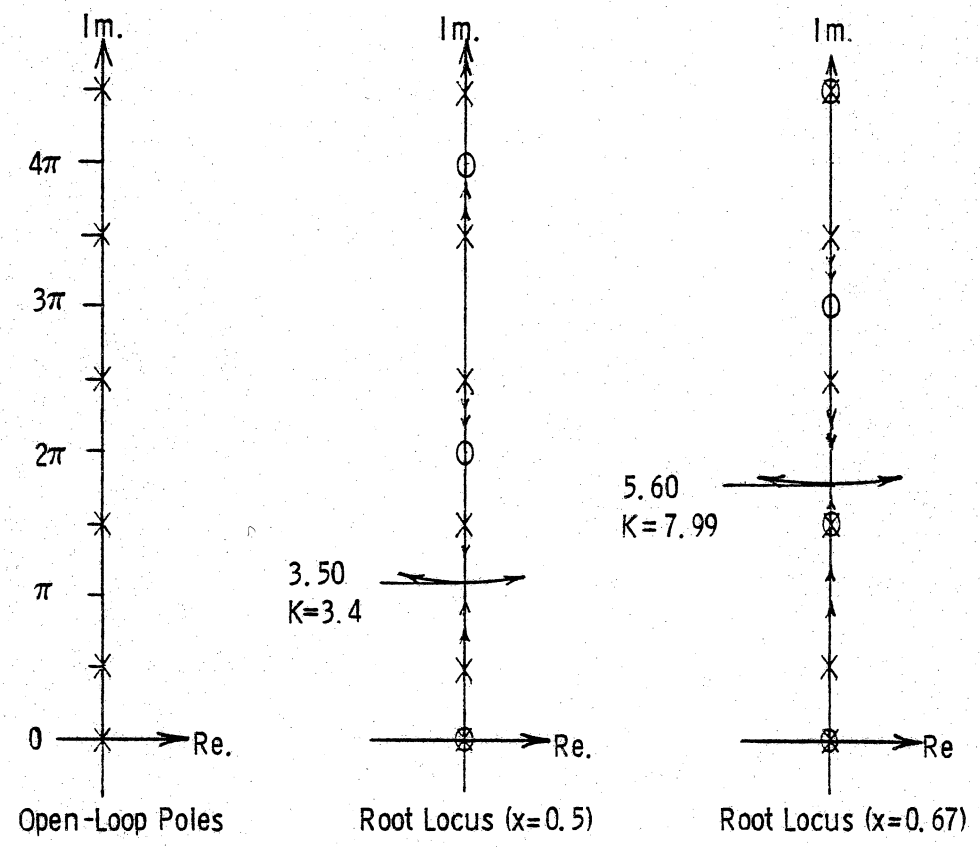

Figure 10. Displacement Feedback to End, x=0.5, 0.67, (Fixed-Free Cable)

$$\cosh s + K \sinh xs = 0$$

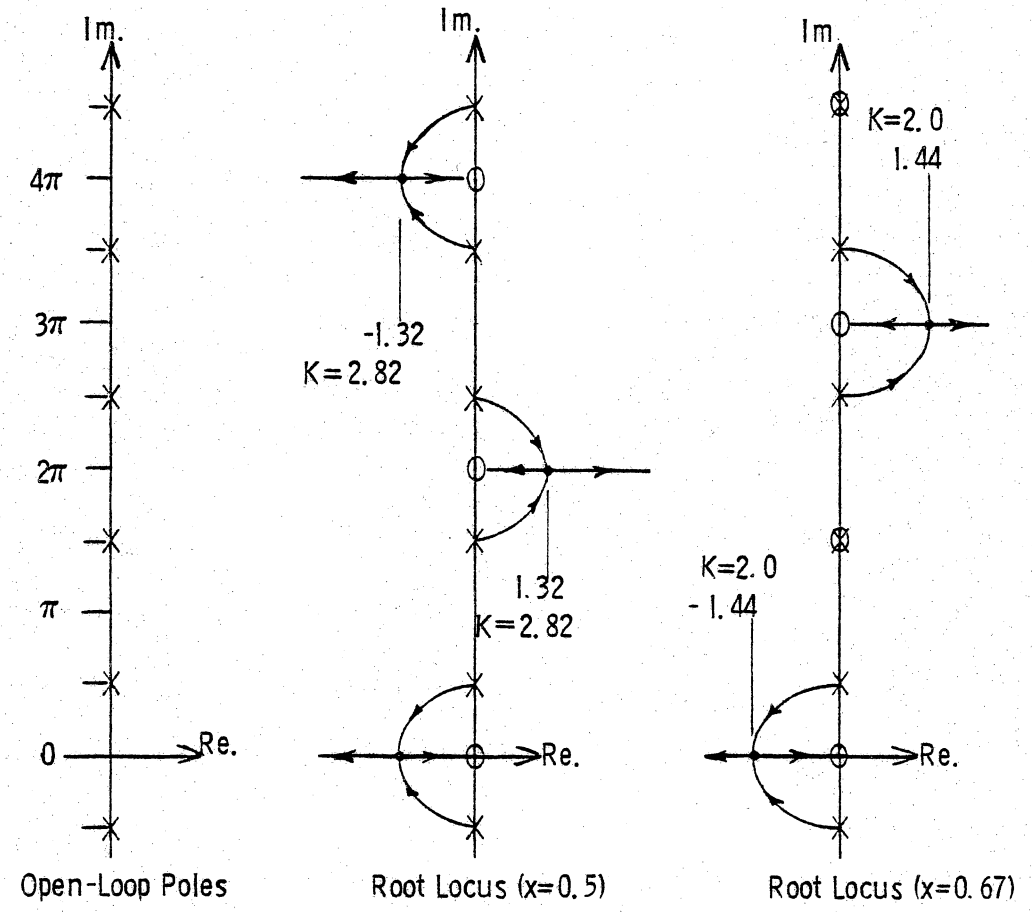

Figure II. Velocity Feedback to End, x=0.5, 0.67, (Fixed-Free Cable)

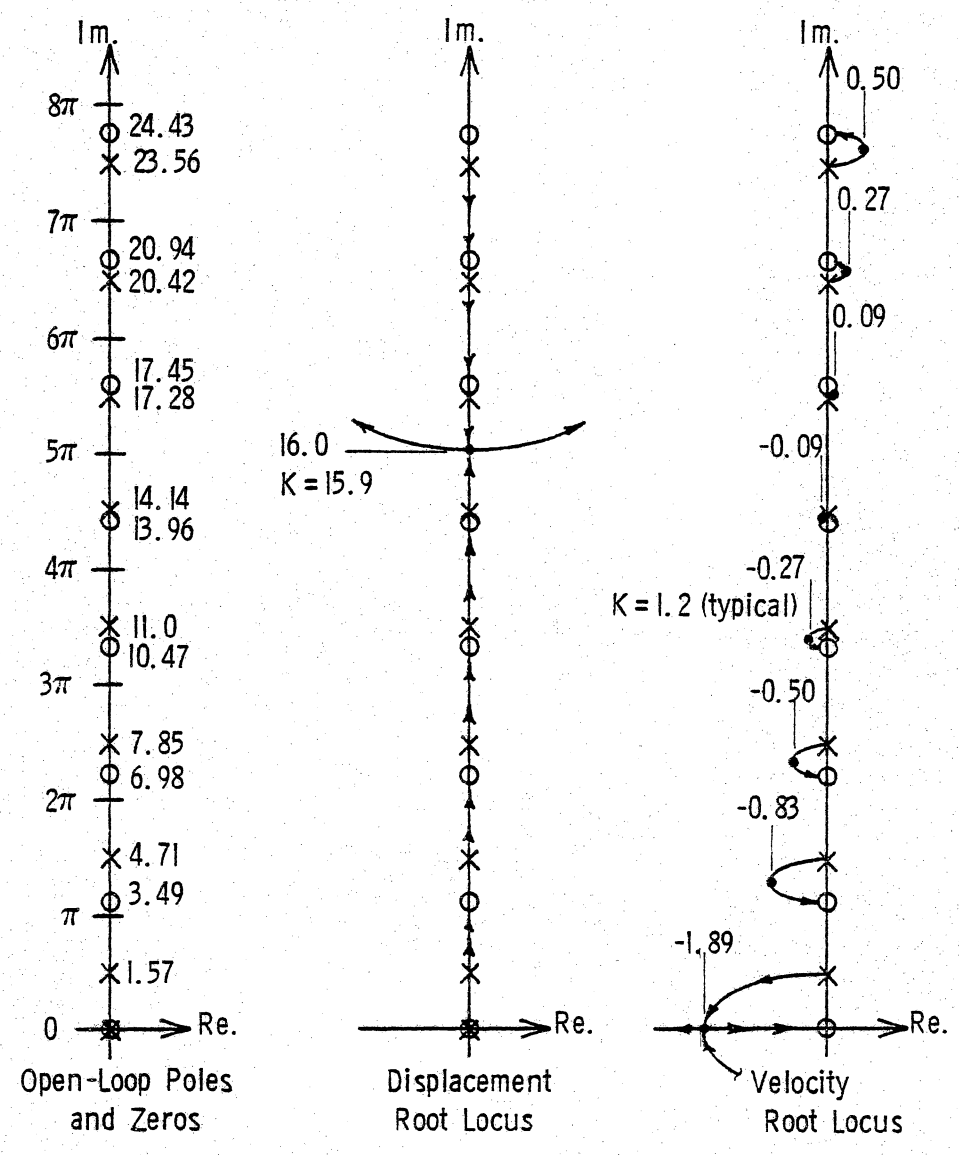

Figure 12. Velocity and Displacement Feedback to End, $x = 0.9$, (Fixed-Free Cable)

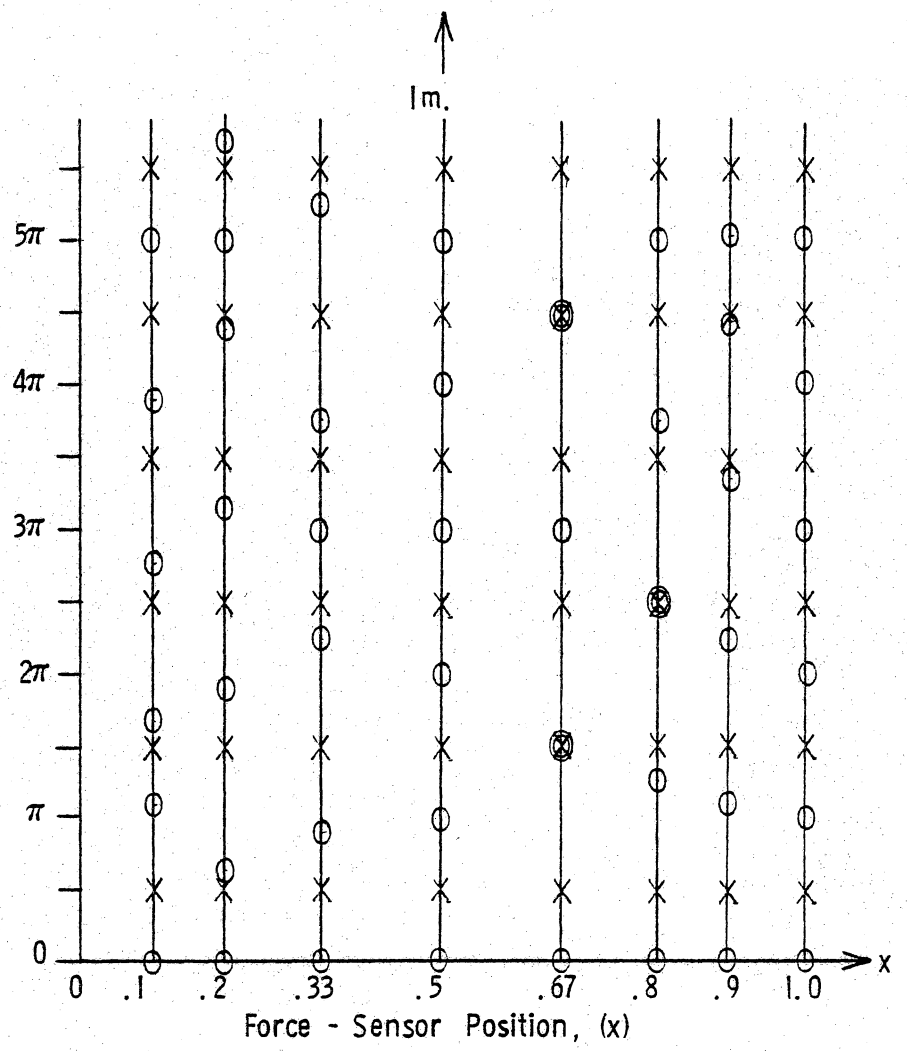

Figure 13. Open-Loop Pole-Zero Locations, Velocity Feedback to Co-located Force, (Fixed-Free Cable)

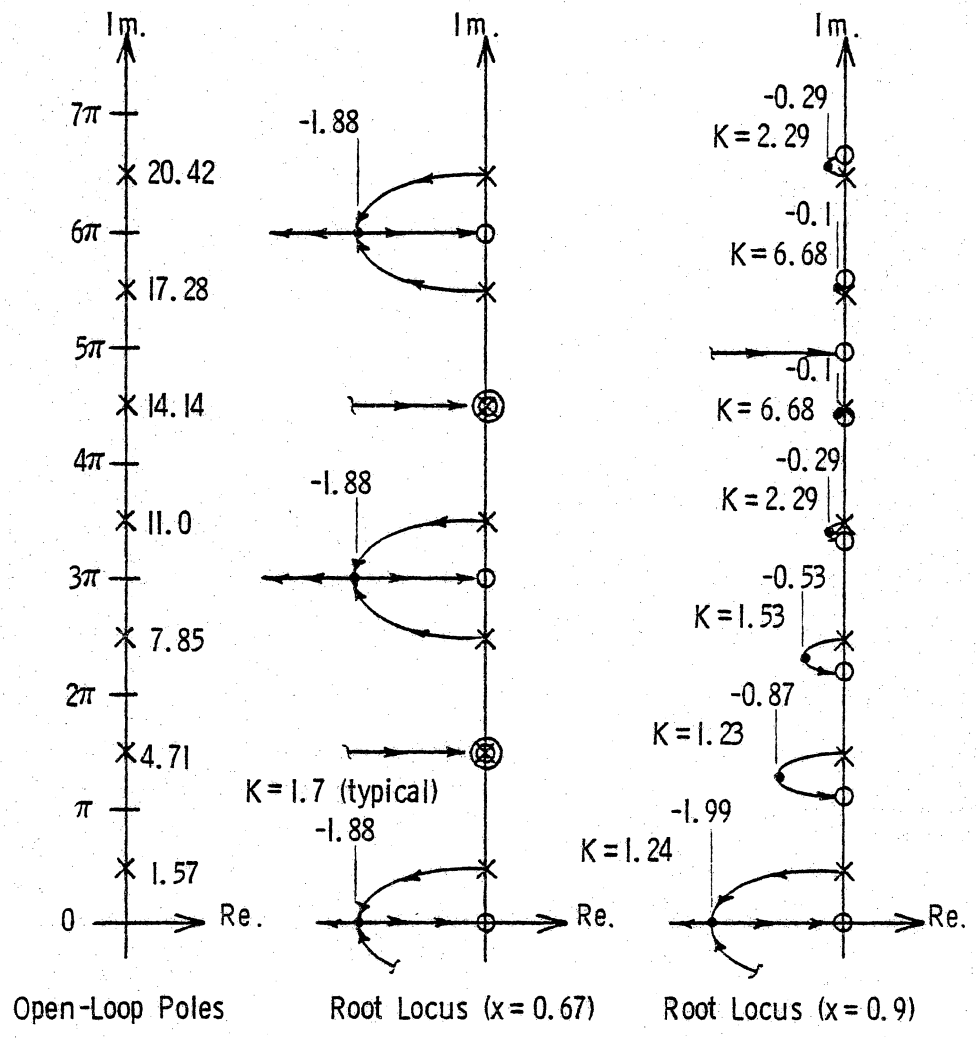

Figure 14. Velocity Feedback to Co-located Force, x = 0.67, 0.9, (Fixed-Free Cable)

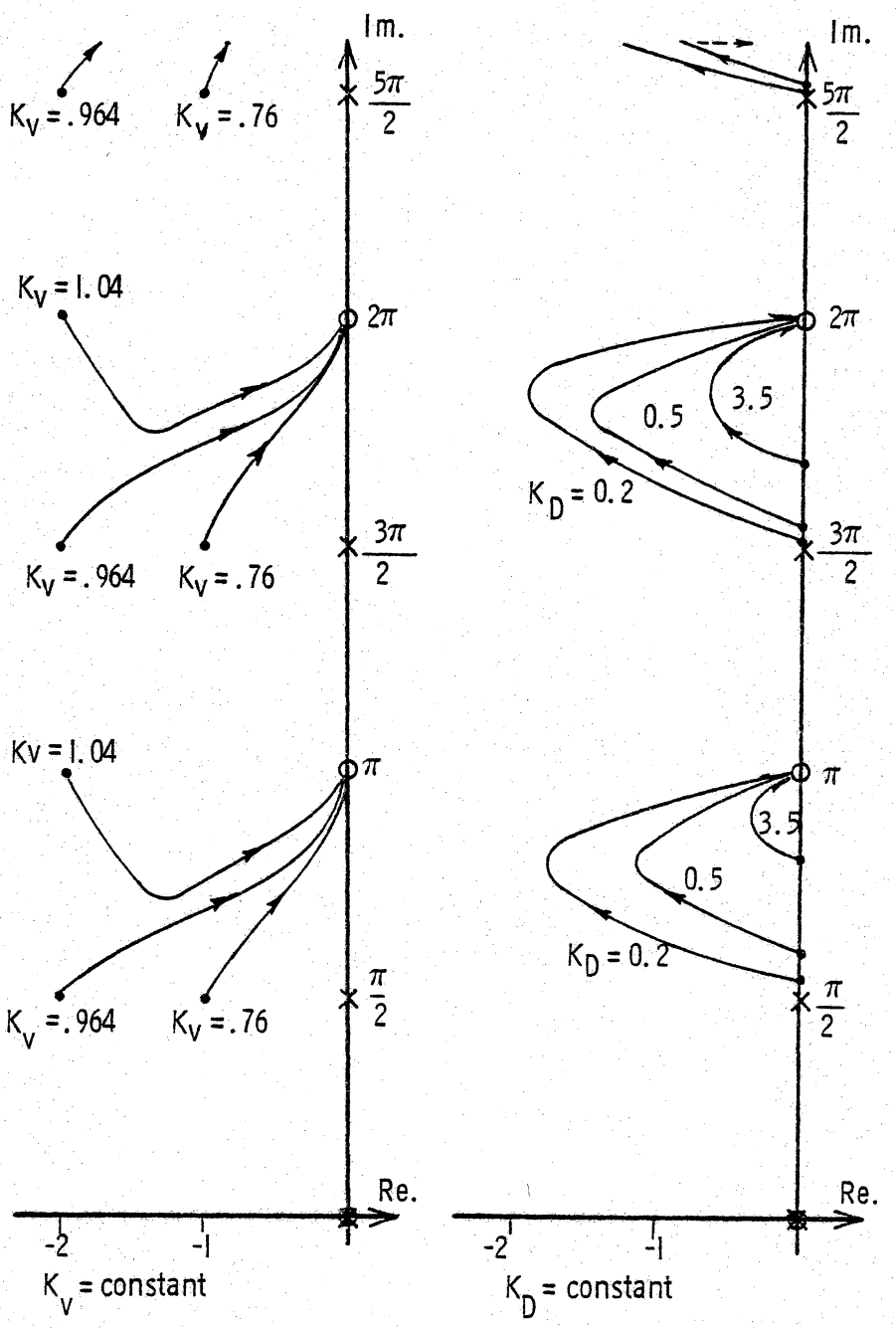

Figure 15. End-End Velocity with Displacement Feedback, Two Gain Root Loci, (Fixed-Free Cable)

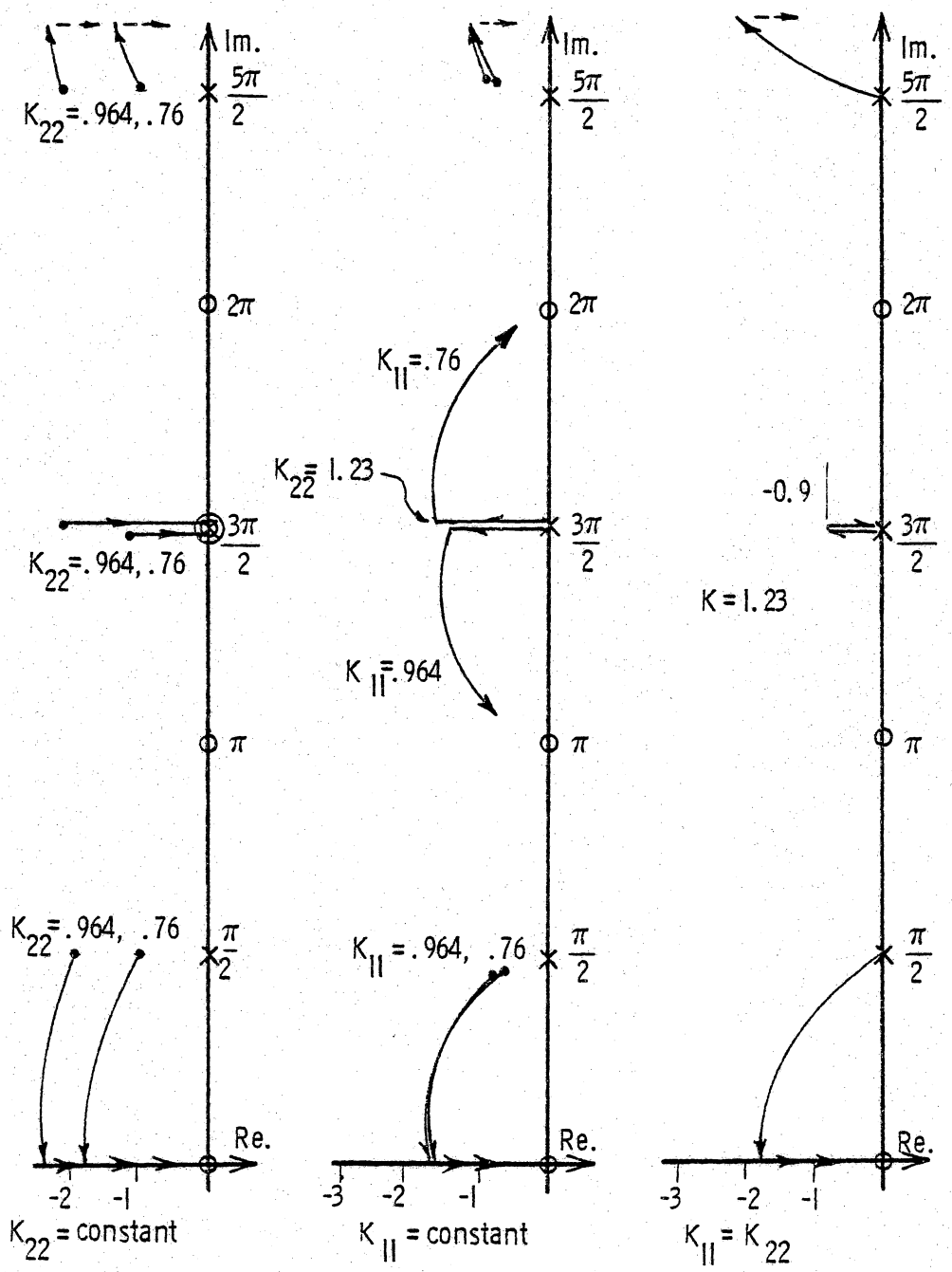

Figure 16. Velocity Feedback to Co-located Forces, x = 0.67, 1.0, Two Gain Root Loci, (Fixed-Free Cable)

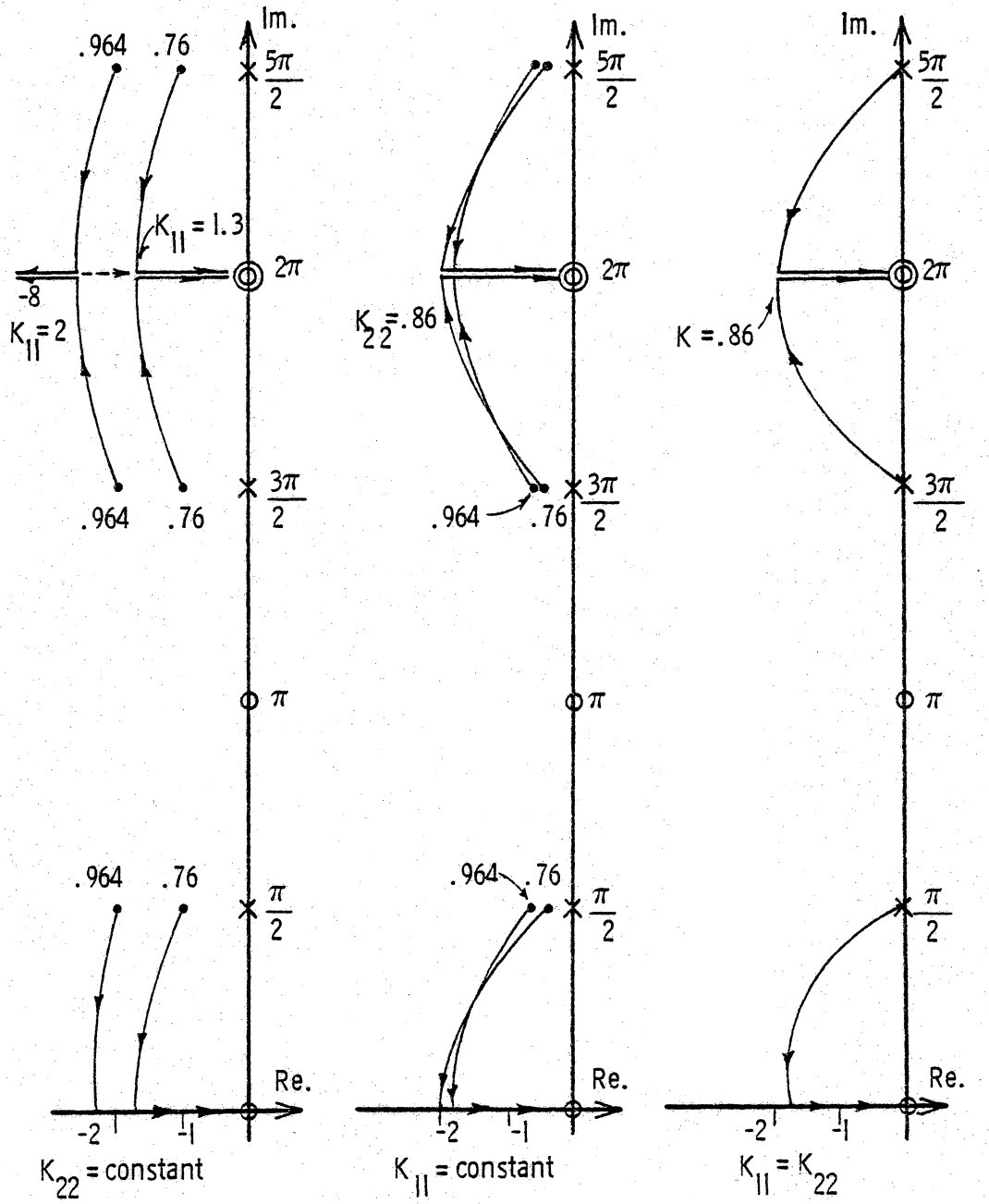

Figure 17. Velocity Feedback to Co-located Forces, x = 0.5, 1.0, Two-Gain Root Loci, (Fixed—Free Cable)

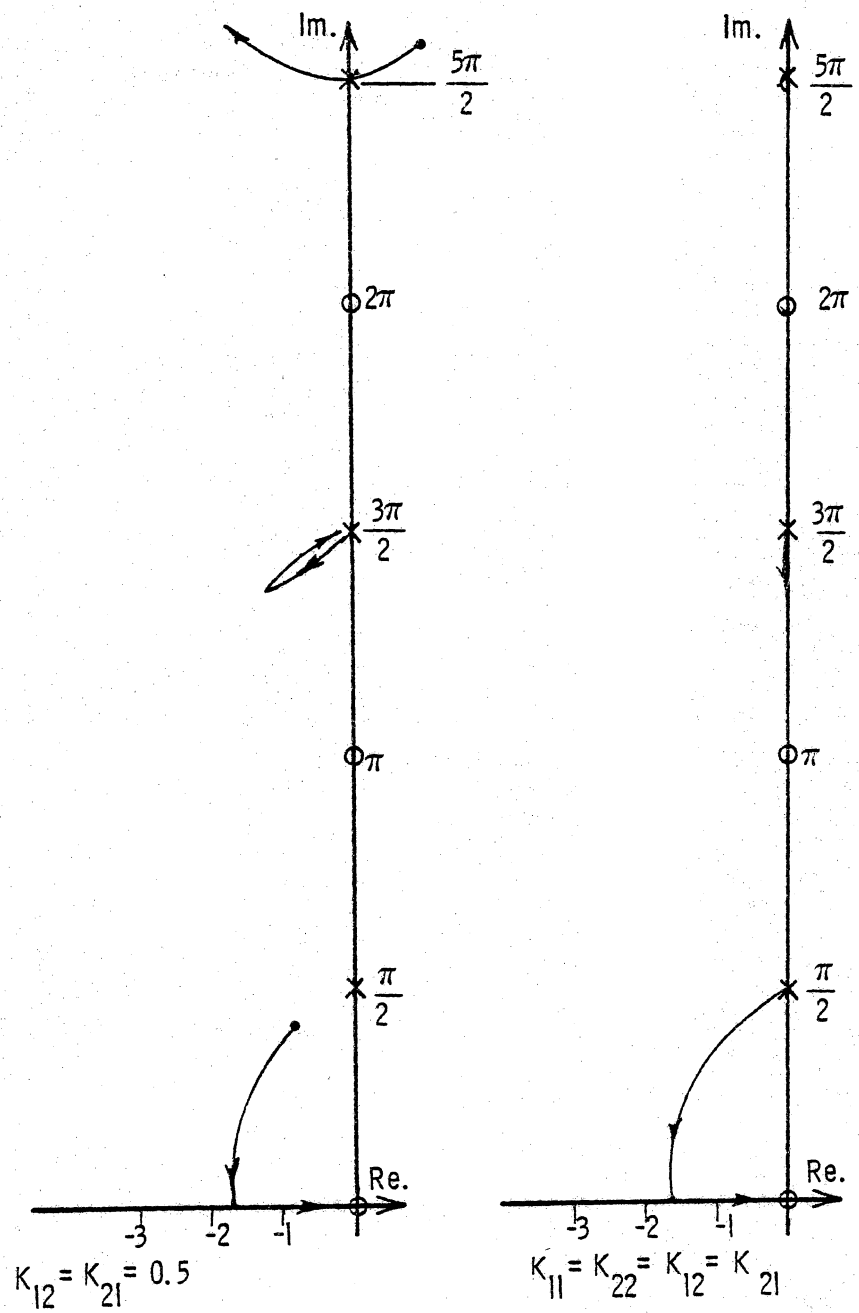

Figure 18. Velocity Feedback to Co-located Forces, with Cross-Gain, x =0.67, 1.0, Four Gain Root Loci, (Fixed-Free Cable)

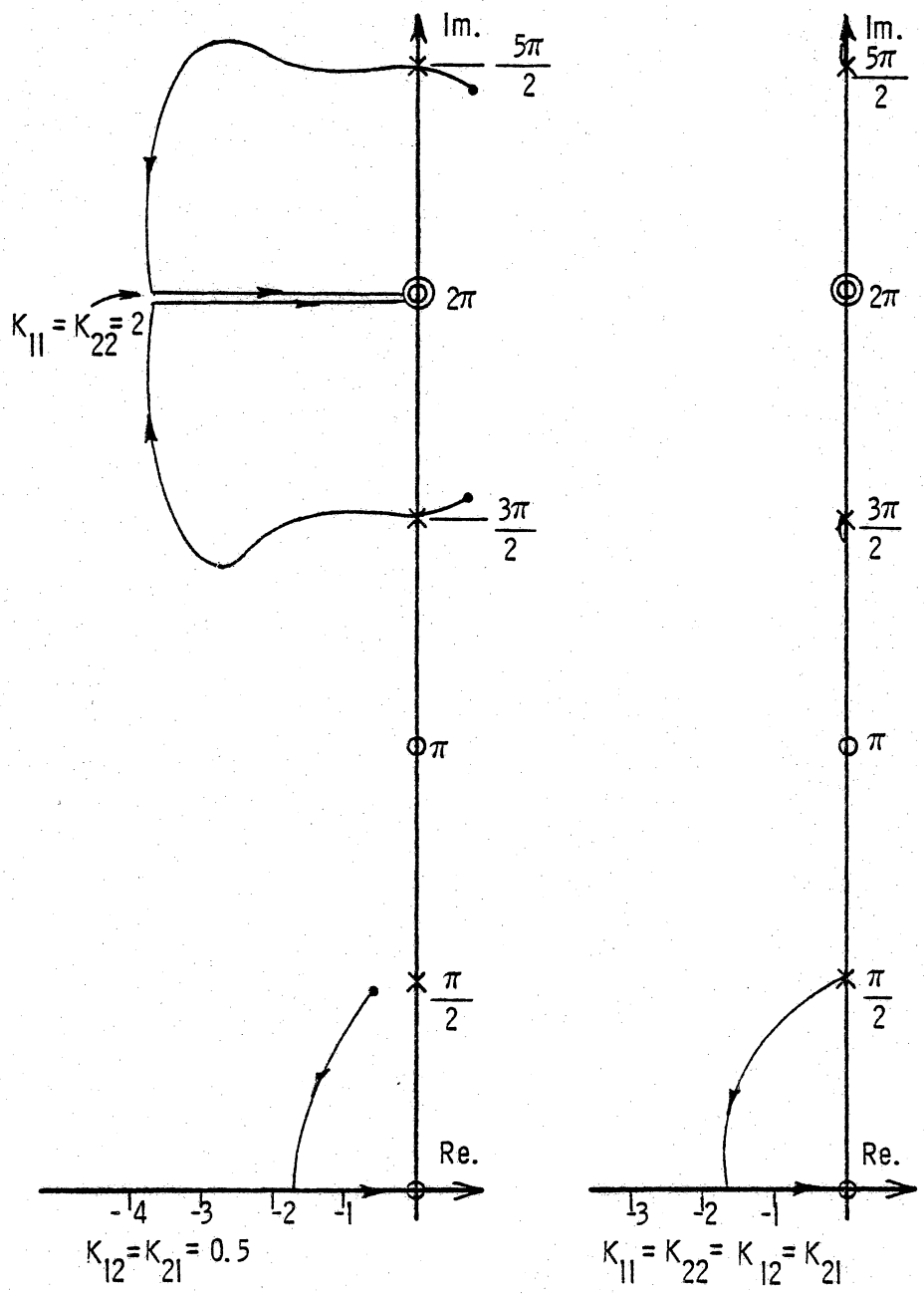

Figure 19. Velocity Feedback to Co-located Forces, with Cross-Gain, x = 0.5, 1.0, Four Gain Root Loci, (Fixed-Free Cable)

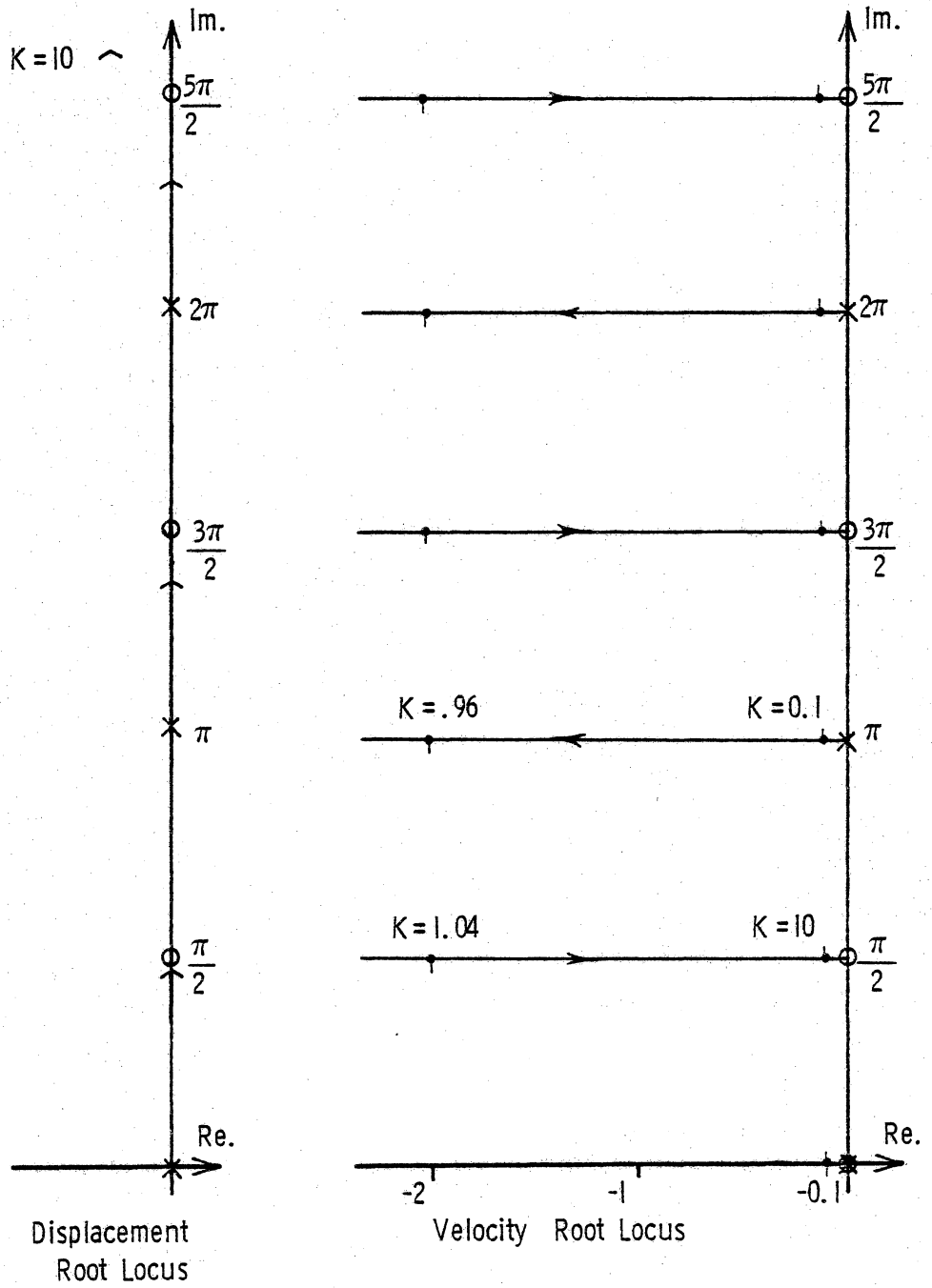

Figure 20. Displacement and Velocity Feedback to Co-Located Force at One End, (Free-Free Cable)

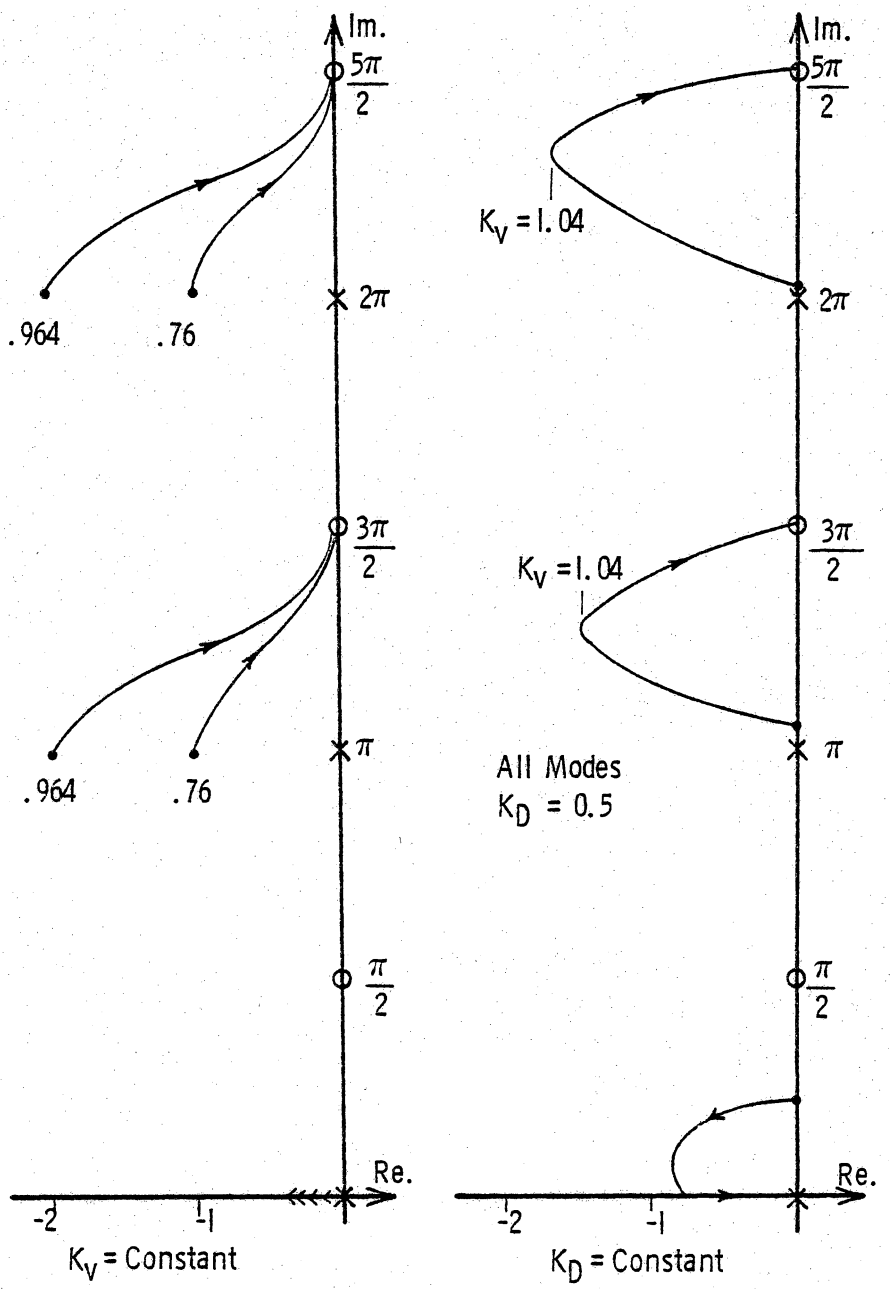

Figure 21. Velocity with Displacement Feedback to Co-Located Force at One End, Two Gain Root Loci, (Free-Free Cable)

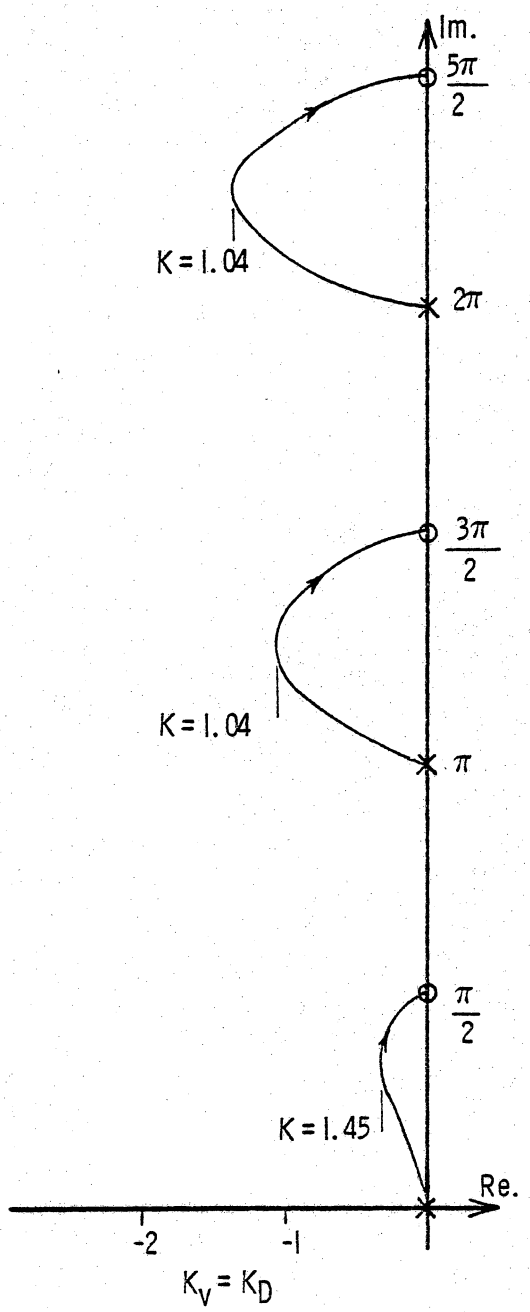

Figure 22. Velocity with Displacement Feedback to Co-Located Force at One End, Two Gain Root Loci, (Free-Free Cable)

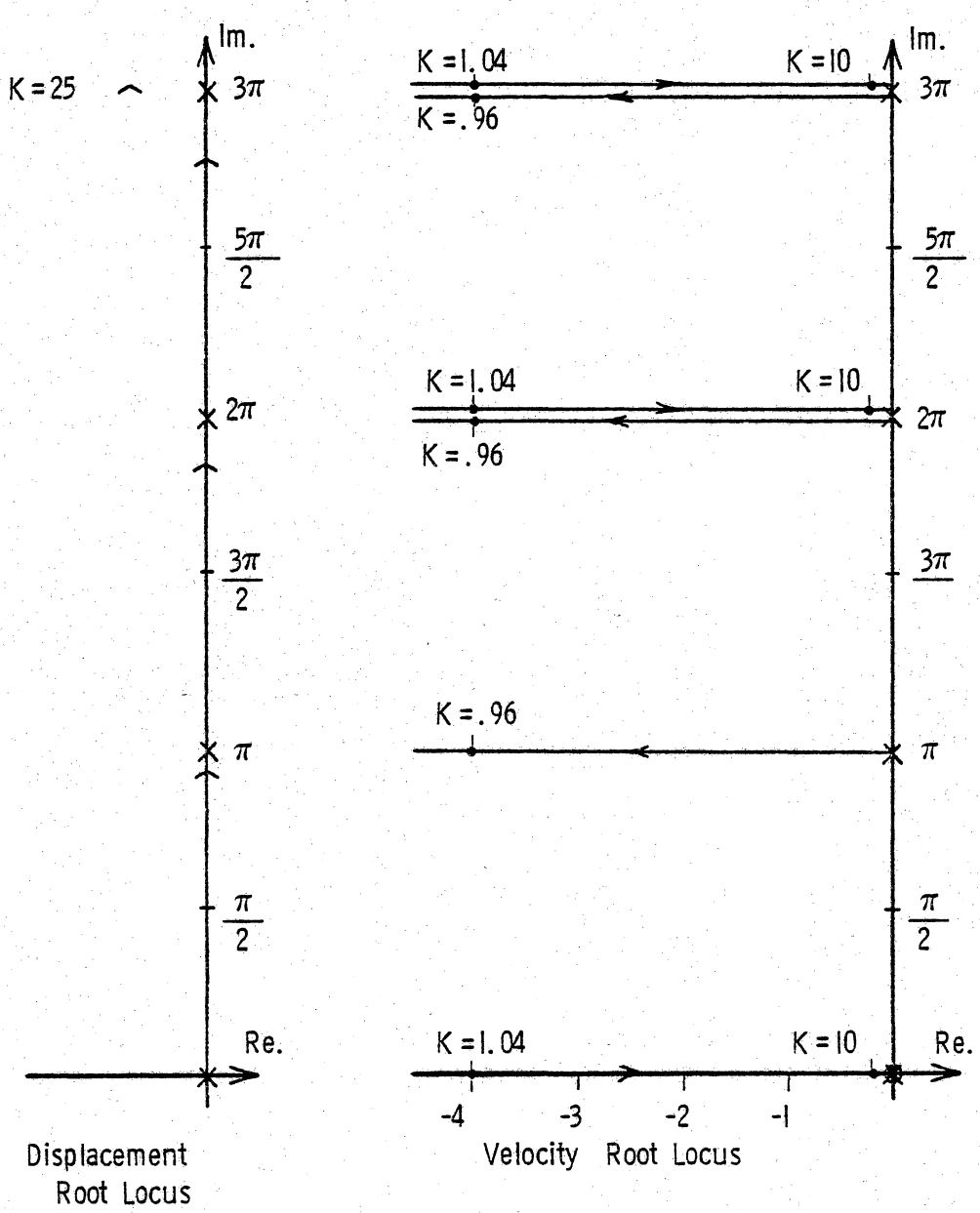

Figure 23. Displacement and Velocity Feedback to Co-Located Forces at Both Ends, (Free-Free Cable)

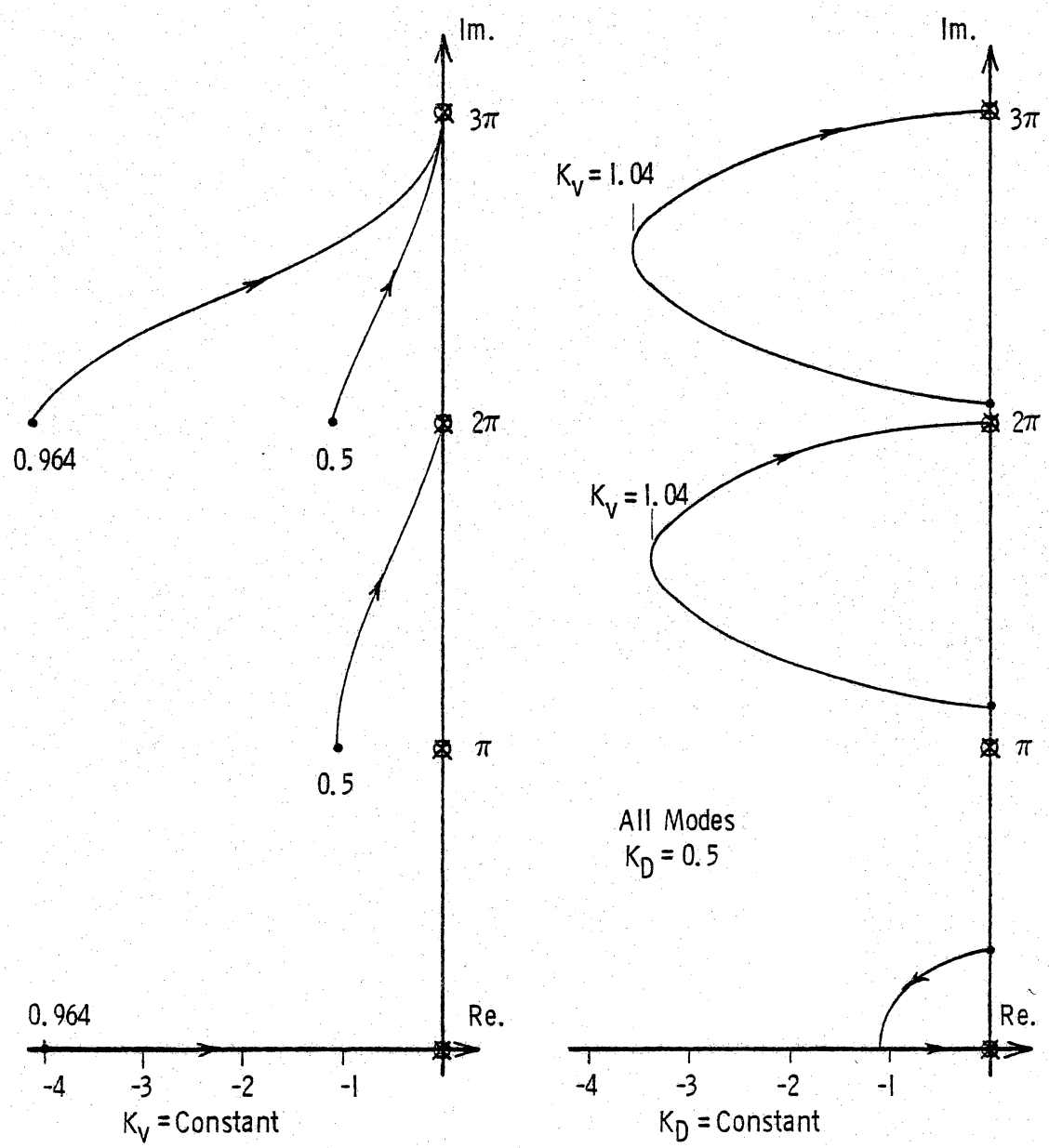

Figure 24. Velocity with Displacement Feedback to Co-Located Forces at Both Ends, Two Gain Root Loci, (Free-Free Cable)

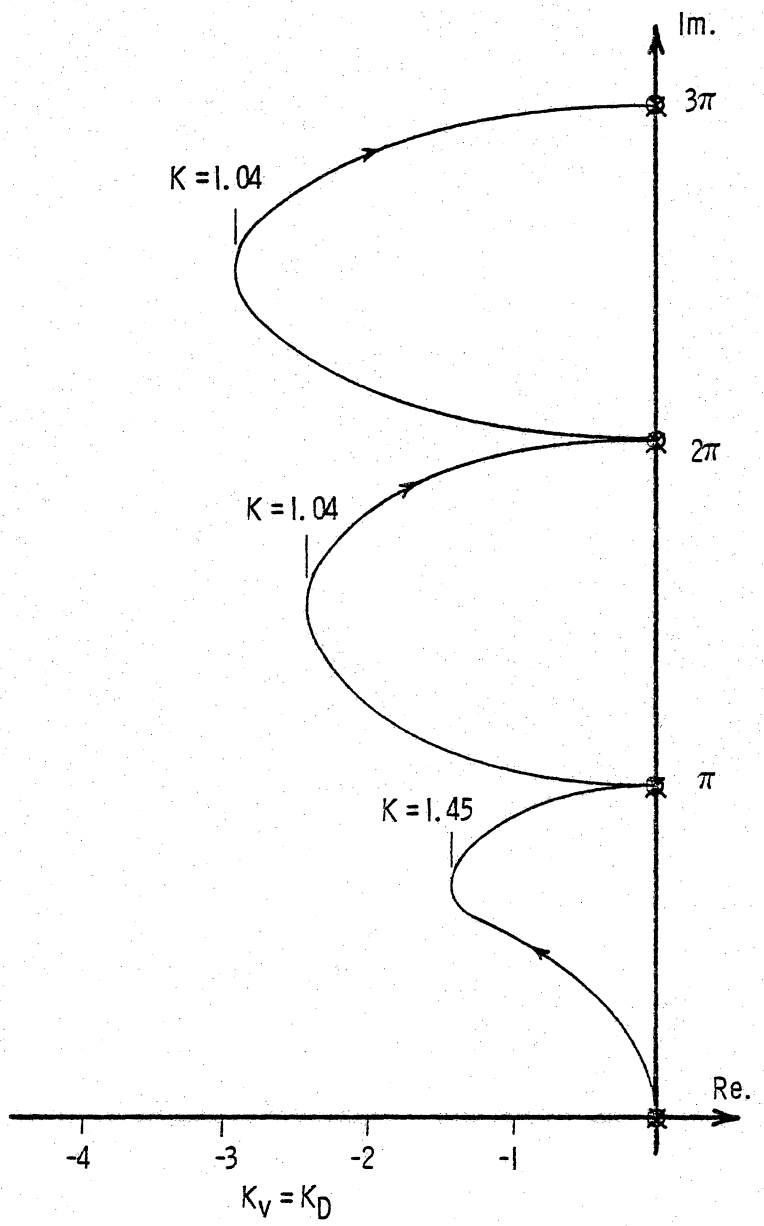

Figure 25. Velocity with Displacement Feedback to Co-Located Forces at Both Ends, Two Gain Root Loci, (Free- Free Cable)

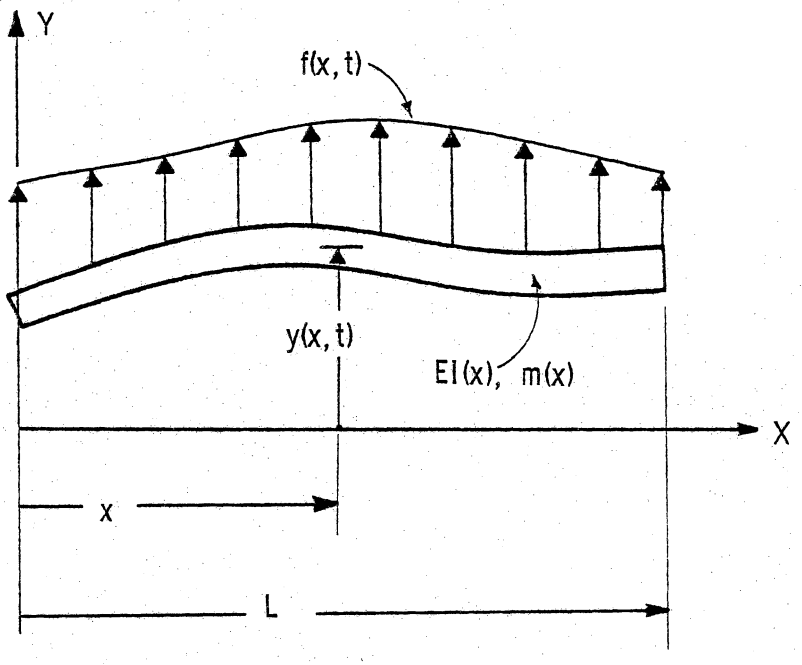

Figure 26. Beam in Bending Vibration

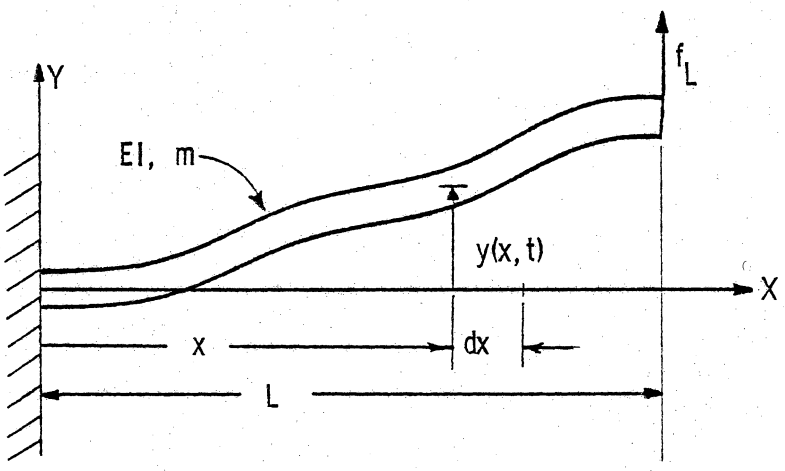

(a) cantilever beam

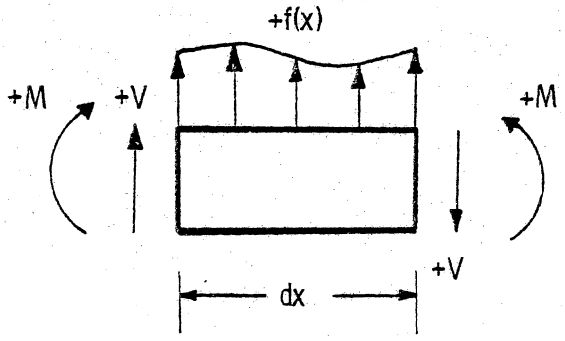

(b)

Figure 27. Cantilever Beam in Bending Vibration, Control Force at Free End

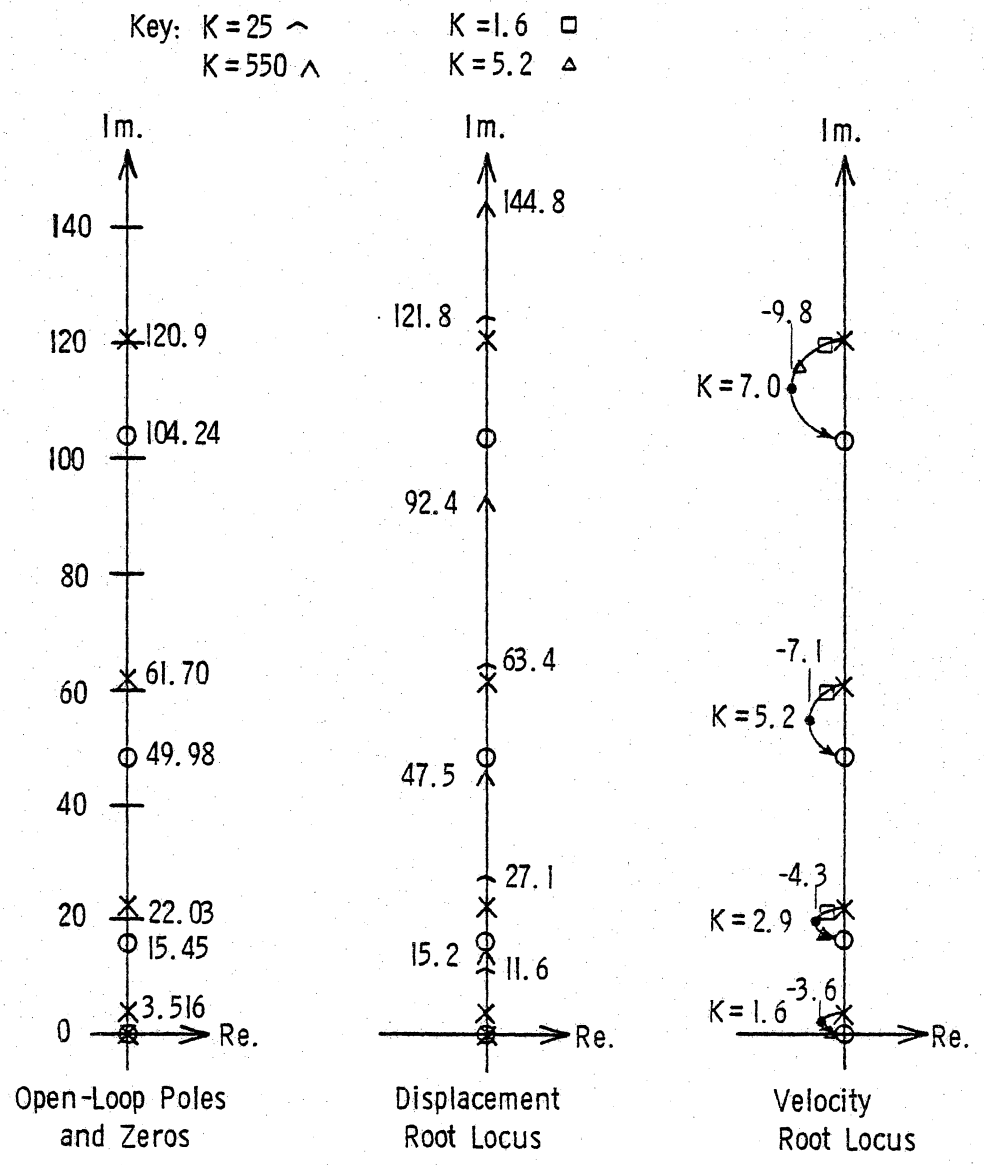

Figure 28. Velocity and Displacement Feedback, End - End, (Cantilever Beam)

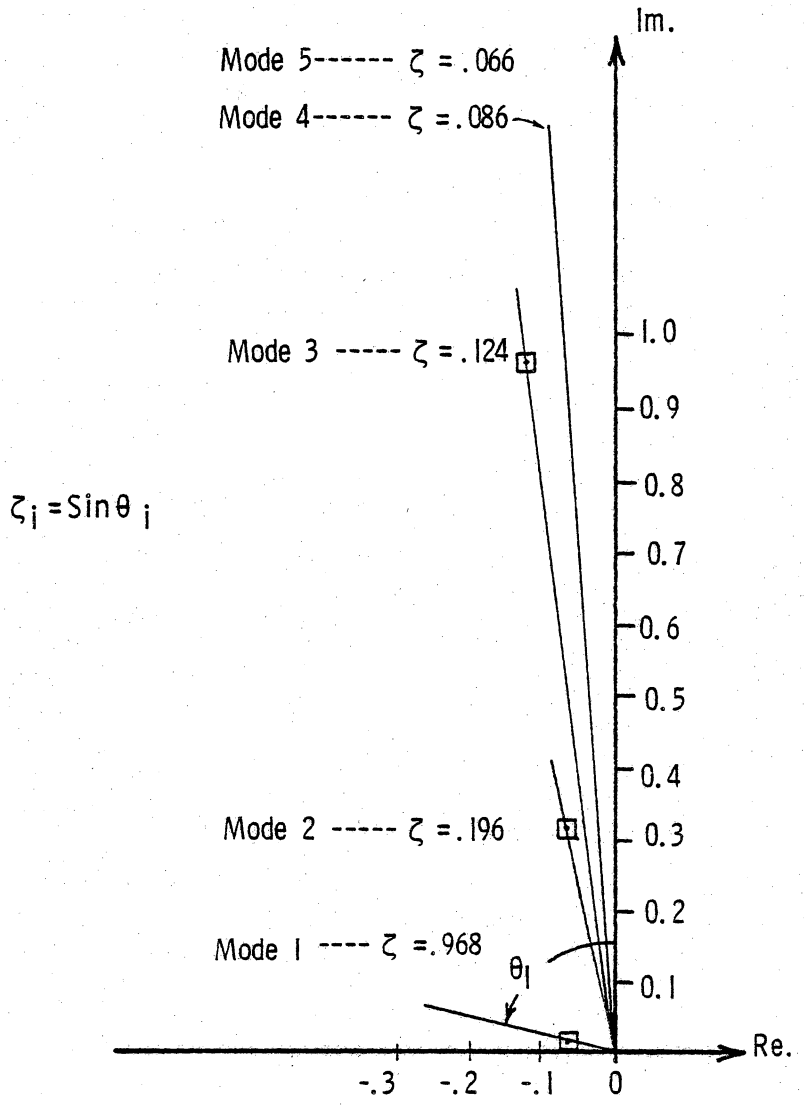

Figure 29. Maximum Damping Ratios for Each Mode, Velocity Feedback, End to End, (Example Graphite-Epoxy Cantilever Beam)

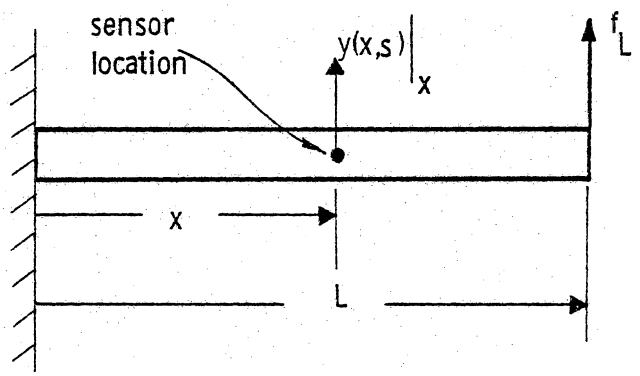

Figure 30. Cantilever Beam, Arbitrary Sensor Location, Force at the Free End

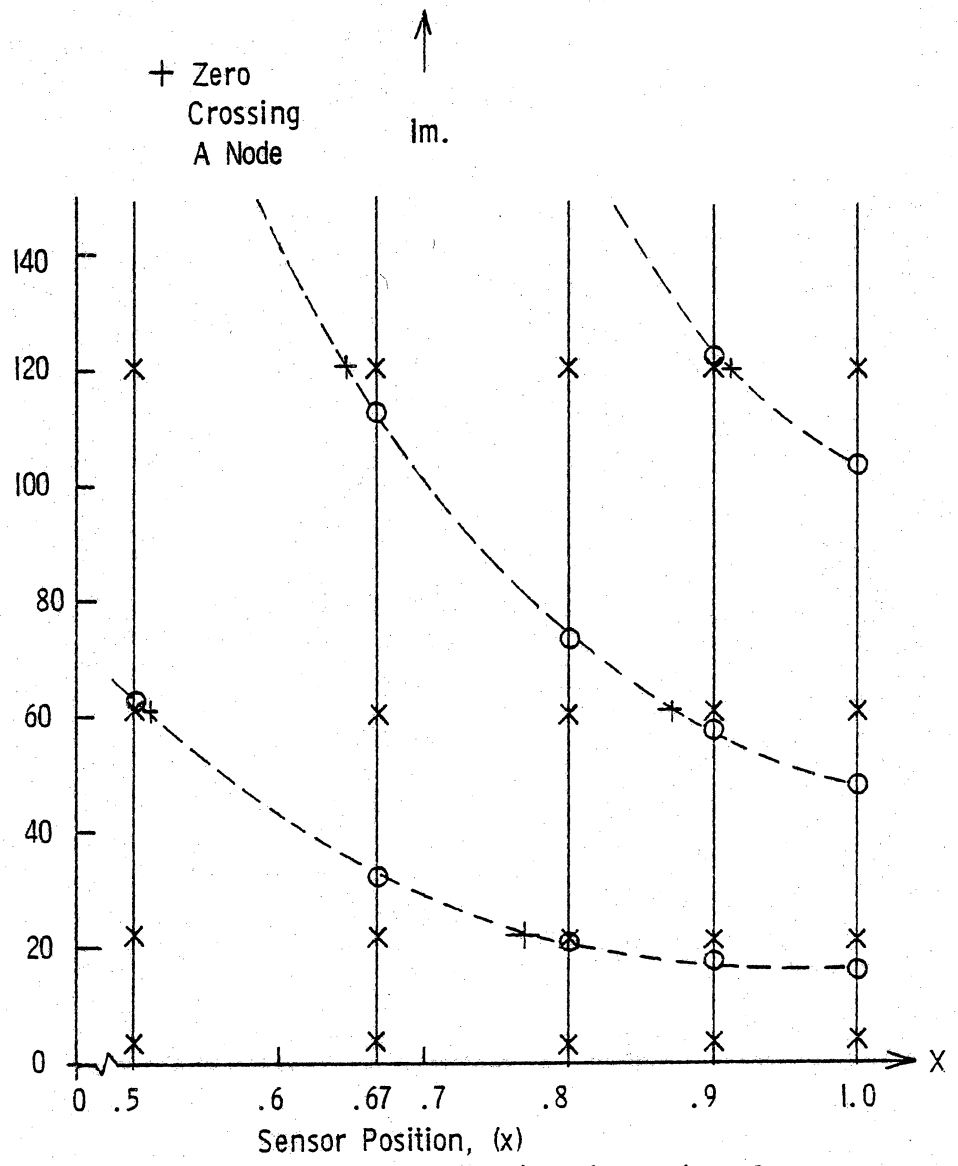

Figure 31. Open-Loop Pole-Zero locations for Various Sensor Positions, (Cantilever Beam)

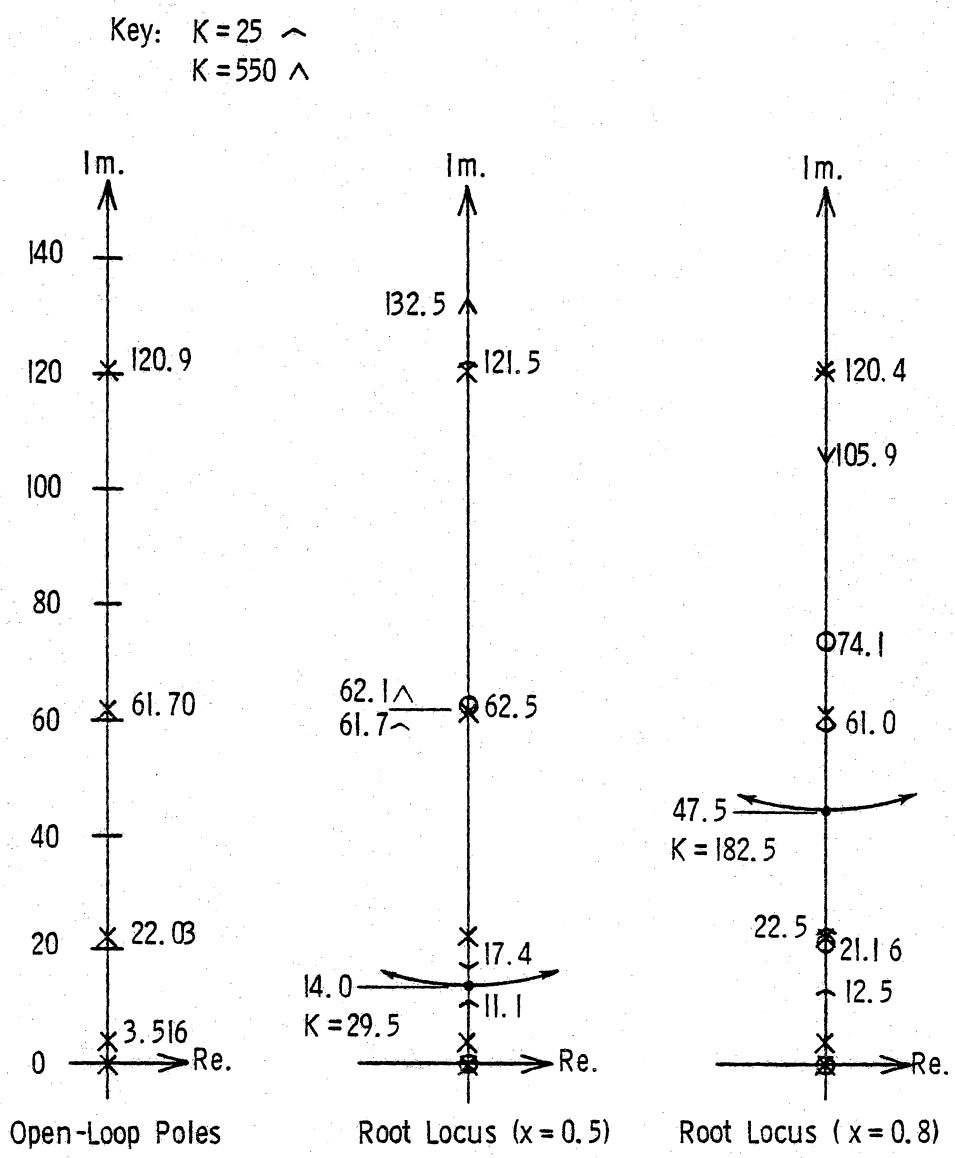

Figure 32. Displacement Feedback to End, x = 0.5, 0.8, (Cantilever Beam)

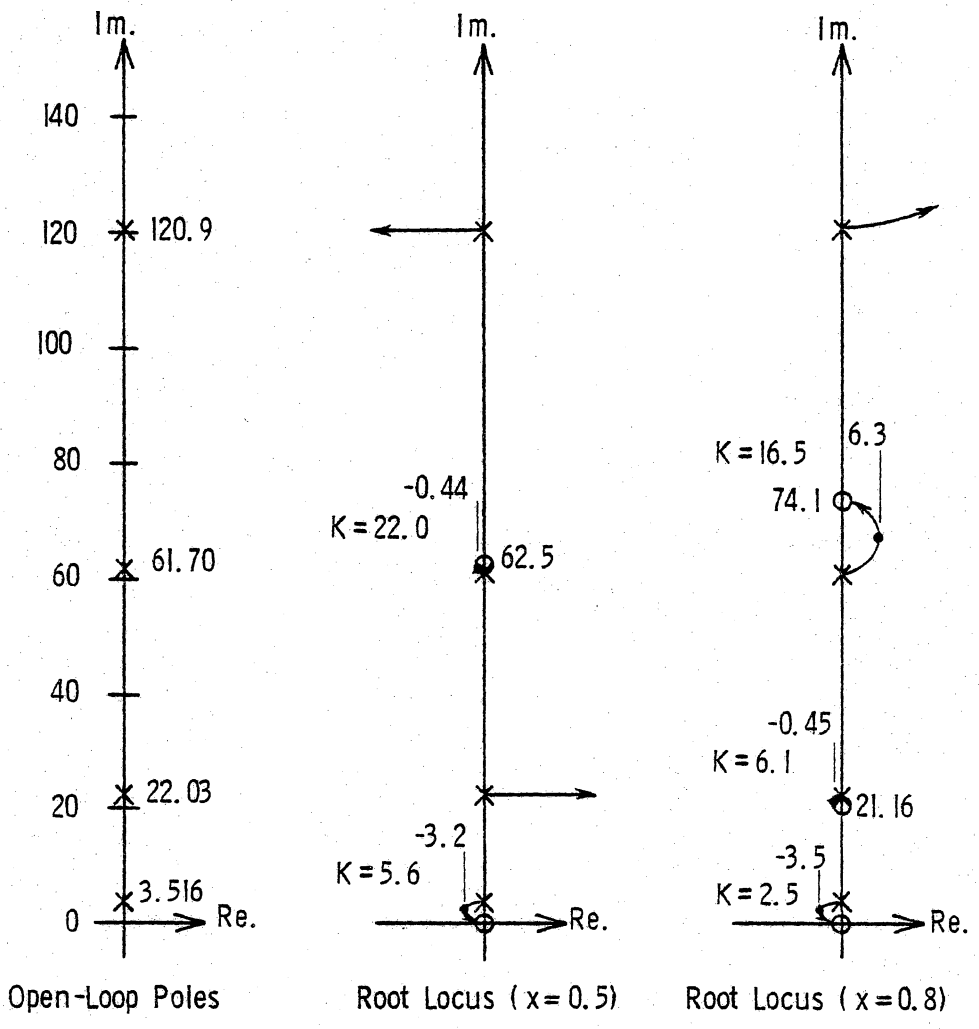

Figure 33. Velocity Feedback to End, x = 0.5, 0.8, (Cantilever Beam)

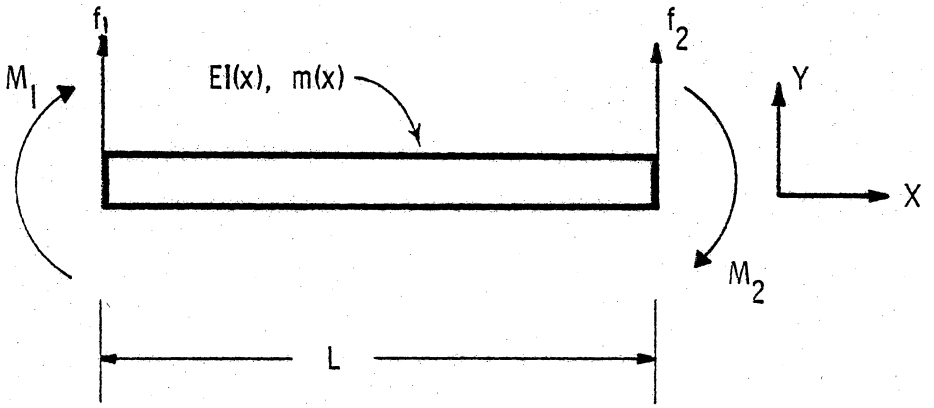

(a)

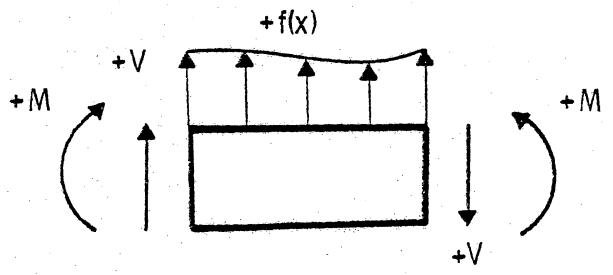

(b)

Figure 34. Free-Free Beam with Control Forces and Moments at Both ends, and Sign Convention

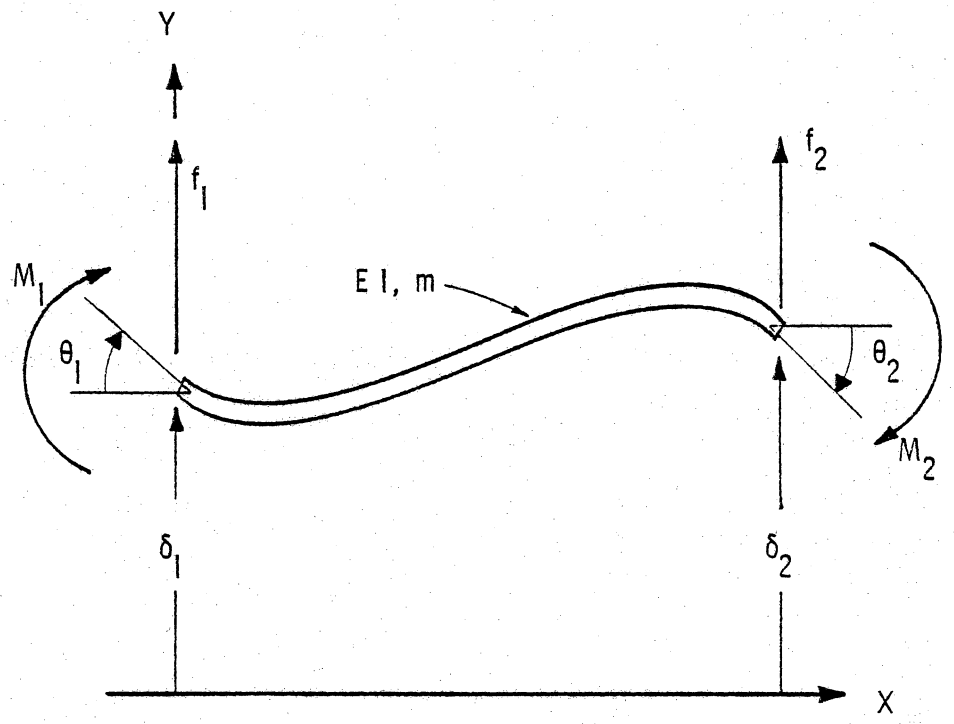

Figure 35. Boundary Forces and Displacements, Uniform Beam Element

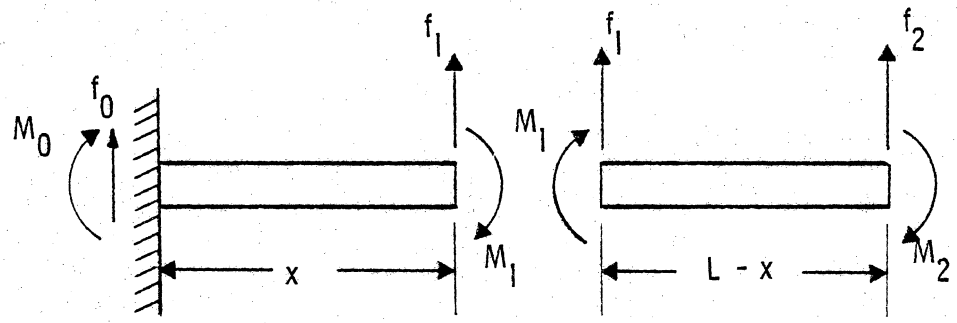

Figure 36. Two Element Beam, Dynamic Stiffness Method

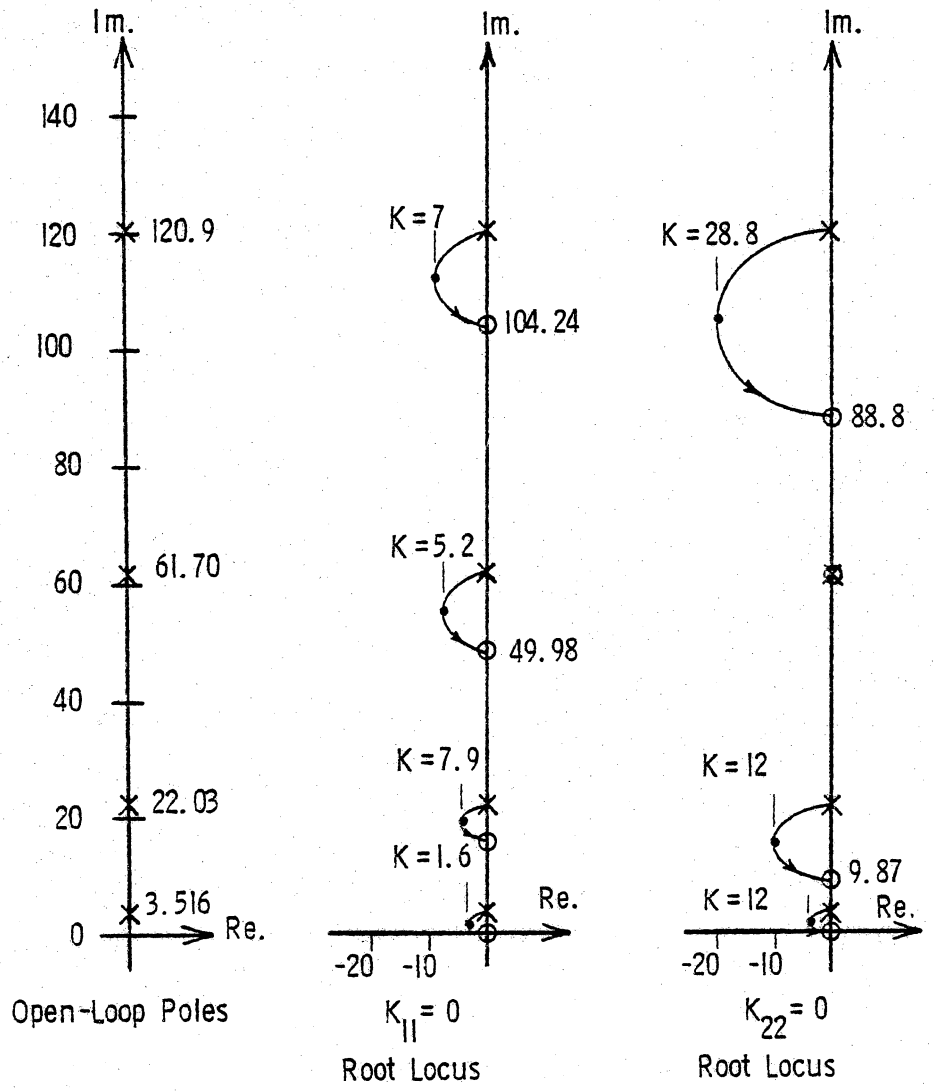

Figure 37. Velocity Feedback to Co-Located Forces, x = 0.5, 1.0, (Cantilever Beam)

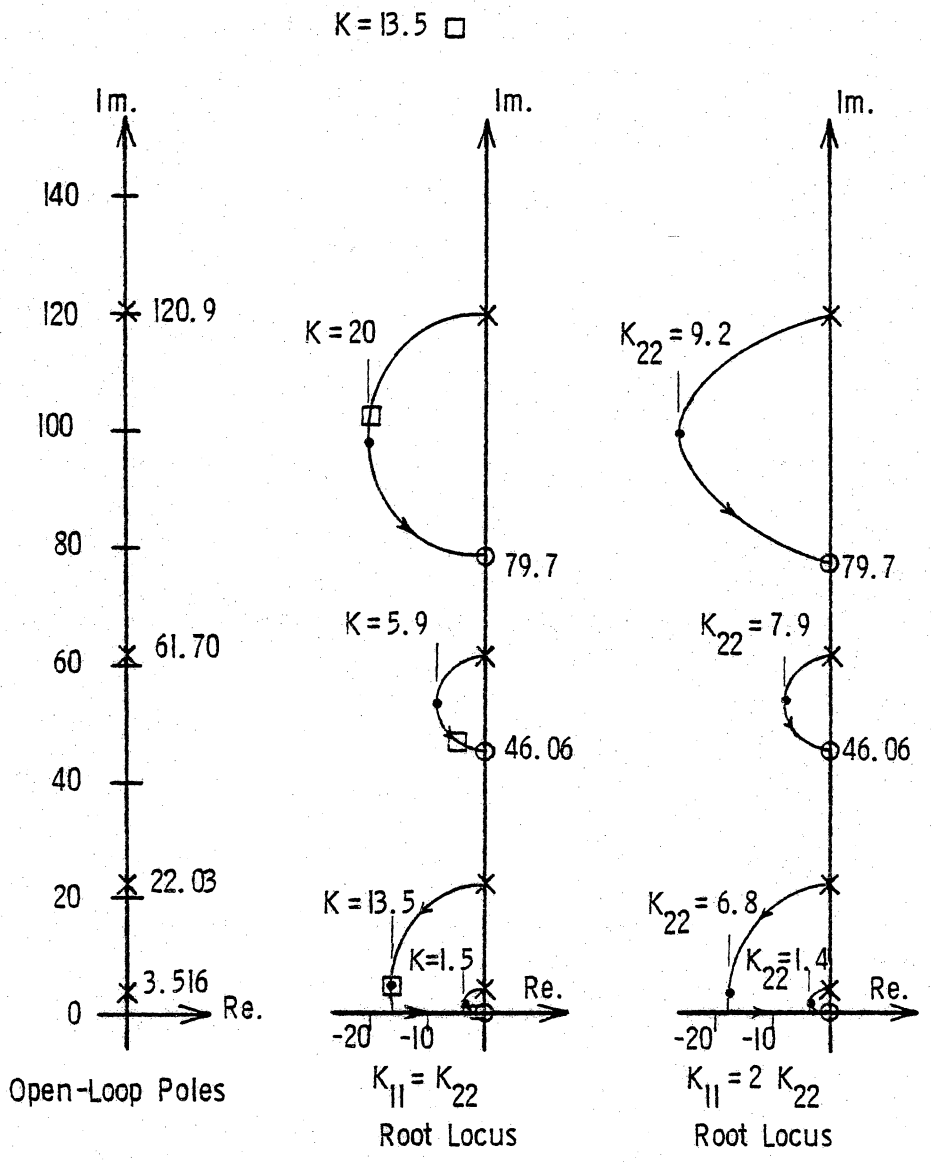

Figure 38. Velocity Feedback to Co-Located Forces, x = 0.5, 1.0, Two Gain Root Loci, (Cantilever Beam)

The vita has been removed from the scanned document

THE USE OF TRANSFER FUNCTION METHODS IN THE FEEDBACK CONTROL OF DISTRIBUTED PARAMETER SYSTEMS

by

Richard Morris Amato Goff

(ABSTRACT)

The design of controllers for structural systems, particularly those associated with large space structures, has received a considerable amount of attention in the past few years. The usual approach to designing these controllers is to apply modern control theory to a reduced linear system obtained from finite element analysis or from a truncated modal analysis. In most of these designs, the sensor signal must be processed to separate out the contributions from each mode so that it may be sent to the appropriate actuators. The analysis presented here, on the other hand, obtains exact solutions for a selected set of sensor and actuator positions for simple structural elements. Sensor signals are fed back directly to the actuators with appropriate gains. The method of analysis is that of classical control theory using Laplace transforms and the associated open and closed-loop transfer functions. Single-input-single-output feedback control is applied to various flexible cable and beam configurations. Root-loci for various values of gain are constructed and the system characteristics and the global system stability are determined.

Although the procedure outlined above can be carried out for basic structural elements, more complex structures and control

configurations are synthesized using the dynamic stiffness matrix method. With this method, the exact relationships of the basic elements can be combined to allow analysis of multi-input-multi-output control of more complex structures. Using this approach, examples for flexible cable and beam configurations are presented. It was found that exact solutions can be obtained using a finite number of sensors and actuators. It was also determined that a single co-located sensor-actuator at the boundary of a fixed-free cable or beam can control all the vibrational modes of the cable or beam. Also, pure signals from a perfect sensor can be used without any additional signal processing. The multi-input-multi-output investigation demonstrates that, even without cross-gain feedback, there is interaction between the sets of co-located sensor-actuator pairs. It appears that this interactive effect needs to be included in any multi-input-multi-output control design. By starting with fundamental elements of beams and cables, it was shown that reasonably sophisticated systems can be modeled. Finally, considerable insight is offered by analyzing the control of flexible structures using exact transfer function relationships.